HIGH-THROUGHPUT FIELD PHENOTYPING IN WHEAT USING UNMANNED AERIAL SYSTEMS (UAS)

A Dissertation

by

MAHENDRA BHANDARI

Submitted to the Office of Graduate and Professional Studies of
Texas A&M University
in partial fulfillment of the requirements for the degree of

DOCTOR OF PHILOSOPHY

Chair of Committee,	Amir M.H. Ibrahim
Co-Chair of Committee,	Qingwu Xue
Committee Members,	Nithya Rajan
	Sorin Popescu
	Xuejun Dong
Head of Department,	David D. Baltensperger

May 2020

Major Subject: Agronomy

ABSTRACT

Precise field phenotyping has always been a bottleneck in wheat breeding. Traditionally, field phenotyping has been done by physically inspecting plots one by one. A substantial amount of time, cost, and labor is required to collect data from many breeding lines. High-throughput phenotyping (HTP) is gaining interest in recent years. Advancement in Unmanned Aerial System (UAS) and sensor technology enabled the collection of high spatial and temporal resolution data which can be used in agricultural research and management. This study was conducted to develop and assess the use of UAS in wheat breeding. The major objectives of this study were to define UAS data collection and processing framework and to investigate the application of UAS data to assess disease, seasonal growth, and yield in wheat (*Triticum aestivum* L.).

The experiment to investigate the application of UAS to assess disease severity was conducted in 2017 and 2018 at Castroville, Texas. RGB images were acquired by flying rotary wing UAS. Images were then processed to develop orthomosaics and three vegetation indices were calculated. Visual notes on field response and leaf rust severity were taken to calculate Coefficient of Infection (CI). A significant variation in vegetation indices was found among the wheat genotypes. Normalized Difference Index (NDI), Green Index (GI), and Green Leaf Index (GLI) were linearly related to CI with coefficient of determination (R^2) values of 0.78 ($p<0.05$), 0.75 ($p<0.05$), and 0.72 ($p<0.05$), respectively. Vegetation indices used in this study showed great potential for their use in leaf rust severity assessment in wheat.

Crop growth analysis was performed to investigate the application of UAS data to assess wheat seasonal growth. This field study was conducted in 2018-2019 winter wheat growing season and RGB-based multi-temporal UAS data were collected throughout the growing season. Canopy Cover (CC) was obtained from UAS images and used to perform growth analysis by fitting several growth functions. Four-parameter logistic growth function had the best fit with R^2 value of 0.99 ($p<0.05$) and lowest Root Mean Square Error (3.43). Grain yield was positively associated with CC obtained during reproductive stage of wheat ($R^2=0.65$, $p<0.05$), and negatively associated with the rate of canopy decay ($R^2=0.65$, $p<0.05$) suggesting the importance of maintaining healthy canopy during grain filling for better yield.

The relationship between UAS obtained canopy features and vegetation indices with grain yield was analyzed to develop a wheat yield prediction model. Eight vegetation indices and two canopy features (CC, canopy height) were extracted from multispectral and RGB imagery. UAS parameters obtained during grain filling stage of wheat were significantly related to grain yield ($R^2>0.30$, $p<0.05$). A three-layered Artificial Neural Network (ANN) model was created using multi-temporal CC, canopy height, Excess Green Index (ExG), Normalized Difference Red Edge Index (NDRE), Normalized Difference Vegetation Index (NDVI), standard deviation of NDRE and ExG measurements as input parameters to predict grain yield. R^2 values between predicted yield and observed yield were 0.78 and 0.60 ($p<0.01$) for training and testing data set, respectively. Satisfactory performance of ANN model shows the potential of using machine learning models to predict grain yield based on UAS parameters.

DEDICATION

To my lovely wife

Chadani Adhikari

And

My parents (Tulsi Bhandari and Saraswati Bhandari)

ACKNOWLEDGEMENTS

There were many helping hands to make this study a success. Foremost, I would like to express my sincere gratitude to Dr. Amir M.H. Ibrahim and Dr. Qingwu Xue for their continuous support and encouragement during my study. Also, I am thankful to my dissertation advisory committee members Dr. Nithya Rajan, Dr. Sorin Popescu, and Dr. Xuejun Dong, for providing the guidance and support during this period. I am grateful to Dr. Juan Landivar for letting me work as an intern at Texas A&M AgriLife Research Center at Corpus Christi, Texas.

Many thanks to the College of Agriculture and Life Science, Texas A&M University for providing me the Excellence Fellowship to pursue my doctoral study. Additionally, I would like to thank Texas A&M AgriLife Research Crop Improvement Program for funding this research. My sincere gratitude goes to Governor's University Research Initiative (GURI) program that provided funding to purchase Unmanned Aerial System (UAS) platforms and sensors.

I am grateful to UAS team at College Station and Texas A&M AgriLife Research at Corpus Christi, Texas. Specifically, Ms. Jessica Flores, Ms. Misty Vidrine were very helpful in taking care of all the legal producers for conducting UAS flights. I thank Mr. Ian Gates and Mr. Eric Pitts for their help to conduct UAS flights. I am thankful to Dr. Anjin Chang, Dr. Jinha Jung, and Dr. Sungchan Oh for their help during UAS image processing. Many thanks to Dr. Nothabo Dube for her help during data analysis.

I am indebted to the entire wheat breeding and genetics team who were always helpful during this study. I would like to thank Dr. Geraldine Opena and Mr. Bryan Simoneaux, and Dr. Brandon Gerrish for logistic support. Many thanks to Mr. Anil Adhikari, Mr. Rahul Raman, and Mr. Jorge Valenzuela for their support in data collection. I am grateful to Ms. Shannon Baker and Dr. Jackie Rudd for their willingness to provide UAS data collected at Bushland, Texas.

I am grateful to faculty members and administrative staff at the Soil and Crop Sciences Department for their support and facilitation of my doctoral study. Thanks to the International Student Services (ISS) staff for all the support during my Curriculum Practicum Training (CPT) authorization.

I am grateful to my friends at College Station for their support, encouragement, and all the fun we had in the last three and half years. Last but not the least; I would like to thank my family: my parents, my lovely wife, my brother, sister-in-law, and sister for supporting and believing in me throughout my life.

NOMENCLATURE

CC	Canopy Cover
CI	Coefficient of Infection
DSM	Digital Surface Model (DSM)
DEM	Digital Elevation Model (DEM)
Kg	Kilogram
DN	Digital Number
ExG	Excess Green Index
GI	Green Index
GLI	Green Leaf Index (GLI)
GNDVI	Green Normalized Difference Vegetation Index
Ha	Hectare
HTP	High Throughput Phenotyping
MSAVI	Modified Soil Adjusted Vegetation Index
MTVI2	Modified Triangular Vegetation Index
NDI	Normalized Difference Index
NDRE	Normalized Difference Red Edge Index
NDVI	Normalized Difference Vegetation Index
SAVI	Soil Adjusted Vegetation Index
SCCCI	Simplified Canopy Chlorophyll Content Index
UAS	Unmanned Aerial System

TABLE OF CONTENTS

Page

LIST OF FIGURES

Page

LIST OF TABLES

Page

CHAPTER I

INTRODUCTION AND LITERATURE REVIEW

Wheat (*Triticum aestivum* L.) is one of the most important staple food crops grown in the world. It is also a major crop in the U.S. Great Plains, including Texas High Plains (Howell *et al.*, 1995). In 2018, it was planted in 90 thousand hectares in the Texas High Plains (USDA-NASS, 2019). The current global annual increase in wheat yield is about 0.9%. With a steady increase in global population, wheat yield needs to increase by 1.7% per year to feed the expected 9.7 billion people by 2050 (Hawkesford *et al.*, 2013). The impact of increasing temperature due to global warming and the decrease in the availability of freshwater resources for irrigation will be a major challenge for wheat production in the future. Development of better wheat cultivars through improved breeding (Donmez *et al.*, 2001; Brancourt-Hulmel *et al.*, 2003; Shearman *et al.*, 2005; Foulkes *et al.*, 2007; Green *et al.*, 2012) and utilization of better crop management techniques (Evenson and Gollin, 2003; Pingali, 2012) have increased wheat production since the green revolution. Wheat breeding has played a crucial role to increase yield through the development of disease resistant (Ausemus, 1943; Sayre *et al*., 1997; Rajaram *et al.*, 2001; Bariana *et al.*, 2007; Hiebert *et al.*, 2010; Paillard *et al.*, 2012; Basnet *et al.*, 2013; Rehman *et al.*, 2013; Li *et al.*, 2014; Ullah *et al.*, 2015; Wu *et al.*, 2015; Tolmay *et al.*, 2016), drought tolerant (Hurd, 1974; Cushman and Bohnert, 2000; Araus *et al.*, 2002; Paulsen, 2002; Cattivelli *et al.*, 2008; Fleury *et al.*, 2010; Blum, 2011; Morran *et al.*, 2011; Fritsche-Neto and Borém, 2012; Panguluri and Kumar, 2013;

Budak, Kantar and Yucebilgili Kurtoglu, 2013; Timmusk *et al.*, 2014; Mwadzingeni *et al.*, 2016; Mohammadi, 2018), and high-yielding cultivars (Slafer *et al.*, 1994; Acreche *et al.*, 2008; Bradshaw, 2017). It is important to improve genetics, agronomy and efficiency of wheat breeding programs to achieve the demand of wheat. Technologies that can complement conventional breeding approaches have the potential to identify new traits, improve genetic gain, widen the gene pool and identify elite progeny efficiently and precisely.

Genetic gain is the improvement in the genetic or phenotypic value of a population due to selections over multiple breeding cycles (Tester and Langridge, 2010). During the variety development process, a population goes through a multiple year of recombination, selection, and evaluation until the best performing cultivar can be released. Evaluation and selection are based on the phenotypic and/or genotypic data collected during the growing season to induce genetic gain in the subsequent generation. The genetic gain is usually defined by the following formula according to the breeder's equation (Rutkoski et al., 2016).

$$R = \frac{\mathrm{ir}\sigma_A^2}{\mathrm{y}}$$

Where R is genetic gain over time, i is selection intensity, r is selection accuracy, σ_A^2 is genetic variance, and y is years per cycle.

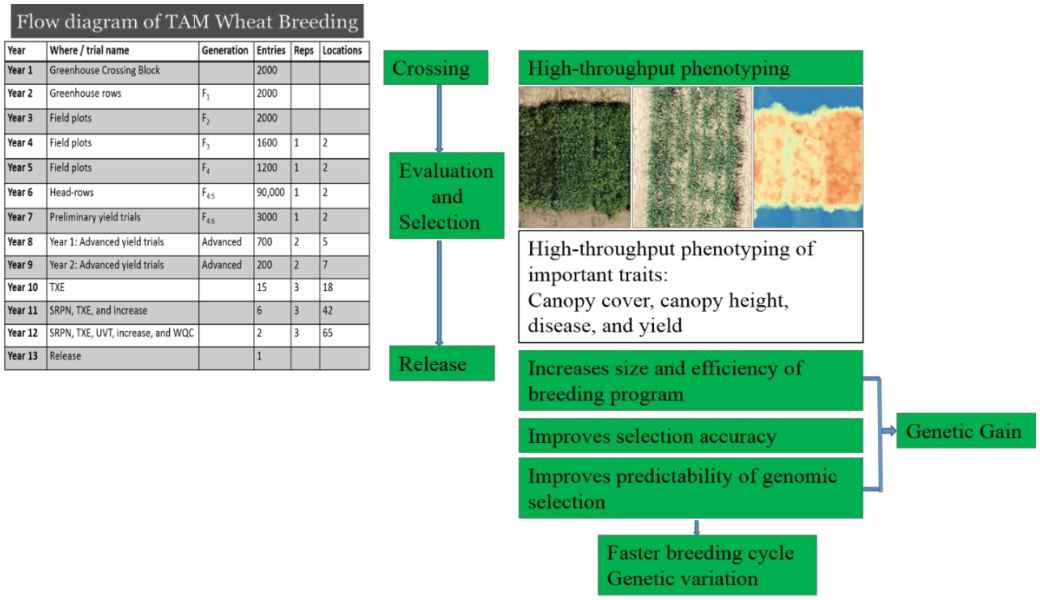

Figure 1. Overall wheat breeding process and the potential of high-throughput phenotyping

Selection intensity is the amount of population that is selected from the total population for a particular trait or traits combined. Population size affects selection intensity. Selection accuracy improves estimation of genetic value of a population. Thus, as outlined and explained by (Barabaschi *et al.*, 2015; Bai *et al.*, 2016; Araus *et al.*, 2018; Sun *et al.*, 2019); increase in the genetic gain can be achieved by (i) expanding breeding program (ii) improving selection accuracy (iii) introducing enough genetic variation, and (iv) shortening the breeding cycles. To achieve the desired output using the components, the breeding program needs a high-throughput data collection and analysis mechanism for obtaining genetic and phenotypic information (Figure **1**).

Use of genomic tools such as Marker Assisted Selection (MAS), gene editing, and genetic engineering can help conventional breeding programs for selecting

genotypes for disease resistance (Jena and Mackill, 2008; G. Miah *et al.*, 2013; Gous Miah *et al.*, 2013). Although difficult, genomic approaches have the ability to assemble desired genes but it is necessary to screen a population for a certain trait under replicated trials across multiple environments (Kang *et al.*, 2016) to finally produce a desirable variety. High throughput genotyping enables indirect selection of genotypes using predictive models prior to phenotyping. This reduces the number of genotypes that are needed to evaluate in the field (Lorenz *et al.*, 2011). The genomic models require phenotypic data for the training population and is tested using an entirely different population. This model is then used to select another population. This process of genomic selection has the potential to improve genetic gain over time by increasing selection intensity, selection accuracy and genetic variance and reducing the time per cycle. However, genomic selection is much more dependent on the accuracy of phenotypic data of the training population. Development of low cost, non-destructive, high-throughput phenotyping (HTP) system not-only addresses the traditional labor and time intensive phenotyping system but also complements genomic selection.

Precise field phenotyping has always been a bottleneck in wheat breeding. Traditionally, field phenotyping has been done by physically inspecting plots one by one. Substantial amount of time, cost and labor is required to collect phenotypic data from large number of breeding lines (Haghighattalab *et al.*, 2016). For example, the Texas A&M wheat breeding program evaluates around 90,000 F_5 head-rows annually and advances them to subsequent generations for derivation and subsequent testing in multiple environments (Figure **1**). The accuracy of the manual data is affected by the

raters and their ability to properly diagnose the disease and other phenotypic features which can reduce the repeatability and reliability of the measured trait (Chakraborty *et al.*, 2014; Mutka and Bart, 2015). HTP is gaining interest in recent years as an improvement to manual phenotyping. Plant phenotyping facilities are developed for green houses, growth chambers with robotics system and remote sensing tools to assess plant growth and development (Araus and Cairns, 2014). High-throughput field phenotyping tools use remote sensing techniques and capture information about a particular trait remotely. These techniques have several advantages over traditional phenotyping approaches (Araus *et al.*, 2002; White *et al.*, 2012; Panguluri and Kumar, 2013b; Fernie and Gutierrez-Marcos, 2019; Furbank *et al.*, 2019; Parmley *et al.*, 2019; Pieruschka and Schurr, 2019; Pratap *et al.*, 2019; York, 2019). HTP has the potential to enable rapid assessments of large breeding nurseries across time and space by providing high spatial and temporal resolution measurements from small plots. This can increase our capability to monitor and quantify field data obtained from multiple breeding nurseries and improve genetic gain in the long run. Ability to obtain precise phenotypic information can replace tedious and subjective ratings of breeding plots with highly dependable phenotypic information about a certain genotype (Mutka and Bart, 2015). If we look at the breeder's equation of genetic gain, the high-throughput field phenotyping can improve genetic gain by improving selection intensity and selection accuracy directly and indirectly to all components of the equation.

Ground-based platforms (Bai *et al.*, 2016; Crain *et al.*, 2016; Tattaris, Reynolds and Chapman, 2016; Thompson *et al.*, 2018), satellite imaging (Tattaris, Reynolds and

Chapman, 2016; G. Yang *et al.*, 2017), manned aerial system (Olanrewaju *et al.*, 2019), Unmanned Aerial Systems (UAS) (Haghighattalab *et al.*, 2016; Tattaris, Reynolds and Chapman, 2016; Chawade *et al.*, 2019; Sun *et al.*, 2019) are four different platforms commonly used to collect data for various agriculture applications (White *et al.*, 2012; Sun *et al.*, 2017; G. Yang *et al.*, 2017; Sankaran *et al.*, 2018; Chawade *et al.*, 2019; Zhang *et al.*, 2019). All these different platforms come with several advantages and disadvantages and can be used for specific applications. Ground-based platforms provide high resolution data (temporal and spatial) but they are time consuming if we collect data from many plots. Crain *et al.* (2016) developed a portable ground-based field phenotyping system (phenocart) by integrating a GreenSeeker, an infrared thermometer (IRT), and a global navigation satellite system (GNSS) receiver to measure Normalized Difference Vegetation Index (NDVI), canopy temperature, and geographic co-ordinates for geo-referencing. Although it allowed faster data collection of multiple traits from wheat breeding trials, it was expensive (~US$12,000) to build the platform compared to the UAS system. The phenotyping platform developed by mounting sensors on a high-clearance tractor becomes even more expensive compared to the UAS (White *et al.*, 2012; Cobb *et al.*, 2013; Yang *et al.*, 2017). Additionally, the ground clearance and variation of canopy height between genotypes makes it even more difficult to obtain uniformity in data collection (Yang *et al.*, 2017). Satellite imaging system have several challenges such as the cost of using the sensor and cloud coverage might obstruct image acquisition. Additionally, lower spatial and temporal resolution limits its use as a tool for HTP as plots in a breeding trial are relatively small in size (Chapman *et al.*, 2014). Low

cost UAS can be used as a rapid, affordable, and efficient field-based crop phenotyping tool in breeding programs to collect data on several phenotypic features (Liebisch *et al.*, 2015; Inostroza *et al.*, 2016). UAS-based remote sensing is gaining interest in recent years in high-throughput field phenotyping. Development of lightweight, low-cost portable sensors had added benefits of using UAS for obtaining high spatial and temporal resolution data which can be helpful for obtaining data from small breeding plots (Ashapure *et al.*, 2019).

UAS equipped with RGB, thermal and multispectral sensors have been used to estimate several crop biophysical parameters such as Leaf Area Index (LAI) (Potgieter *et al.*, 2017; Yang *et al.*, 2017), the fraction of intercepted photosynthetically active radiation (Guillen-Climent *et al.*, 2012), biomass (Bendig *et al.*, 2014, 2015; Bendig, 2015; Brocks and Bareth, 2018; Acorsi *et al.*, 2019), plant height (Bendig *et al.*, 2014; Bendig, 2015; Anderson *et al.*, 2019; Hassan *et al.*, 2019), plant density (Yang *et al.*, 2017), disease assessment (Su *et al.*, 2018), water stress (Hoffmeister *et al.*, 2016), Canopy Cover (CC) (Chu et al., 2016), growth status (Du and Noguchi, 2017; Shafian *et al.*, 2018) and yield (Yang and Everitt, 2002; Stroppiana *et al.*, 2015; Hoffmeister *et al.*, 2016; Shi *et al.*, 2016; Q. Yang *et al.*, 2017; Zhou *et al.*, 2017; Su *et al.*, 2018; Anderson *et al.*, 2019; Wang *et al.*, 2019; Yang *et al.*, 2019). The sensors capture the amount of light reflected by different objects in the surface of the earth. If we analyze the spectral reflectance curve of vegetation, soil and water in the electromagnetic spectrum then we can find the variation in the reflectance in the visible region, Near Infrared Region (NIR) and beyond. For healthy green vegetation, the reflectance is low in both the blue and red

regions of the spectrum, due to absorption by chlorophyll for photosynthesis while the reflectance is high in the green region (Wang *et al.*, 2016). As NIR is affected by the cellular structure of leaves, the reflectance is much higher in this region. While the reflectance from soil is higher in the visible region than the vegetation and lower in the NIR region. UAS collect aerial image data, which can be converted into reflectance dataset to obtain meaningful information. These images can further be processed to generate plot level high throughput measurements. These measurements can be used as an indirect approach to study the agronomic and physiological traits of plants, which can be useful to evaluate genotypes in wheat breeding programs, thus increasing size and efficiency (Haghighattalab *et al.*, 2016). These measurements will help to select parents and evaluate progenies on a large scale. One of the commonly used indirect approach of estimating a plant physiological trait is based on spectral vegetation indices (VIs).

RGB and multispectral imagery can be used to obtain reflectance measurements in the red (R), green (G), blue (B), Red edge and NIR wavebands and calculate the spectral vegetation indices (VIs). Numerous VIs has been developed so far and are used to study the growth and development of vegetation. Table **1** provides a list of several VIs that has been used to assess disease severity, drought stress, and plant growth and can be derived from RGB and multispectral sensors. For example, the reflectance observed in the G, NIR and R channels can be used to obtain indices such as NDVI, Green Normalized Vegetation Index (GNDVI), and Normalized Difference Red edge Index (NDRE), Simplified Canopy Chlorophyll Content Index (SCCCI), and Green Normalized Difference Vegetation Index (GNDVI). NDVI is used to estimate green

biomass (Bendig *et al.*, 2015; Olanrewaju *et al.*, 2019; Zhang *et al.*, 2019), canopy health, LAI (Araus *et al.*, 2018) and yield (Goodwin *et al.*, 2018). NDRE, which uses the reflectance obtained in the red edge region of the spectrum, can be used in vegetation stress detection and crop canopy senescence (Gitelson *et al.*, 1996). GNDVI was used to estimate LAI, chlorophyll content, nitrogen, protein content and water content of the canopy (Prasad *et al.*, 2007; Garcia-Ruiz *et al.*, 2013). Potgieter *et al.* (2017) evaluated the use of NDVI, NDRE, and Enhanced Vegetation Index (EVI) to assess the seasonal leaf area dynamics of sorghum breeding lines. They found a good correlation of NDVI and EVI with plant number per plot, CC, and LAI. They also found that NDRE can be used to estimate chlorophyll content and was useful to characterize the leaf area dynamics and senescence. The indices in this study were obtained from a multispectral sensor flown using UAS. Shafian *et al.* (2018) evaluated UAS-derived NDVI, GNDVI, Enhanced Vegetation Index (EVI), and Modified Triangular Vegetation Index (MTVI2) to quantify LAI, fractional vegetation cover, and yield in sorghum. Of the four indices, NDVI was highly correlated with LAI, fractional vegetation cover, and yield. NDVI was strongly correlated with LAI followed by vegetation cover, and yield. They also stated that NDVI obtained during the flowering stage of sorghum (*Sorghum bicolor* L.) was highly correlated with grain yield. NDVI measured during grain filling had a higher correlation with wheat grain yield in a study conducted by Hassan *et al.* (2019). They concluded that the multispectral sensor mounted on a UAS platform can be a reliable high-throughput platform to measure NDVI and use it to predict biomass and grain yield. Additionally, a higher heritability estimates of NDVI obtained during flowering

and grain-filling stages suggested that grain-filling can be an appropriate stage to make selections based on UAS measurements. Strong correlations were found between UAS-based NDVI measured around flowering and final grain yield (Duan *et al.*, 2019). NDVI is strongly associated with aboveground biomass and total green area (Cabrera-Bosquet *et al.*, 2011). Green leaf Index (GLI), Green Index (GI) and Normalized Difference Index (NDI) are some of the indices that can be developed by using only the RGB band information. GLI values range from -1 to +1. Feature with negative GLI values represent non-living objects while positive values represent green canopy features. This index was originally formulated to measure CC in wheat (Louhaichi *et al.*, 2001). GI, which is the ratio of reflectance in the R and G region is negatively associated with leaf rust severity in wheat (Ashourloo *et al.*, 2014). NDI was developed to filter soil and residue background and select green vegetation in the images (Perez et al., 2000).

Table 1. List of spectral vegetation indices

Reflectance obtained in the red band is denoted by R, green band by G, red edge by RE, and near infrared by NIR.

Vegetation indices	**Formula**	**References**
Green Leaf Index (GLI)	$\frac{2G - R - B}{2G + R + B}$	Louhaichi *et al.*, 2001
Green Index (GI)	$\frac{R}{G}$	Zarco-Tejada *et al.*, 2005
Normalized Difference Index (NDI)	$\frac{G - R}{G + R}$	Perez *et al.*, 2000
Normalized Difference Vegetation Index (NDVI)	$\frac{NIR - R}{NIR + R}$	Rouse *et el.*, 1974
Normalized Difference Red Edge Index (NDRE)	$\frac{NIR - RE}{NIR + RE}$	Barnes *et al.*, 2000
Simplified Canopy Chlorophyll Content Index (SCCCI)	$\frac{NDRE}{NDVI}$	Raper and Varco, 2015
Green Normalized Difference Vegetation Index (GNDVI)	$\frac{NIR - G}{NIR + G}$	Giletson *et al*., 2003
Soil Adjusted Vegetation Index (SAVI)	$\frac{1.5(NIR - R)}{NIR + R + 0.5}$	Huete, 1988
Modified Soil Adjusted Vegetation Index (MSAVI)	$\frac{2NIR + 1 - \sqrt{(2NIR + 1)^2 - 8(NIR - R)}}{2}$	Qi *et al.* (1994)

Although, VIs can be used to measure and estimate several crop biophysical parameters, they are subjected to limitations. One of the major limiting factors is the influence of soil background on the measurements. Additionally, the vegetation indices are saturated when the plot is fully covered by the canopy. Other factors that influence

the VIs measurements are crop type and climate. The proper time and growth stage for collecting spectral data is still a topic of discussion. Some researchers propose that data collection should be done when the crop canopy is fully covered. However, others argue that the data collection should be done before the ground is fully covered by the canopy so that there will be enough threshold between the soil and canopy to filter the later from former. The color of the soil on other hand play an important role when calculating vegetation indices as the canopy during senescence sometimes can resemble to the soil in wheat (Colwell, 1974). Yang *et al.* (2001) reported that the NDVI measured between soft to hard dough to before physiological maturity can be important in predicting yield. The use of including threshold values in the vegetation indices can be another approach to estimate green biomass. For example, an NDVI value of 0.5 or higher can be considered as the canopy pixels in the image while the lower values can be classified as soil pixels (Potgieter *et al.*, 2017). Duan *et al.* (2019) suggested a data fusion technique in which the ground and aerial sensing system can be integrated to improve the accuracy of the estimates across multiple resolution and scales. Thus, it is important to reduce the contribution of the soil in the VI measurements to determine the canopy VI. Therefore, it is necessary to test the ability of VIs according to the crop and the growing conditions. The influence of the climate and environmental variability on the UAS data collected multiple times during the growing season is the use of radiometric calibration technique to maintain the uniformity in the reflectance data despite changing weather conditions during the crop growing season.

Using the radiometric calibration approach, image digital numbers (DN) are converted into surface reflectance values so that the uniformity can be obtained across multiple measurements throughout the growing season. The data obtained from UAS imagery are in the form of DN and are converted into reflectance data following different procedures. Radiometric correction is done to calibrate the pixel values and correct errors in the values. During this process, DN from the imagery data sets are converted into reflectance values to derive meaningful interpretation of remotely sensed data. Most importantly, if we are comparing multiple imagery data sets gathered for monitoring crop growth dynamics, radiometric correction is essential as climatic conditions vary during the growing season. If we use satellite imagery, atmospheric correction is needed to discard the effects of atmospheric absorption and scattering on imagery dataset. However, the UAS platforms are usually flown in lower altitudes (20 m-120 m) in which the reflected light passes through a small atmospheric column. This results in small difference in radiance in the sensor, and in the surface. Therefore, the work of atmospheric correction is discarded. However, radiometric calibration should be done on the UAS imagery. There are several different approaches to conduct radiometric calibration such as vicarious calibration, absolute radiometric calibration, and relative radiometric calibration. Vicarious calibration is usually performed on satellite imagery. When the satellite overpasses a certain region, at that same time, hyperspectral surface reflectance data and atmosphere transmittance data are measured. These measurements along with local meteorological data are used with the satellite measured values to develop a calibration coefficient. This type of calibration is performed by MODTRAN

software (Berk *et al.*, 2014). Absolute radiometric calibration is also performed in satellite imagery data. In this approach, Pseudo Invariant Calibration Sites (PICS) are constructed on the earth surface where the surface reflectance properties are constant. The reflectance obtained on these sites are used as calibration sources. These sites are made in the regions where there is minimal atmospheric variation. In relative radiometric calibration, calibration from one detector is done to another in the system. One of the most common methods of radiometric calibration of UAS imagery is the empirical line method (Haghighattalab *et al.*, 2016). In this method calibration targets of known reflectance are placed in the field during the UAS flight. The spectral measurements (reflectance) of these calibration targets are recorded using spectrometer and the DN are extracted during image processing. The DN values of the target are plotted against the reflectance values to obtain a regression equation. With the advancement of sensors, real time radiometric corrections are performed based on the amount of light incident and reflection from the objects. One of such sensors is SlantRange 3p which has onboard sunlight correction ambient illumination sensor that calibrates the imagery data based on the proportion of the amount of light incident on and reflected from the surface. It captures the incoming solar radiation and the reflected radiation. Radiometric correction of the sensor coupled with radiometric calibration of the UAS imagery would be a better option for obtaining precise results. UAS provides higher flexibility in data collection as that can be arranged in a day without cloud coverage. Also, UAS can collect data when the sky is completely covered by clouds. As the UAS platforms fly in lower altitude, the radiations reflected to the sensors incur less error because of atmospheric conditions

such as clouds, dusts, aerosols, etc. For example, clouds and snow tend to be bright in the red and dark in the NIR region of the spectrum. This can significantly vary the results of vegetation indices obtained from UAS and satellite imagery.

Canopy height is another important trait that can be used to study the crop phenology and growth. It can be used as a measure to estimate crop biomass and final yield. Traditionally, plant height is measured by using a scale meter in wheat breeding. This requires substantial amount of time if we are required to take multiple plant height measurements in a single plot. One of the common approaches to obtain canopy height is the photogrammetric method using the principal of stereo vision (Xiao et al., 2010). Another approach is the use of airborne or ground-based LiDAR sensor (Popescu *et al.*, 2003). Although the LiDAR measurements are relatively accurate, the sensor is costly, and it is difficult to handle in a wheat breeding trial. RGB images obtained by flying UAS platforms at low altitude can be used to develop Digital Surface Model (DSM) of the bare ground and the surface of the canopy which can be used to determine canopy height (Jensen and Mathews, 2016). Biomass can be estimated using the plant height derived from DSM in wheat. Khan *et al.* (2018) evaluated UAS and mobile ground platform (MGP) to estimate canopy height and canopy vigor in wheat. They found that the MGP imaging system provided better estimates of height while the UAS was able to provide better estimates of canopy vigor. One of the reasons for obtaining better results using MGP system was the acquisition of high-resolution imagery. This shows that the development and use of sensors on UAS platforms capable of flying at lower altitude can provide better estimates of canopy height measurements. Higher resolution images

can be useful to differentiate wheat canopy from the soil as the leaves of the wheat plants are small. UAS can be used to obtain high resolution images which can be used to generate 3D point clouds and produce DSM using the Structure from Motion (SfM) approach. This technique has been used by several researchers to obtain canopy height in maize (*Zea mays* L.) (Anderson et al., 2019), sorghum (Hu et al., 2018), and wheat (Holmen et al., 2016). Bendig (2015) used UAS-based RGB imagery to develop crop surface models (CSMs) multiple times during the growing season to estimate canopy height. The results obtained in these studies were highly correlated with ground measurements. Anderson *et al.* (2019) used this same method to determine canopy height of maize and estimate grain yield. In this method, digital terrain model (DTM) developed from the UAS images of bare ground is acquired immediately after planting. Once the plants emerge and canopy is developed, UAS flights are conducted to obtain images to develop CSM. Ground control points are placed in the field to obtain the geographic coordinates so that each image can be geo-referenced when developing the point cloud data sets. The canopy height model is developed by subtracting DTM from CSM. Many studies have shown that the results obtained from this method are reliable and accurate. However, the accuracy of the measurement depends on the absolute accuracy of the 3D point cloud data, image overlap, spatial resolution, and accurate coordinate measurement of the ground control points. Although, UAS platforms are mounted with their own GPS system, their accuracy is affected by the wind and the motion during the flight mission. Therefore, it is suggested to place permanent/semi-permanent ground control points in the field while flights are conducted. Additionally,

accurate geo-referencing is highly desirable to extract phenotypic data from orthomosaic images in plant breeding. During data extraction plot boundary shape file is generated that constitute polygon shape file for each plot and accurate geo-referencing can save the amount of time required to generate the plot boundary shape files.

Developing wheat genotypes for better yield, quality, disease resistance, and drought tolerance is the primary goal of any wheat breeding. Development of disease resistance varieties is important as wheat is threatened by one or several diseases every year in most of the wheat producing regions in the world. In the United States, leaf rust caused by fungus *Puccinia triticina f. sp. tritici*, is one of the most important diseases (Kolmer and Hughes, 2018). It is important to grow resistant varieties on the southern region of the US as the uredospores survive the winter in this region and become the source of inoculum for leaf rust infection in the wheat grown in the Central and Northern Great Plains. Additionally, continuous development of resistant varieties to leaf rust is critical as new virulent leaf rust races develop every year and overcome the varietal resistance (Oelke and Kolmer, 2004). Precise and efficient disease phenotyping can play an important role in the development of wheat cultivar resistant to leaf rust. The use of UAS to assess disease severity in different crops such as yellow rust (*Puccinia striiformis f. sp. tritici*) in wheat (Su *et al.*, 2018), rice sheath blight (*Rhizoctonia solani*) in rice (*Oryza sativa* L.) (Qin and Zhang, 2005; Zhang *et al.*, 2018), anthracnose (*Colletotrichum sublineola*) in sorghum (*Sorghum bicolor* L.) (Pugh *et al.*, 2018) has been studied and it was shown as a potentially useful tool for assessing plant diseases. Wheat yield is the culmination of several directly and indirectly related factors.

Incorporating several phenotypic features obtained from imagery dataset can help to develop precise yield prediction models and explain yield variation among genotypes. Strong relationship between UAS-based NDVI and grain yield were observed at grain-filling stage (R^2 = 0.40, 0.49 and 0.45) of wheat grown under irrigated condition in a study conducted by Hassan et al. (2019). Additionally, NDRE and normalized green red difference index (NGRDI) correlated in a similar way with grain yield. UAS equipped with multispectral sensor can be a reliable tool to predict biomass and grain yield. Anthesis and grain-filling stages (10.51 to 11.1 in Feekes scale; Large (1954)) of wheat development are the best periods for making selection based on UAS measurements. Genotypes with higher NDVI have faster growth, higher vegetative biomass, delayed senescence and have higher yields. Multi-temporal measurements throughout the wheat growing season can help to predict yield based on UAS parameters (Goodwin *et al.*, 2018). Thus, UAS can be considered as having a great potential to be incorporated into wheat breeding programs but its technical capabilities should be studied to make its use specific to wheat breeding programs. This study was conducted to develop and evaluate the use of high-throughput field phenotypic system for disease and yield phenotyping in wheat breeding with the following objectives:

1. Develop a procedure for image acquisition, processing and data extraction using UAS,
2. Develop image processing methodology to determine canopy height, canopy volume, canopy area, and vegetation indices specific to wheat,

3. Validate the UAS-based canopy features results with the field measurements for disease severity, and use UAS derived canopy features to assess disease severity in wheat, and
4. Use UAS derived canopy features to perform growth analysis and estimate grain yield in wheat

REFERENCES

Acorsi, M. G., Abati Miranda, F. das D., Martello, M., Smaniotto, D. A., & Sartor, L. R. (2019). Estimating biomass of black oat using UAV-based RGB imaging. *Agronomy*. https://doi.org/10.3390/agronomy9070344

Acreche, M. M., Briceño-Félix, G., Sánchez, J. A. M., & Slafer, G. A. (2008). Physiological bases of genetic gains in Mediterranean bread wheat yield in Spain. *European Journal of Agronomy*, *28*(3), 162–170. https://doi.org/10.1016/j.eja.2007.07.001

Anderson, S. L., Murray, S. C., Malambo, L., Ratcliff, C., Popescu, S., Cope, D., ... & Thomasson, J. A. (2019). Prediction of maize grain yield before maturity using improved temporal height estimates of unmanned aerial systems. *The Plant Phenome Journal*, *2*(1). https://doi.org/10.2135/tppj2019.02.0004

Araus, J. L., Slafer, G. A., Reynolds, M. P., & Royo, C. (2002). Plant breeding and drought in C3 cereals: What should we breed for? *Annals of Botany*, *89*(SPEC. ISS.), 925–940. https://doi.org/10.1093/aob/mcf049

Araus, J. L., & Cairns, J. E. (2014). Field high-throughput phenotyping: The new crop breeding frontier. In *Trends in Plant Science*. https://doi.org/10.1016/j.tplants.2013.09.008

Araus, J. L., Kefauver, S. C., Zaman-Allah, M., Olsen, M. S., & Cairns, J. E. (2018). Translating High-Throughput Phenotyping into Genetic Gain. In *Trends in Plant Science* (Vol. 23, Issue 5, pp. 451–466). https://doi.org/10.1016/j.tplants.2018.02.001

Ashapure, A., Jung, J., Yeom, J., Chang, A., Maeda, M., Maeda, A., & Landivar, J. (2019). A novel framework to detect conventional tillage and no-tillage cropping system effect on cotton growth and development using multi-temporal UAS data. *ISPRS Journal of Photogrammetry and Remote Sensing*, *152*, 49–64. https://doi.org/10.1016/j.isprsjprs.2019.04.003

Ashourloo, D., Mobasheri, M. R., & Huete, A. (2014). Evaluating the effect of different wheat rust disease symptoms on vegetation indices using hyperspectral measurements. *Remote Sensing*. https://doi.org/10.3390/rs6065107

Ausemus, E. R. (1943). Breeding for disease resistance in wheat, oats, barley and flax. *The Botanical Review*, *9*(4), 207–260. https://doi.org/10.1007/BF02872472

Bai, G., Ge, Y., Hussain, W., Baenziger, P. S., & Graef, G. (2016). A multi-sensor system for high throughput field phenotyping in soybean and wheat breeding. *Computers and Electronics in Agriculture*, *128*, 181–192. https://doi.org/10.1016/j.compag.2016.08.021

Barabaschi, D., Tondelli, A., Desiderio, F., Volante, A., Vaccino, P., Valè, G., & Cattivelli, L. (2015). Next generation breeding. *Plant Science*, *242*, 3–13. https://doi.org/10.1016/j.plantsci.2015.07.010

Bariana, H. S., Miah, H., Brown, G. N., Willey, N., & Lehmensiek, A. (2007). Molecular Mapping of Durable Rust Resistance in Wheat and its Implication in Breeding. In *Wheat Production in Stressed Environments* (pp. 723–728). https://doi.org/10.1007/1-4020-5497-1_88

Basnet, B. R., Singh, R. P., Herrera-Foessel, S. A., Ibrahim, A. M. H., Huerta-Espino, J.,

Calvo-Salazar, V., & Rudd, J. C. (2013). Genetic analysis of adult plant resistance to yellow rust and leaf rust in common spring wheat Quaiu 3. *Plant Disease*, *97*(6), 728–736. https://doi.org/10.1094/PDIS-02-12-0141-RE

Bendig, J., Bolten, A., Bennertz, S., Broscheit, J., Eichfuss, S., & Bareth, G. (2014). Estimating biomass of barley using crop surface models (CSMs) derived from UAV-based RGB imaging. *Remote Sensing*. https://doi.org/10.3390/rs61110395

Bendig, J. (2015). Unmanned aerial vehicles (UAVs) for multi-temporal crop surface modelling. A new method for plant height and biomass estimation based on RGB-imaging. Doctoral dissertation, Universität zu Köln.

Bendig, J., Yu, K., Aasen, H., Bolten, A., Bennertz, S., Broscheit, J., Gnyp, M. L., & Bareth, G. (2015). Combining UAV-based plant height from crop surface models, visible, and near infrared vegetation indices for biomass monitoring in barley. *International Journal of Applied Earth Observation and Geoinformation*. https://doi.org/10.1016/j.jag.2015.02.012

Berk, A., Conforti, P., Kennett, R., Perkins, T., Hawes, F., & Van Den Bosch, J. (2014). MODTRAN® 6: A major upgrade of the MODTRAN® radiative transfer code. *Workshop on Hyperspectral Image and Signal Processing, Evolution in Remote Sensing*. https://doi.org/10.1109/WHISPERS.2014.8077573

Blum, A. (2011). Plant breeding for water-limited environments. In *Plant Breeding for Water-Limited Environments*. https://doi.org/10.1007/978-1-4419-7491-4

Bradshaw, J. E. (2017). Plant breeding: past, present and future. *Euphytica*, *213*(3). https://doi.org/10.1007/s10681-016-1815-y

Brancourt-Hulmel, M., Doussinault, G., Lecomte, C., Bérard, P., Le Buanec, B., & Trottet, M. (2003). Genetic improvement of agronomic traits of winter wheat cultivars released in France from 1946 to 1992. *Crop Science*, *43*(1), 37–45. https://doi.org/10.2135/cropsci2003.3700

Brocks, S., & Bareth, G. (2018). Estimating barley biomass with crop surface models from oblique RGB imagery. *Remote Sensing*. https://doi.org/10.3390/rs10020268

Budak, H., Kantar, M., & Yucebilgili Kurtoglu, K. (2013). Drought tolerance in modern and wild wheat. In *The Scientific World Journal* (Vol. 2013). https://doi.org/10.1155/2013/548246

Cabrera-Bosquet, L., Molero, G., Stellacci, A., Bort, J., Nogués, S., & Araus, J. (2011). NDVI as a potential tool for predicting biomass, plant nitrogen content and growth in wheat genotypes subjected to different water and nitrogen conditions. *Cereal Research Communications*. https://doi.org/10.1556/CRC.39.2011.1.15

Cattivelli, L., Rizza, F., Badeck, F. W., Mazzucotelli, E., Mastrangelo, A. M., Francia, E., Marè, C., Tondelli, A., & Stanca, A. M. (2008). Drought tolerance improvement in crop plants: An integrated view from breeding to genomics. In *Field Crops Research* (Vol. 105, Issues 1–2, pp. 1–14). https://doi.org/10.1016/j.fcr.2007.07.004

Chakraborty, A., Ghosh, S., Mukhopadhyay, P., Dinara, S. M., Bag, A., Mahata, M. K., Kumar, R., Das, S., Sanjay, J., Majumdar, S., & Biswas, D. (2014). Trapping effect analysis of AlGaN/InGaN/GaN Heterostructure by conductance frequency measurement. *MRS Proceedings*, *XXXIII*(2), 81–87. https://doi.org/10.1007/s13398-014-0173-7.2

Chapman, S. C., Merz, T., Chan, A., Jackway, P., Hrabar, S., Dreccer, M. F., Holland, E., Zheng, B., Ling, T. J., & Jimenez-Berni, J. (2014). Pheno-copter: A low-altitude, autonomous remote-sensing robotic helicopter for high-throughput field-based phenotyping. *Agronomy*. https://doi.org/10.3390/agronomy4020279

Chawade, A., Van Ham, J., Blomquist, H., Bagge, O., Alexandersson, E., & Ortiz, R. (2019). High-throughput field-phenotyping tools for plant breeding and precision agriculture. In *Agronomy*. https://doi.org/10.3390/agronomy9050258

Cobb, J. N., DeClerck, G., Greenberg, A., Clark, R., & McCouch, S. (2013). Next-generation phenotyping: Requirements and strategies for enhancing our understanding of genotype-phenotype relationships and its relevance to crop improvement. In *Theoretical and Applied Genetics*. https://doi.org/10.1007/s00122-013-2066-0

Crain, J. L., Wei, Y., Barker, J., Thompson, S. M., Alderman, P. D., Reynolds, M., Zhang, N., & Poland, J. (2016). Development and deployment of a portable field phenotyping platform. *Crop Science*. https://doi.org/10.2135/cropsci2015.05.0290

Cushman, J. C., & Bohnert, H. J. (2000). Genomic approaches to plant stress tolerance. In *Current Opinion in Plant Biology* (Vol. 3, Issue 2, pp. 117–124). https://doi.org/10.1016/S1369-5266(99)00052-7

Donmez, E., Sears, R. G., Shroyer, J. P., & Paulsen, G. M. (2001). Genetic gain in yield attributes of winter wheat in the Great Plains. *Crop Science*, *41*(5), 1412–1419. https://doi.org/10.2135/cropsci2001.4151412x

Du, M., & Noguchi, N. (2017). Monitoring of wheat growth status and mapping of

wheat yield's within-field spatial variations using color images acquired from UAV-camera System. *Remote Sensing*, *9*(3). https://doi.org/10.3390/rs9030289

Duan, B., Fang, S., Zhu, R., Wu, X., Wang, S., Gong, Y., & Peng, Y. (2019). Remote estimation of rice yield with unmanned aerial vehicle (uav) data and spectral mixture analysis. *Frontiers in Plant Science*. https://doi.org/10.3389/fpls.2019.00204

Evenson, R. E., & Gollin, D. (2003). Assessing the impact of the Green Revolution, 1960 to 2000. In *Science* (Vol. 300, Issue 5620, pp. 758–762). https://doi.org/10.1126/science.1078710

Fernie, A. R., & Gutierrez-Marcos, J. (2019). From genome to phenome: genome-wide association studies and other approaches that bridge the genotype to phenotpe gap. In *Plant Journal*. https://doi.org/10.1111/tpj.14219

Fleury, D., Jefferies, S., Kuchel, H., & Langridge, P. (2010). Genetic and genomic tools to improve drought tolerance in wheat. In *Journal of Experimental Botany* (Vol. 61, Issue 12, pp. 3211–3222). https://doi.org/10.1093/jxb/erq152

Foulkes, M. J., Snape, J. W., Shearman, V. J., Reynolds, M. P., Gaju, O., & Sylvester-Bradley, R. (2007). Genetic progress in yield potential in wheat: Recent advances and future prospects. *Journal of Agricultural Science*, *145*(1), 17–29. https://doi.org/10.1017/S0021859607006740

Fritsche-Neto, R., & Borém, A. (2012). Plant breeding for abiotic stress tolerance. In *Plant Breeding for Abiotic Stress Tolerance* (Vol. 9783642305). https://doi.org/10.1007/978-3-642-30553-5

Furbank, R. T., Jimenez-Berni, J. A., George-Jaeggli, B., Potgieter, A. B., & Deery, D. M. (2019). Field crop phenomics: enabling breeding for radiation use efficiency and biomass in cereal crops. In *New Phytologist*. https://doi.org/10.1111/nph.15817

Garcia-Ruiz, F., Sankaran, S., Maja, J. M., Lee, W. S., Rasmussen, J., & Ehsani, R. (2013). Comparison of two aerial imaging platforms for identification of Huanglongbing-infected citrus trees. *Computers and Electronics in Agriculture*. https://doi.org/10.1016/j.compag.2012.12.002

Gitelson, A. A., Kaufman, Y. J., & Merzlyak, M. N. (1996). Use of a green channel in remote sensing of global vegetation from EOS- MODIS. *Remote Sensing of Environment*. https://doi.org/10.1016/S0034-4257(96)00072-7

Goodwin, A. W., Lindsey, L. E., Harrison, S. K., & Paul, P. A. (2018). Estimating wheat yield with normalized difference vegetation index and fractional green canopy cover. *Crop, Forage and Turfgrass Management*. https://doi.org/10.2134/cftm2018.04.0026

Green, A. J., Berger, G., Griffey, C. A., Pitman, R., Thomason, W., Balota, M., & Ahmed, A. (2012). Genetic yield improvement in soft red winter wheat in the Eastern United States from 1919 to 2009. *Crop Science, 52*(5), 2097–2108. https://doi.org/10.2135/cropsci2012.01.0026

Guillen-Climent, M. L., Zarco-Tejada, P. J., Berni, J. A. J., North, P. R. J., & Villalobos, F. J. (2012). Mapping radiation interception in row-structured orchards using 3D simulation and high-resolution airborne imagery acquired from a UAV. *Precision Agriculture*. https://doi.org/10.1007/s11119-012-9263-8

Haghighattalab, A., González Pérez, L., Mondal, S., Singh, D., Schinstock, D., Rutkoski, J., Ortiz-Monasterio, I., Singh, R. P., Goodin, D., & Poland, J. (2016). Application of unmanned aerial systems for high throughput phenotyping of large wheat breeding nurseries. *Plant Methods*, *12*(1). https://doi.org/10.1186/s13007-016-0134-6

Harwin, S., & Lucieer, A. (2012). Assessing the accuracy of georeferenced point clouds produced via multi-view stereopsis from Unmanned Aerial Vehicle (UAV) imagery. *Remote Sensing*. https://doi.org/10.3390/rs4061573

Hassan, M. A., Yang, M., Rasheed, A., Yang, G., Reynolds, M., Xia, X., Xiao, Y., & He, Z. (2019). A rapid monitoring of NDVI across the wheat growth cycle for grain yield prediction using a multi-spectral UAV platform. *Plant Science*. https://doi.org/10.1016/j.plantsci.2018.10.022

Hawkesford, M. J., Araus, J. L., Park, R., Calderini, D., Miralles, D., Shen, T., Zhang, J., & Parry, M. A. J. (2013). Prospects of doubling global wheat yields. In *Food and Energy Security* (Vol. 2, Issue 1, pp. 34–48). https://doi.org/10.1002/fes3.15

Hiebert, C. W., Thomas, J. B., McCallum, B. D., Humphreys, D. G., DePauw, R. M., Hayden, M. J., Mago, R., Schnippenkoetter, W., & Spielmeyer, W. (2010). An introgression on wheat chromosome 4DL in RL6077 (Thatcher*6/PI 250413) confers adult plant resistance to stripe rust and leaf rust (Lr67). *Theoretical and Applied Genetics*, *121*(6), 1083–1091. https://doi.org/10.1007/s00122-010-1373-y

Hoffmeister, D., Waldhoff, G., Korres, W., Curdt, C., & Bareth, G. (2016). Crop height variability detection in a single field by multi-temporal terrestrial laser scanning.

Precision Agriculture. https://doi.org/10.1007/s11119-015-9420-y

Howell, T. A., Steiner, J. L., Schneider, A. D., & Evett, S. R. (1995). Evapotranspiration of irrigated winter wheat - Southern high plains. *Transactions of the American Society of Agricultural Engineers*, *38*(3), 745–759. https://doi.org/10.13031/2013.27888

Hurd, E. A. (1974). Phenotype and drought tolerance in wheat. *Agricultural Meteorology*, *14*(1–2), 39–55. https://doi.org/10.1016/0002-1571(74)90009-0

Inostroza, L., Acuña, H., Munoz, P., Vásquez, C., Ibáñez, J., Tapia, G., Pino, M. T., & Aguilera, H. (2016). Using aerial images and canopy spectral reflectance for high-throughput phenotyping of white clover. *Crop Science*. https://doi.org/10.2135/cropsci2016.03.0156

Jena, K. K., & Mackill, D. J. (2008). Molecular markers and their use in marker-assisted selection in rice. In *Crop Science* (Vol. 48, Issue 4, pp. 1266–1276). https://doi.org/10.2135/cropsci2008.02.0082

Jensen, J. L. R., & Mathews, A. J. (2016). Assessment of image-based point cloud products to generate a bare earth surface and estimate canopy heights in a woodland ecosystem. *Remote Sensing*. https://doi.org/10.3390/rs8010050

Kang, Y. J., Lee, T., Lee, J., Shim, S., Jeong, H., Satyawan, D., Kim, M. Y., & Lee, S. H. (2016). Translational genomics for plant breeding with the genome sequence explosion. In *Plant Biotechnology Journal* (Vol. 14, Issue 4, pp. 1057–1069). https://doi.org/10.1111/pbi.12449

Khan, Z., Chopin, J., Cai, J., Eichi, V. R., Haefele, S., & Miklavcic, S. J. (2018).

Quantitative estimation of wheat phenotyping traits using ground and aerial imagery. *Remote Sensing*. https://doi.org/10.3390/rs10060950

Kolmer, J. A., & Hughes, M. E. (2018). Physiologic specialization of Puccinia triticina on wheat in the United States in 2016. *Plant Disease*, *102*(6), 1066–1071. https://doi.org/10.1094/PDIS-11-17-1701-SR

Li, Z., Lan, C., He, Z., Singh, R. P., Rosewarne, G. M., Chen, X., & Xia, X. (2014). Overview and application of QTL for adult plant resistance to leaf rust and powdery mildew in wheat. In *Crop Science* (Vol. 54, Issue 5, pp. 1907–1925). https://doi.org/10.2135/cropsci2014.02.0162

Liebisch, F., Kirchgessner, N., Schneider, D., Walter, A., & Hund, A. (2015). Remote, aerial phenotyping of maize traits with a mobile multi-sensor approach. *Plant Methods*. https://doi.org/10.1186/s13007-015-0048-8

Lorenz, A. J., Chao, S., Asoro, F. G., Heffner, E. L., Hayashi, T., Iwata, H., Smith, K. P., Sorrells, M. E., & Jannink, J. L. (2011). Genomic Selection in Plant Breeding. Knowledge and Prospects. In *Advances in Agronomy* (Vol. 110, Issue C). https://doi.org/10.1016/B978-0-12-385531-2.00002-5

Louhaichi, M., Borman, M. M., & Johnson, D. E. (2001). Spatially located platform and aerial photography for documentation of grazing impacts on wheat. *Geocarto International*, *16*(1), 65–70. https://doi.org/10.1080/10106040108542184

Miah, G., Rafii, M. Y., Ismail, M. R., Puteh, A. B., Rahim, H. A., Asfaliza, R., & Latif, M. A. (2013). Blast resistance in rice: A review of conventional breeding to molecular approaches. *Molecular Biology Reports*, *40*(3), 2369–2388.

https://doi.org/10.1007/s11033-012-2318-0

Mohammadi, R. (2018). Breeding for increased drought tolerance in wheat: A review. In *Crop and Pasture Science* (Vol. 69, Issue 3, pp. 223–241). https://doi.org/10.1071/CP17387

Morran, S., Eini, O., Pyvovarenko, T., Parent, B., Singh, R., Ismagul, A., Eliby, S., Shirley, N., Langridge, P., & Lopato, S. (2011). Improvement of stress tolerance of wheat and barley by modulation of expression of DREB/CBF factors. *Plant Biotechnology Journal*, *9*(2), 230–249. https://doi.org/10.1111/j.1467-7652.2010.00547.x

Mutka, A. M., & Bart, R. S. (2015). Image-based phenotyping of plant disease symptoms. In *Frontiers in Plant Science* (Vol. 5, Issue JAN). https://doi.org/10.3389/fpls.2014.00734

Mwadzingeni, L., Shimelis, H., Dube, E., Laing, M. D., & Tsilo, T. J. (2016). Breeding wheat for drought tolerance: Progress and technologies. In *Journal of Integrative Agriculture* (Vol. 15, Issue 5, pp. 935–943). https://doi.org/10.1016/S2095-3119(15)61102-9

Oelke, L. M., & Kolmer, J. A. (2004). Characterization of leaf rust resistance in hard red spring wheat cultivars. *Plant Disease*, *88*(10), 1127–1133. https://doi.org/10.1094/PDIS.2004.88.10.1127

Olanrewaju, S., Rajan, N., Ibrahim, A. M. H., Rudd, J. C., Liu, S., Sui, R., Jessup, K. E., & Xue, Q. (2019). Using aerial imagery and digital photography to monitor growth and yield in winter wheat. *International Journal of Remote Sensing*, *40*(18), 6905–

6929. https://doi.org/10.1080/01431161.2019.1597303

Paillard, S., Trotoux-Verplancke, G., Perretant, M. R., Mohamadi, F., Leconte, M., Coëdel, S., de Vallavieille-Pope, C., & Dedryver, F. (2012). Durable resistance to stripe rust is due to three specific resistance genes in French bread wheat cultivar Apache. *Theoretical and Applied Genetics*, *125*(5), 955–965. https://doi.org/10.1007/s00122-012-1885-8

Panguluri, S. K., & Kumar, A. A. (2013a). Phenotyping for plant breeding: Applications of phenotyping methods for crop improvement. In *Phenotyping for Plant Breeding: Applications of Phenotyping Methods for Crop Improvement*. https://doi.org/10.1007/978-1-4614-8320-5

Panguluri, S. K., & Kumar, A. A. (2013b). Phenotyping for plant breeding: Applications of phenotyping methods for crop improvement. In *Phenotyping for Plant Breeding: Applications of Phenotyping Methods for Crop Improvement*. https://doi.org/10.1007/978-1-4614-8320-5

Parmley, K., Nagasubramanian, K., Sarkar, S., Ganapathysubramanian, B., & Singh, A. K. (2019). Development of Optimized Phenomic Predictors for Efficient Plant Breeding Decisions Using Phenomic-Assisted Selection in Soybean. *Plant Phenomics*. https://doi.org/10.34133/2019/5809404

Paulsen, G. (2002). Application of Physiology in Wheat Breeding. *Crop Science*, *42*(6), 2228–2228. https://doi.org/10.2135/cropsci2002.2228

Pieruschka, R., & Schurr, U. (2019). Plant Phenotyping: Past, Present, and Future. *Plant Phenomics*. https://doi.org/10.34133/2019/7507131

Pingali, P. L. (2012). Green revolution: Impacts, limits, andthe path ahead. In *Proceedings of the National Academy of Sciences of the United States of America* (Vol. 109, Issue 31, pp. 12302–12308). https://doi.org/10.1073/pnas.0912953109

Popescu, S. C., Wynne, R. H., & Nelson, R. F. (2003). Estimating plot-level tree heights with lidar: Local filtering with a canopy-height based variable window size. *Computers and Electronics in Agriculture*. https://doi.org/10.1016/S0168-1699(02)00121-7

Potgieter, A. B., George-Jaeggli, B., Chapman, S. C., Laws, K., Cadavid, L. A. S., Wixted, J., Watson, J., Eldridge, M., Jordan, D. R., & Hammer, G. L. (2017). Multi-spectral imaging from an unmanned aerial vehicle enables the assessment of seasonal leaf area dynamics of sorghum breeding lines. *Frontiers in Plant Science*. https://doi.org/10.3389/fpls.2017.01532

Prasad, A. K., Singh, R. P., Tare, V., & Kafatos, M. (2007). Use of vegetation index and meteorological parameters for the prediction of crop yield in India. *International Journal of Remote Sensing*. https://doi.org/10.1080/01431160601105843

Pratap, A., Gupta, S., Nair, R. M., Gupta, S. K., Schafleitner, R., Basu, P. S., Singh, C. M., Prajapati, U., Gupta, A. K., Nayyar, H., Mishra, A. K., & Baek, K. H. (2019). Using plant phenomics to exploit the gains of genomics. In *Agronomy*. https://doi.org/10.3390/agronomy9030126

Pugh, N. A., Horne, D. W., Murray, S. C., Carvalho, G., Malambo, L., Jung, J., Chang, A., Maeda, M., Popescu, S., Chu, T., Starek, M. J., Brewer, M. J., Richardson, G., & Rooney, W. L. (2018). Temporal Estimates of Crop Growth in Sorghum and

Maize Breeding Enabled by Unmanned Aerial Systems. *Tppj*, *1*(1), 0. https://doi.org/10.2135/tppj2017.08.0006

Rajaram, S. R., Pena, R. J. P., Villareal, R. L. V., Mujeeb-KAZI, A. M., Singh, R. S., & Gilchrist, L. G. (2001). Utilization of wild and cultivated emmer and of diploid wheat relatives in breeding. *Israel Journal of Plant Sciences*, *49*, 93–104. https://doi.org/10.1560/2W61-9294-FH8U-BYQY

Rehman, A. U., Sajjad, M., Khan, S. H., & Ahmad, N. (2013). Prospects of wheat breeding for durable resistance against brown, yellow and black rust fungi. In *International Journal of Agriculture and Biology* (Vol. 15, Issue 6, pp. 1209–1220).

Rutkoski, J., Poland, J., Mondal, S., Autrique, E., Pérez, L. G., Crossa, J., Reynolds, M., & Singh, R. (2016). Canopy temperature and vegetation indices from high-throughput phenotyping improve accuracy of pedigree and genomic selection for grain yield in wheat. *G3: Genes, Genomes, Genetics*. https://doi.org/10.1534/g3.116.032888

Sankaran, S., Zhou, J., Khot, L. R., Trapp, J. J., Mndolwa, E., & Miklas, P. N. (2018). High-throughput field phenotyping in dry bean using small unmanned aerial vehicle based multispectral imagery. *Computers and Electronics in Agriculture*. https://doi.org/10.1016/j.compag.2018.05.034

Sayre, K. D., Rajaram, S., & Fischer, R. A. (1997). Yield potential progress in short bread wheats in northwest Mexico. *Crop Science*, *37*(1), 36–42. https://doi.org/10.2135/cropsci1997.0011183X003700010006x

Shafian, S., Rajan, N., Schnell, R., Bagavathiannan, M., Valasek, J., Shi, Y., &

Olsenholler, J. (2018). Unmanned aerial systems-based remote sensing for monitoring sorghum growth and development. *PLoS ONE*, *13*(5). https://doi.org/10.1371/journal.pone.0196605

Shearman, V. J., Sylvester-Bradley, R., Scott, R. K., & Foulkes, M. J. (2005). Physiological processes associated with wheat yield progress in the UK. *Crop Science*, *45*(1), 175–185. https://doi.org/10.2135/cropsci2005.0175

Shi, Y., Murray, S. C., Rooney, W. L., Valasek, J., Olsenholler, J., Pugh, N. A., Henrickson, J., Bowden, E., Zhang, D., & Thomasson, J. A. (2016). Corn and sorghum phenotyping using a fixed-wing UAV-based remote sensing system. *Autonomous Air and Ground Sensing Systems for Agricultural Optimization and Phenotyping*. https://doi.org/10.1117/12.2228737

Slafer, G. A., Satorre, E. H., & Andrade, F. H. (1994). Slicer PDF. *Genetic Improvement of Field Crops*, *30*(9), 1–68. https://doi.org/10.1016/j.mri.2012.05.001.3D

Stroppiana, D., Migliazzi, M., Chiarabini, V., Crema, A., Musanti, M., Franchino, C., & Villa, P. (2015). Rice yield estimation using multispectral data from UAV: A preliminary experiment in northern Italy. *International Geoscience and Remote Sensing Symposium (IGARSS)*. https://doi.org/10.1109/IGARSS.2015.7326869

Su, J., Liu, C., Coombes, M., Hu, X., Wang, C., Xu, X., Li, Q., Guo, L., & Chen, W. H. (2018). Wheat yellow rust monitoring by learning from multispectral UAV aerial imagery. *Computers and Electronics in Agriculture*. https://doi.org/10.1016/j.compag.2018.10.017

Sun, J., Poland, J. A., Mondal, S., Crossa, J., Juliana, P., Singh, R. P., Rutkoski, J. E.,

Jannink, J. L., Crespo-Herrera, L., Velu, G., Huerta-Espino, J., & Sorrells, M. E. (2019). High-throughput phenotyping platforms enhance genomic selection for wheat grain yield across populations and cycles in early stage. *Theoretical and Applied Genetics*, *132*(6), 1705–1720. https://doi.org/10.1007/s00122-019-03309-0

Sun, J., Rutkoski, J. E., Poland, J. A., Crossa, J., Jannink, J. L., & Sorrells, M. E. (2017). Multitrait, random regression, or simple repeatability model in high-throughput phenotyping data improve genomic prediction for wheat grain yield. *Plant Genome*. https://doi.org/10.3835/plantgenome2016.11.0111

Tattaris, M., Reynolds, M. P., & Chapman, S. C. (2016). A direct comparison of remote sensing approaches for high-throughput phenotyping in plant breeding. *Frontiers in Plant Science*. https://doi.org/10.3389/fpls.2016.01131

Tester, M., & Langridge, P. (2010). Breeding technologies to increase crop production in a changing world. In *Science* (Vol. 327, Issue 5967, pp. 818–822). https://doi.org/10.1126/science.1183700

Thompson, A. L., Thorp, K. R., Conley, M., Andrade-Sanchez, P., Heun, J. T., Dyer, J. M., & White, J. W. (2018). Deploying a proximal sensing cart to identify drought-adaptive traits in upland cotton for high-throughput phenotyping. *Frontiers in Plant Science*. https://doi.org/10.3389/fpls.2018.00507

Timmusk, S., Abd El-Daim, I. A., Copolovici, L., Tanilas, T., Kännaste, A., Behers, L., Nevo, E., Seisenbaeva, G., Stenström, E., & Niinemets, Ü. (2014). Drought-tolerance of wheat improved by rhizosphere bacteria from harsh environments: Enhanced biomass production and reduced emissions of stress volatiles. *PLoS*

ONE, *9*(5). https://doi.org/10.1371/journal.pone.0096086

Tolmay, V. L., Sydenham, S. L., Boshoff, W. H. P., Wentzel, B. S., Miles, C. W., & Booyse, M. (2016). Registration of five spring wheat lines resistant to russian wheat aphid, stem rust (Ug99), leaf rust, and stripe rust. *Journal of Plant Registrations*, *10*(1), 80–86. https://doi.org/10.3198/jpr2015.03.0013crg

Ullah, N., Bux, H., Mumtaz, A. S., Qureshi, S. T., Sial, M. A., & Budak, H. (2015). Phenotypic and genotypic variability for durable resistance to yellow rust (Puccinia striiformis f. sp. tritici) in Pakistan wheat cultivars. *Archives of Phytopathology and Plant Protection*, *48*(2), 181–187. https://doi.org/10.1080/03235408.2014.882534

Wang, F., Wang, F., Zhang, Y., Hu, J., Huang, J., & Xie, J. (2019). Rice yield estimation using parcel-level relative spectral variables from uav-based hyperspectral imagery. *Frontiers in Plant Science*. https://doi.org/10.3389/fpls.2019.00453

Wang, H., Qin, F., Ruan, L., Wang, R., Liu, Q., Ma, Z., Li, X., Cheng, P., & Wang, H. (2016). Identification and severity determination of wheat stripe rust and wheat leaf rust based on hyperspectral data acquired using a black-paper-based measuring method. *PLoS ONE*. https://doi.org/10.1371/journal.pone.0154648

White, J. W., Andrade-Sanchez, P., Gore, M. A., Bronson, K. F., Coffelt, T. A., Conley, M. M., Feldmann, K. A., French, A. N., Heun, J. T., Hunsaker, D. J., Jenks, M. A., Kimball, B. A., Roth, R. L., Strand, R. J., Thorp, K. R., Wall, G. W., & Wang, G. (2012). Field-based phenomics for plant genetics research. In *Field Crops Research*. https://doi.org/10.1016/j.fcr.2012.04.003

Wu, L., Xia, X., Rosewarne, G. M., Zhu, H., Li, S., Zhang, Z., & He, Z. (2015). Stripe

rust resistance gene Yr18 and its suppressor gene in Chinese wheat landraces. *Plant Breeding*, *134*(6), 634–640. https://doi.org/10.1111/pbr.12311

Yang, C., & Everitt, J. H. (2002). Relationships between yield monitor data and airborne multidate multispectral digital imagery for grain sorghum. *Precision Agriculture*. https://doi.org/10.1023/A:1021544906167

Yang, G., Liu, J., Zhao, C., Li, Z., Huang, Y., Yu, H., Xu, B., Yang, X., Zhu, D., Zhang, X., Zhang, R., Feng, H., Zhao, X., Li, Z., Li, H., & Yang, H. (2017). Unmanned aerial vehicle remote sensing for field-based crop phenotyping: Current status and perspectives. In *Frontiers in Plant Science*. https://doi.org/10.3389/fpls.2017.01111

Yang, Q., Shi, L., Han, J., Zha, Y., & Zhu, P. (2019). Deep convolutional neural networks for rice grain yield estimation at the ripening stage using UAV-based remotely sensed images. *Field Crops Research*. https://doi.org/10.1016/j.fcr.2019.02.022

Yang, Q., Ye, H., Huang, K., Zha, Y., & Shi, L. (2017). Estimation of leaf area index of sugarcane using crop surface model based on UAV image. *Nongye Gongcheng Xuebao/Transactions of the Chinese Society of Agricultural Engineering*. https://doi.org/10.11975/j.issn.1002-6819.2017.08.014

York, L. M. (2019). Functional phenomics: An emerging field integrating high-throughput phenotyping, physiology, and bioinformatics. *Journal of Experimental Botany*. https://doi.org/10.1093/jxb/ery379

Zhang, D., Zhou, X., Zhang, J., Lan, Y., Xu, C., & Liang, D. (2018). Detection of rice sheath blight using an unmanned aerial system with high-resolution color and

multispectral imaging. *PLoS ONE*, *13*(5). https://doi.org/10.1371/journal.pone.0187470

Zhang, J., Virk, S., Porter, W., Kenworthy, K., Sullivan, D., & Schwartz, B. (2019). Applications of unmanned aerial vehicle based imagery in turfgrass field trials. *Frontiers in Plant Science*. https://doi.org/10.3389/fpls.2019.00279

Zhou, X., Zheng, H. B., Xu, X. Q., He, J. Y., Ge, X. K., Yao, X., Cheng, T., Zhu, Y., Cao, W. X., & Tian, Y. C. (2017). Predicting grain yield in rice using multi-temporal vegetation indices from UAV-based multispectral and digital imagery. *ISPRS Journal of Photogrammetry and Remote Sensing*. https://doi.org/10.1016/j.isprsjprs.2017.05.003

CHAPTER II

ASSESSING WINTER WHEAT FOLIAGE DISEASE SEVERITY USING AERIAL IMAGERY ACQUIRED FROM UNMANNED AERIAL SYSTEM (UAS)

INTRODUCTION

Wheat (*Triticum aestivum* L.) is one of the most important cereal crops and is widely grown around the world. However, in most of the wheat producing regions, it is threatened by one or several fungal, bacterial, or viral diseases that can cause partial or complete canopy damage (Prescott, Burnett and Saari, 1986). In most of the U.S. wheat producing areas, leaf rust, caused by the fungus *Puccinia triticina f. sp. tritici*, is one of the most important diseases (Line and Chen, 1995; Kolmer and Hughes, 2018). When the plant is infected by leaf rust, small brown pustules develop on the leaf surface. These pustules are the fruiting bodies (uredinia) and produce urediospores. A single uredinium can produce numerous spores on the leaf surface within a short time under favorable conditions(Stubbs *et al.*, 1986). Once the leaf is infected, chlorophyll content and photosynthesis are reduced (Carretero, Bancal and Miralles, 2011) which can cause severe yield losses in highly susceptible cultivars. Severe epidemics of leaf rust occurred in 2007 in the U.S. Great Plains and caused almost 14% yield losses in some places (Wegulo and Byamukama, 2012). If the disease appears early in the season it can reduce yield by more than 20% (Roelfs *et al.*, 1992). The reduction in grain yield is primarily attributed to reduced floral set (Roelfs *et al.*, 1992) and kernel weight (Singh and Huerta-Espino, 1997). Growing resistant varieties and the effective use of pesticides have

decreased the severity and incidence of leaf rust in the US. However, varietal resistance is the most economical method in controlling the disease (Oelke and Kolmer, 2004; Ponce-Molina *et al.*, 2018).

Growing resistant varieties in the southern region of the U.S. is important as the uredospores survive the winter in this region and become the source of inoculum for leaf rust infection in the wheat growing in the Central and Northern Great Plains during spring (Wegulo and Byamukama, 2012). Additionally, continuous development of resistant varieties to leaf rust is critical as new virulent leaf rust races develop every year and overcome varietal resistance (Oelke and Kolmer, 2004; Ponce-Molina *et al.*, 2018). Precise and efficient disease phenotyping can play an important role in the development of wheat variety resistant to leaf rust (Zhang *et al.*, 2018). Traditionally, disease phenotyping is done by trained personnel through visual assessment of infection type and severity (Ali and Hodson, 2017). The accuracy of visual data is affected by the raters and their ability to properly diagnose the disease, which can reduce the repeatability and reliability of disease estimates (Mutka and Bart, 2015). Moreover, a significant amount of time, labor, and money is required to collect data from large breeding nurseries (Haghighattalab *et al.*, 2016; Wang *et al.*, 2016). The development and use of phenotyping tool that can provide precise disease estimates can assist breeders to evaluate genotypes for disease severity and make selection decisions. Low cost Unmanned Aerial System (UAS) can be used as a rapid, affordable, and efficient field-based crop phenotyping tool in breeding programs (Haghighattalab *et al.*, 2016; Potgieter *et al.*, 2017). The use of UAS to assess disease severity in different crops such

as yellow rust (*Puccinia striiformis f. sp. tritici*) in wheat (Su *et al.*, 2018), rice sheath blight (*Rhizoctonia solani*) in rice (*Oryza sativa* L.) (Qin and Zhang, 2005; Zhang *et al.*, 2018), anthracnose (*Colletotrichum sublineola*) in sorghum (*Sorghum bicolor* L.) (Pugh *et al.*, 2018) has been studied. UAS can provide rapid and non-destructive HTP measurements for detecting and monitoring plant diseases and have several advantages of being low cost, flexible, convenient, and high-spatial resolution data collection tools (Dash *et al.*, 2017).

UAS platforms equipped with red, green, blue (RGB), multispectral, hyperspectral, and thermal sensors can provide real time data for several phenotypic traits of plants (Yang *et al.*, 2017). All these sensors have their own advantages and disadvantages in terms of resolution, precision, weight, size, and cost. Compared to hyperspectral and multispectral sensors, the RGB camera has lower spectral resolution but it has the advantages of low cost, high spatial resolution, light weight, small size, easy operational procedure, and convenience in image processing (Yang *et al.*, 2017). The data obtained from RGB camera can further be processed to develop reflectance data and obtain vegetation indices (Du and Noguchi, 2017). These indices can be used as an indirect approach for disease phenotyping in wheat breeding programs.

The amount of light reflected in the visible region is significantly different between leaf rust infected and healthy leaves (Wang *et al.*, 2016). When the chlorophyll content is reduced in the diseased leaf, the reflectance is higher in the red region and lower in the green region of the spectrum (Wang *et al.*, 2016). This variation offers a potential to use RGB camera for assessing leaf rust severity in wheat. Some of the

commonly used spectral vegetation indices derived from RGB sensors are Green leaf Index (GLI), Green Index (GI) and Normalized Difference Index (NDI). GLI values range from -1 to +1. Feature with negative GLI values represent non-living objects while the positive values represent green vegetation. This index was originally formulated to measure Canopy Cover (CC) in wheat (Louhaichi *et al.*, 2001). GI, which is the ratio of reflectance in the red and green region is negatively associated with leaf rust severity in wheat (Ashourloo *et al.*, 2014). NDI was developed to separate plants from soil and residue background in the images (Pérez *et al.*, 2000). There are several other indices that use reflectance data obtained beyond the visible region of the spectrum. Su *et al.* (2018) examined different vegetation indices and found Ratio Vegetation Index (RVI), Normalized Difference Vegetation Index (NDVI), Optimized Soil Adjusted Vegetation Index (OSAVI) as top three indices and red and NIR bands to be the top two spectral bands to classify healthy and yellow rust infected wheat plants. Although this low-cost technology offers great potential in field phenotyping for disease severity, there are few studies in the literature primarily focused on improving its technical capabilities and use for assessing leaf rust severity in wheat. In this study, a multirotor UAS equipped with a digital camera (Red, Green, and Blue bands) was flown over the Multi-state Wheat Rust Evaluation Nursery (MSREN) at Castroville, TX to capture high-spatial resolution images of wheat genotypes infected with leaf rust. The specific objectives of this study were to: 1) outline the procedure of UAS image acquisition, processing and data extraction, 2) determine the relationship between UAS-based vegetation indices and

field measurements of disease severity, and 3) discuss the opportunities and limitations of using UAS to assess disease severity in wheat.

MATERIALS AND METHODS

Study area

A field experiment was conducted at the MSREN located at Castroville, Texas (35º11'N, 102º06'W, and elevation 1170 m) in 2017 and 2018 wheat growing seasons. Major screening of Texas A&M's (TAM) wheat breeding lines for leaf rust resistance takes place in this nursery. The nursery is in the southern region of Texas and has favorable weather conditions for leaf rust inoculum to survive the winter. The overwintering fungi in this region develops spores in the spring (usually third week of March) when the weather is moist and temperature is below 20°C. Wheat grown in Castroville is mainly infected by leaf rust and the urediospores appear in the flag leaf during the third week of April. Thirty-four and 45 winter wheat genotypes representing Uniform Varietal Trial (UVT) of TAM wheat breeding program were grown in 2017 and 2018, respectively. Genotypes were replicated three times in a randomized complete block design. Plots were 3.4 m × 1.52 m in size consisting of seven rows with 0.18 m spacing. Seeds were sown on November 13, 2016 and November 15, 2017. Irrigation was maintained at optimum level throughout the growing season and other agronomic practices such as nutrient management and weed control were carried out as needed (Kimura et al., 2018).

Image acquisition, geo-referencing, and radiometric calibration

DJI phantom 4 pro (SZ DJI Technology Co., Ltd, Shenzhen, China) was flown in this study. Phantom 4 pro is a low cost, light weight multi-rotor UAS equipped with 20 megapixels one-inch CMOS (Complementary metal-oxide-semiconductor) RGB sensor. This platform also has an additional advantage of flying at low altitude, which is helpful for obtaining ultra-high resolution orthomosaic images. In this study, UAS was flown at 25 m altitude to obtain sub-centimeter (~0.7 cm/pixel) ground resolution. Pix4Dcapture (Pix4D S. A, Switzerland), a UAS mission planning software was used to plan UAS flights. The flight plan was set to 85% forward and backward overlap and the camera was set to face vertically downwards at nadir. UAS data were collected on April 14 and April 15 in 2017 and 2018 respectively when the leaf rust infection was visible in the flag leaf. Images were captured during the solar noon and field data were taken after the UAS flights on the same date.

Portable ground control points (GCPs) were placed across the field before flying the UAS. The GCPs were 0.6 m × 0.6 m square plywood board, painted black and white to make them easily identifiable during image processing. V-Map Post Processing Kinematic (PPK) system (Micro Aerial Projects LLC., Gainsville, FL) was used to survey precise coordinates of GCPs. GCPs were placed in the field before the flight and were collected once the flights were conducted and coordinate date was taken.

Radiometric calibration is the conversion of image digital numbers (DN) to surface reflectance values to compare data obtained across different dates and different crop growing seasons (Mafanya *et al.*, 2018). Airborne sensor ground calibration panels

(Group 8 technology, Inc., Utah, USA) were used to convert digital number (DN) values into reflectance measurements. Four level gray panels of 3%, 12%, 33%, and 56% reflectance were placed in the field during UAS data collection. These panels were 0.6 m × 0.6 m square in size and made from type 822 fabric providing uniform reflective surface. The spectral reflectance of the panels was measured using ASD Spectroradiometer (Malvern Panalytical, Malvern, UK). Mean DN value of the reflectance panel was extracted from the orthomosaic for all the RGB bands separately. An equation was developed for all the red, green and blue bands after regressing the DN values with the surface reflectance values of the reflectance panels. In this study, the relationship between reflectance data and DN values of calibration target was exponential for all the three bands. Therefore, a simplified empirical line method of radiometric calibration proposed by Wang and Myint (2015) was followed. According to this method, a natural log transformation was carried out on reflectance values and again regressed to obtain a linear relationship between image DN values and reflectance as follows.

$$-\ln(y) = m \times (DN) + C$$

Where y is reflectance, m is slope for each individual band, DN as the digital number of that respective band, and C is the calibration parameter.

Image processing and data extraction

After each flight, images were processed using Agisoft metashape software (Agisoft LLC, St. Petersburg, Russia, 191144) to generate 3D point cloud, Digital Surface Model (DSM), and orthomosaic images. Once the orthomosaic was developed,

vegetation index maps were created on QGIS software (www.qgis.org) using raster calculator tool. Plot boundary shape file was created using plot boundary tool available in the UAS hub (https://uashub.tamucc.edu) for plot level data extraction. Each plot has a boundary of 3 m × 1.2 m leaving boarders on each side of the plot. Plot boundary shape file was overlaid on the vegetation index map and plot level data was extracted using zonal statistics tool in QGIS software.

Spectral vegetation indices

Spectral vegetation indices are the combination of two or more bands to obtain information about the vegetation. Compared to hyperspectral and multispectral imagery, the vegetation indices obtained from RGB imagery are limited because of the limited number of bands and wider spectral band width. However, it has the advantages of using low cost UAS platform, easy operational procedure, and convenience in image processing. It also serves as a useful tool to visually screen the spread and intensity of disease. Vegetation indices have been used to determine disease severity in different crops (Zang *et al.,* 2018; Ashourloo *et al.,* 2014; Su *et al.,* 2018; Pugh *et al.,* 2018). In this study, we adopted four different vegetation indices that could be used to assess leaf rust severity based on previous literature findings (Table **2**). These indices estimate chlorophyll content and greenness of the canopy and can provide indirect assessment of the damage caused by the disease.

Table 2. Spectral vegetation indices used in this study

Reflectance obtained in the red band is denoted by R, green band by G, blue band by B, and near infrared by NIR. GLI, GI, and NDI were obtained from Unmanned Aerial System (UAS) and NDVI measurements were taken using handheld green seeker.

Vegetation indices	Formula	References
Green Leaf Index (GLI)	$\frac{2G - R - B}{2G + R + B}$	Louhaichi *et al.,* 2001
Green Index (GI)	$\frac{R}{G}$	Zarco-Tejada et al., 2005
Normalized Difference Index (NDI)	$\frac{G - R}{G + R}$	Perez *et al.,* 2000
Normalized Difference Vegetation Index (NDVI)	$\frac{NIR - R}{NIR + R}$	Rouse *et al.,* 1974

Ground measurements

A handheld GreenSeeker (Trimble Navigation Limited, California, US) was used to collect NDVI data from each plot. This device has an active sensor and measures the amount of light reflected in the red and NIR regions to calculate NDVI (Rouse et al., 1973). Seven NDVI measurements were made in each plot on the same date when UAS data were collected, and they were averaged to obtain the plot-wise average NDVI value. For ground truthing, visual notes on field response, a.k.a, infection type and disease severity, were taken for leaf rust infection following the rust scoring guide from International Maize and Wheat Improvement Center (CIMMYT) (Rust-scoring guide, CIMMYT, 1986). Infection type measures the nature of disease reaction and is expressed as Resistant (R), Moderately Resistant (MR), Moderately Susceptible (MS), and Susceptible (S). Severity is the percentage of rust infection on the plants and is largely determined by the number of pustules present in the leaf surface. Visual rating of disease severity was recorded on a scale of 0-100% after inspecting the damage on the

flag leaves. Numerical values were given to infection type, as R = 0.2, MR = 0.4, MS = 0.8 and S = 1.0. Infection type and severity were multiplied to calculate Coefficient of Infection (CI) (Pathan and Park, 2006; Draz *et al.*, 2015).

Statistical analysis

Data analysis was conducted using SAS version 9.4 (Statistical Analysis System Institute, Cary, NC, USA). Analysis of variance (ANOVA) was performed using General Linear Model (GLM) in SAS to compute variance components to evaluate genotypic variation. Repeatability (R), which is the ratio of genotypic variance to the phenotypic variance was calculated for each individual trait measured in 2017 and 2018. Repeatability measures the precision and accuracy of a given trait and is used to determine if the trait measured in a breeding trial can be repeatable. In this study, we computed repeatability for 2017 and 2018 separately using the following equation.

$$R = \frac{\sigma_g^2}{\sigma_p^2} = \frac{\sigma_g^2}{\sigma_g^2 + \sigma_e^2}$$

Where R is the repeatability, σ_g^2 is the genotypic variance, σ_p^2 is the phenotypic variance, and σ_e^2 is error variance.

To evaluate the precision, accuracy and reliability of the phenotypic information derived from UAS data and the associated traits, the vegetation indices were correlated with CI. Coefficient of determination (R^2) was obtained to study the relationship between CI and individual vegetation indices. R^2 is used to assess the variability in dependent variable caused by the independent variable. Multiple regression analysis with stepwise variable selection procedure was used to obtain a predictive model for CI using

aerial imagery indices. The decision for model selection was based on high adjusted R^2, low Akaike Information Criteria (AIC), and low Root Mean Square Error (RMSE). AIC provides a means for model selection from a set of available models. Models with low AIC values are considered to have a better quality relative to those with high AIC values. RMSE measures the error obtained between the observed and predicted values. It is calculated using the following formula:

$$RMSE = \sqrt{\sum_{i}^{n} \frac{(\widehat{Y}i - Yi)^2}{n}}$$

Where $\widehat{Y}i$ are predicted values, Yi are observed values, and n is the number of observations

RESULTS

Radiometric calibration

The regression relationships between the DN values obtained from the images of ground calibration panels and reflectance measurements in the R, G, and B band are shown in Figure **2**. A linear relationship with R^2 values greater than 0.97 ($p<0.01$) was obtained for all the three wavebands in 2017 and 2018. Orthomosaic image DN values for both years were converted into reflectance values using the obtained linear regression equation. Converted reflectance values were used to further calculate vegetation indices.

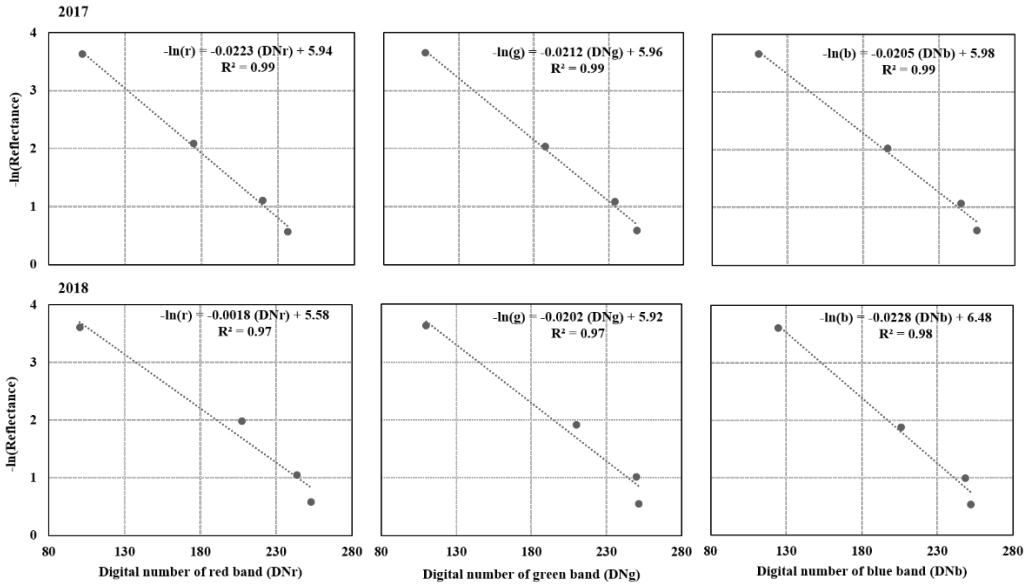

Figure 2. Relationship between digital number (DN) values obtained from ground calibration panels and reflectance measurements in the red, green, and blue wavebands for 2017 and 2018

The reflectance measurements for red, green, and blue wavebands are r, g, and b, respectively. DN_r, DN_g, and DN_b are the DN values for red, green, and blue wavebands, respectively. All R^2 values are significant at $p<0.05$. R^2: coefficient of determination.

Assessing leaf rust severity based on vegetation index map

Figure **3** shows the RGB orthomosaic and vegetation indices map obtained from April 14, 2017 UAS flight. The three vegetation indices maps were developed using NDI (2B), GLI (2C), and GI (2D) indices. The differences between healthy and severely infested wheat canopies are depicted by the color scale of the vegetation indices. All the index's maps show significant variations in disease severity in the field. Red and green color intensity in the map represent the severity level of leaf rust infestation. Plots with dark red color had highly severe leaf rust infestation while the plots with dark green color had either less leaf rust infestation or no infection.

The RGB orthomosaic in combination with the vegetation index maps can be useful for breeders to locate plots that are severely damaged by the disease. The differences in the color of canopy after being infected by leaf rust provided the opportunity to visually inspect the field for disease spread and identification of genotypes that are resistant to leaf rust. However, caution should be taken as the exposed soil in the plot can cause the plot to look dark red in color. Suitable date of disease severity assessment and UAS data acquisition play an important role to visually scan the field based on the orthomosaic images.

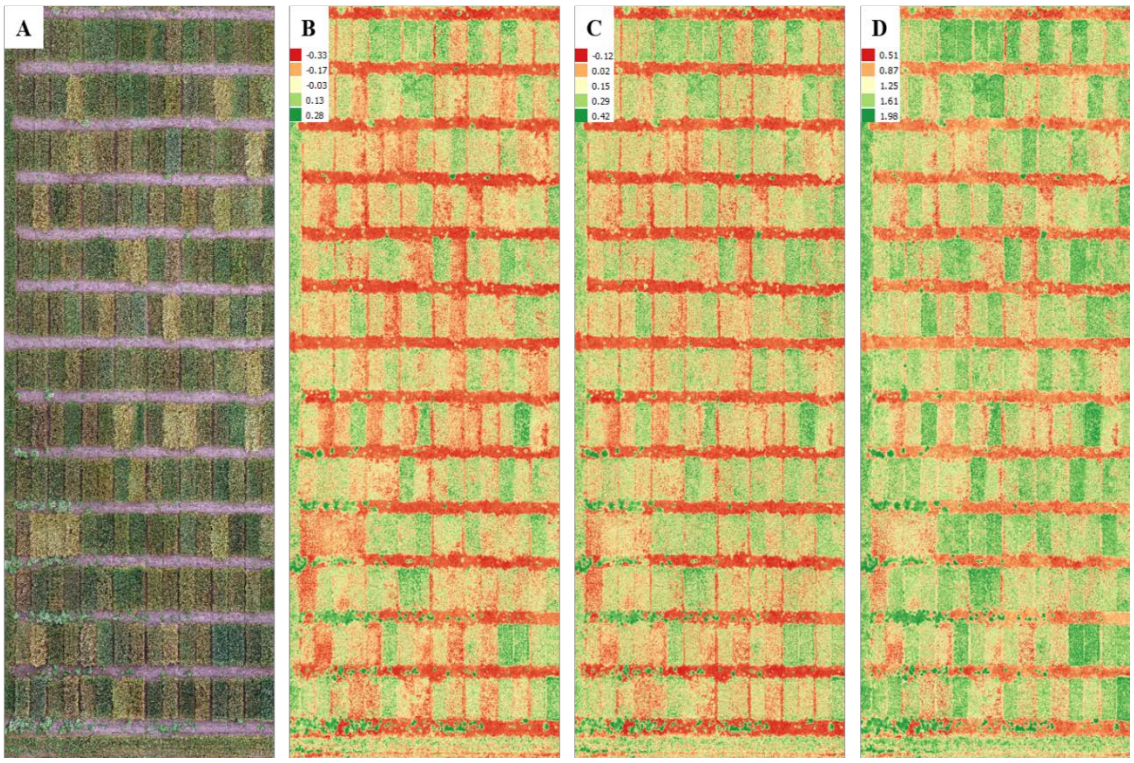

Figure 3. Visualization of plots on Unmanned Aerial System (UAS) imagery and different vegetation maps
Original RGB image (A) captured on April 14, 2017 at Castroville, Texas, B. Normalized Difference Index (NDI), C. Green Leaf Index (GLI), and D. Green Index (GI) maps

Relationship between vegetation indices and coefficient of infection (CI)

The relationship between vegetation indices obtained from UAS imagery and CI is presented in Figure **4**. To evaluate the consistency of UAS tool for disease assessment across years, data obtained from 2017 and 2018 were analyzed separately. All the vegetation indices had significant relations with CI ($p<0.01$). The R^2 estimate was higher (0.72 to 0.78; $p<0.01$) for NDI, GI, and GLI in 2017 compared to 2018 (0.63 to 0.68; $p<0.01$). NDI and GLI were negatively correlated with CI whereas GI was positively correlated with CI in both years. Figure **5** shows the relationship between ground based NDVI and CI in 2017 and 2018. A significant negative relation (R^2 =0.86 in 2017 and R^2 =0.83 in 2018; $p<0.01$) was found between NDVI and CI. NDVI had highest R^2 value compared to those obtained from RGB UAS imagery in both years.

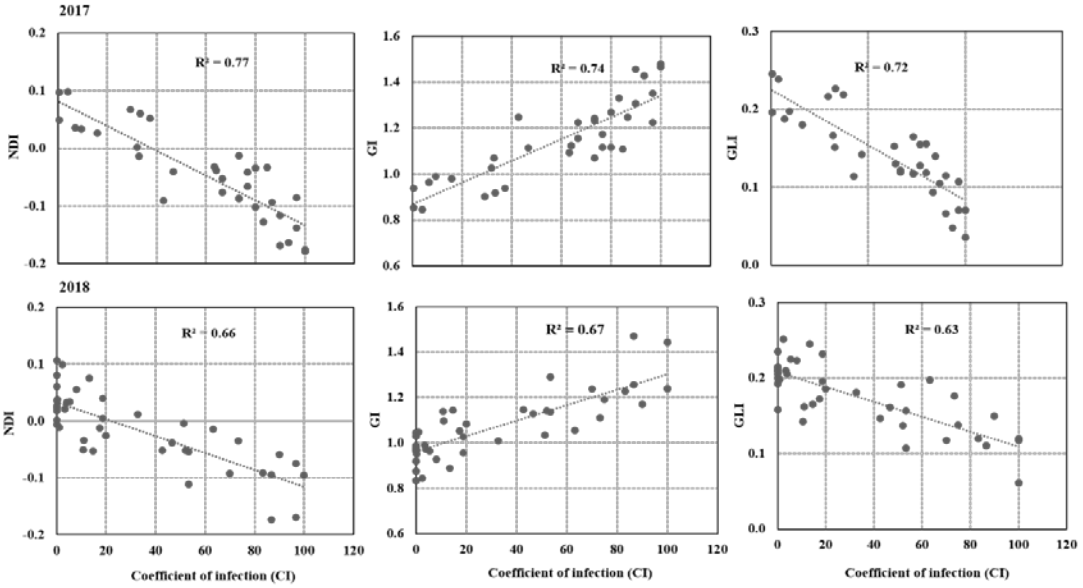

Figure 4. Relationship between Unmanned Aerial System (UAS)-based vegetation indices and Coefficient of Infection (CI) for 2017 and 2018

Each data point represents a winter wheat genotype which is the average of three replicates. Normalized Difference Index (NDI), Green Index (GI), and Green Leaf Index (GLI) are vegetation indices derived from UAS. CI was obtained by multiplying visual ratings of wheat leaf rust disease severity and infection type. R^2: coefficient of determination and all R^2 values are significant at $p<0.05$.

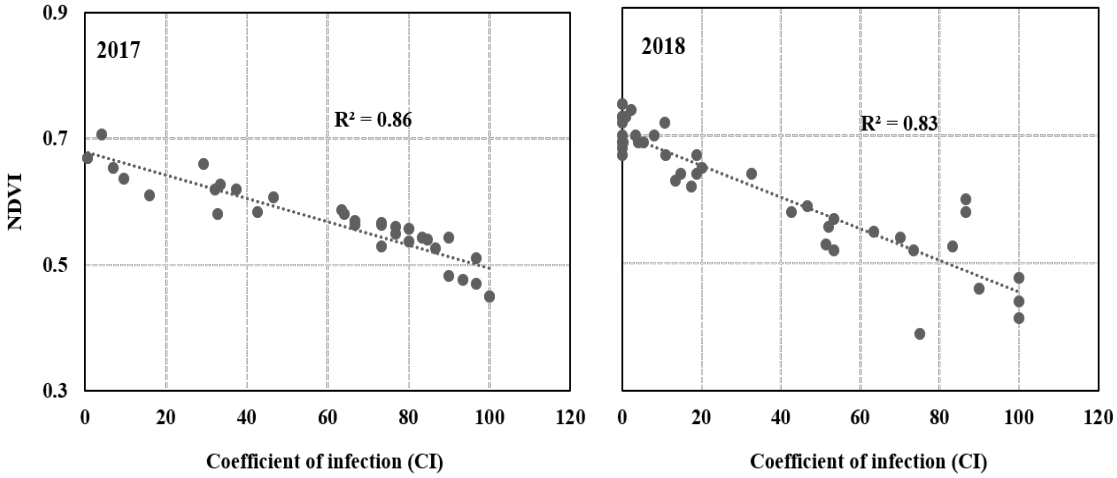

Figure 5. Relationship between green seeker-based Normalized Difference Vegetation Index (NDVI) and Coefficient of Infection (CI) for 2017 and 2018

Each data point represents a winter wheat genotype which is the average value of three replicates. CI was obtained by multiplying visual ratings of wheat leaf rust disease severity and infection type. R^2: coefficient of determination and all R^2 values are significant at $p<0.05$.

Genotypic variation and repeatability

Significant differences were found for all the vegetation indices obtained from UAS as well as the ground measurements of NDVI and CI (Table **3**) in 2017 and 2018. GI values ranged from 0.8 to 1.6, GLI ranged from 0.015 to 0.26, and NDI ranged from -0.20 to 0.13. NDVI values were from 0.4 to 0.73 and CI from 0 to 100. Every year, the time for screening genotypes for disease resistance in the winter wheat nursery at Castroville, TX is determined based on the climatic conditions and the rate at which leaf rust develops. The screening usually takes place in the third week of April. April 14 and April 15 were selected for 2017 and 2018, respectively. Optimum time for data acquisition plays a critical role in using UAS for disease phenotyping as it is important to reduce the errors caused by other physiological changes in the canopy. Consistent results obtained in 2017 and 2018 shows that the aerial imaging tool can be useful to

collect disease phenotyping data and can complement traditional screening of genotypes for leaf rust resistance.

Repeatability for each vegetation index derived from UAS imagery was calculated on an entry mean basis. Traits with higher repeatability estimates can be interpreted to have higher accuracy of measurements. Repeatability values for all the vegetation indices were above 0.8 in both the years (Table **4**). Values were higher in 2017 compared to 2018. NDI had higher repeatability values compared to GI and GLI in both the years. CI had higher repeatability values compared to vegetation indices.

Table 3. Statistical summary of the vegetation indices and Coefficient of Infection (CI) of winter wheat measured in 2017 and 2018

Green Index (GI), Green Leaf Index (GLI), Normalized Difference Index (NDI) were obtained from Unmanned Aerial System (UAS) and Normalized Difference Vegetation Index (NDVI) was obtained using green seeker, CI was obtained by multiplying visual ratings of wheat leaf rust disease severity and infection type.

Genotypes	GI	GLI	NDI	NDVI	CI
2017					
Min.	0.81	0.01	-0.21	0.39	0
Max.	1.58	0.25	0.11	0.72	100
Mean	1.15**	0.14**	-0.04*	0.57***	59***
2018					
Min.	0.79	0.01	-0.19	0.4	0
Max.	1.53	0.26	0.13	0.73	100
Mean	1.07***	0.17***	-0.01**	0.57***	33.98***

*, **, and *** indicate significance at $p<0.05$, 0.01, and 0.001 respectively.

Table 4. Repeatability estimates for vegetation indices and Coefficient of Infection (CI) in winter wheat measured in 2017 and 2018

GI, GLI, NDI were obtained from Unmanned Aerial System (UAS) and NDVI was obtained using green seeker, CI was obtained by multiplying visual ratings of wheat leaf rust disease severity and infection type.

Vegetation indices	Repeatability (R)	
	2017	2018
Green Index (GI)	0.86	0.84
Green Leaf Index (GLI)	0.82	0.80
Normalized Difference Index (NDI)	0.88	0.87
Normalized Difference Vegetation Index (NDVI)	0.90	0.88
Coefficient of Infection (CI)	0.91	0.89

Predictive models

The data from 2017 and 2018 was combined to perform multivariate regression analysis using NDI, GLI, GI, and NDVI as independent variables to predict CI. To test the predictability of the model, data collected from 2017 and 2018 were combined to get a total of 77 observation in which each data point is the average value of three replicates. It consists of four predictor variables (NDI, GLI, GI, and NDVI) and one response variable (CI). The response variable was categorized into four classes based on CI values and training and testing sets were developed by stratified random sampling. Training set comprised 70% of the observations randomly assigned from each class and testing set comprised 30% of the remaining observations in each class. In total, training set consists of 54 observations and testing set consists of 23 observations. Best predictive variables and models are presented in Table **5**. Among four vegetation indices, NDVI was found to be the best index explaining 83% variability in CI. On a separate multivariate analysis using the UAS-based indices, the multivariate model was insignificant for all the variable combinations. However, GLI explained highest variability (80%) alone in the

model. Among 11 different multivariate models, the combination of NDVI and GLI was the best multivariate model which explained 88% variability in CI. The performance of these two models was evaluated using the testing data set to estimate CI from NDVI and combining GLI with NDVI (Figure **6**). A strong linear relationship with R^2 values of 0.89 and 0.90 ($p<0.01$) was found between the observed and predicted CI in both cases.

Table 5. Best regression models developed between vegetation indices and Coefficient of Infection (CI) from the training dataset

Green Index (GI), Green Leaf Index (GLI), Normalized Difference Index (NDI) were obtained from Unmanned Aerial System (UAS) and Normalized Difference Vegetation Index (NDVI) was obtained using green seeker, CI was obtained by multiplying wheat leaf rust disease severity and infection type

No.	Predictors	R^2	adj. R^2	AIC	RMSE	Regression model
1	NDVI	0.83	0.83	449	14.9	COI=276.8-389.35(NDVI)
2	NDVI GLI	0.88	0.87	431	12.6	COI=257.5-293.2(NDVI)-227.9(GLI)
3	NDVI GI GLI	0.88	0.86	433	15.6	
4	NDVI NDI GI GLI	0.88	0.86	435	15.6	

R^2: coefficient of determination; adj. R^2: adjusted coefficient of determination; AIC: Akaike Information C riterion; RMSE: root-mean-square error. All R^2 values are significant at $p<0.05$.

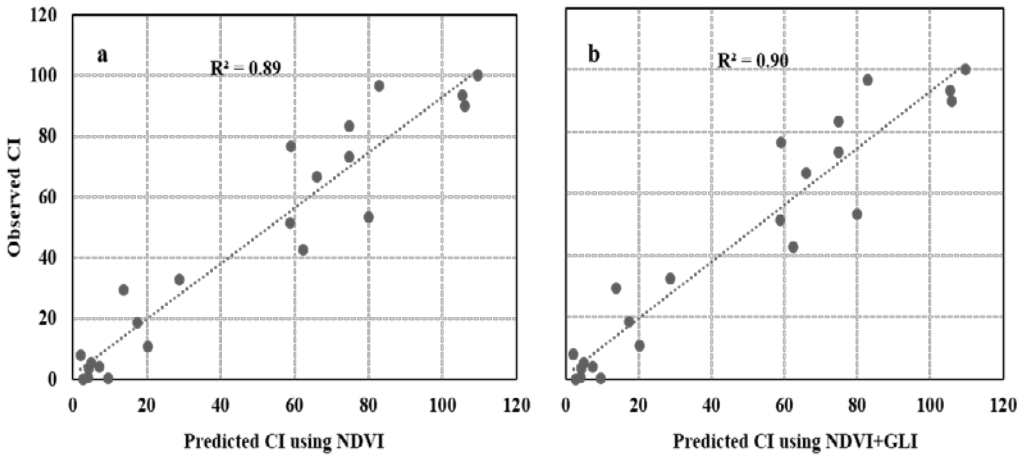

Figure 6. Relationship between actual Coefficient of Infection (CI) and predicted CI using vegetation indices

a. Normalized Difference Vegetation Index (NDVI) and b. NDVI and Green Leaf Index (GLI), R^2: coefficient of determination, NDVI was obtained using hand-held green seeker, GLI was obtained from Unmanned Aerial System (UAS), CI was obtained by multiplying visual ratings of wheat leaf rust disease severity and infection type.

DISCUSSION

The variation in environmental conditions such as solar radiation, angle of the sun, and cloud coverage across different measurement dates may result in inconsistent images obtained by digital cameras flown using UAS platforms. Therefore, calibration of remotely captured images to the physical units of reflectance is important to achieve consistent quantitative analysis (Smith and Milton, 1999). The need for developing vegetation indices to assess and quantify disease severity in this study required radiometric calibration as calibrated images improve accuracy of the vegetation indices (Nguyen *et al.*, 2015). In this study, we adopted the empirical line method to perform radiometric calibration using ground calibration panels. The relationship between image DN values of the calibration panels and known reflectance measurements was exponential for R, G, and B wavebands which was also observed in other studies (Smith and Milton, 1999; Wang and Myint, 2015). Therefore, a natural log transformation was carried out on reflectance values obtained from the calibration panels to obtain linear relationship between image DN values and reflectance. Shafian *et al.* (2018) found a linear relationship between image DN values and known reflectance values of the calibration tarps for a multispectral sensor. The exponential relationship obtained in this study might be the result of using more than two calibration targets (Smith and Milton, 1999). Multispectral sensors such as Micaense RedEdge (MicaSense, Inc., Seattle, USA) come with its own calibration panel to normalize the reflectance differences and calibrate the orthomosaic image. However, the use of calibration tarps or panels is common for accounting environmental errors when measurements are compared across

different dates (Haghighattalab *et al.*, 2016; Shafian *et al.*, 2018). Pseudo-invariant (PIF) method was used by Du and Noguchi (2017) to perform radiometric normalization of the multi-temporal orthomosaic images to monitor the wheat growth status. Iqbal, Lucieer and Barry (2018) proposed a pseudo target-based calibration method for accurate UAV image calibration. The linear relationship results between image DN values and reflectance measurement of the calibration for R, G, and B bands obtained in this study shows that the empirical line method can be used to calibrate orthomosaic images. This study shows the significance of radiometric calibration while comparing UAS imagery data obtained from multiple days and seasons.

The significant genotypic variation found for all the vegetation indices and CI showed the potential of UAS tool to differentiate genotypes for disease resistance. Numerous studies have shown the potential of UAS in breeding program to study physiological traits (Louhaichi *et al.*, 2001; White *et al.*, 2012; Potgieter *et al.*, 2017; Yu *et al.*, 2017; Zhang *et al.*, 2018). The change in color of the canopy because of disease infection was captured by the digital imagery and is reflected by the variation in vegetation indices. CI measured on the ground comprised of infection type and severity of leaf rust. This might be the reason for higher repeatability values of CI compared to vegetation indices. Close inspection of infection type and severity produce precise results. UAS was unable to capture infection type as it requires very high resolution to isolate the infected area based on symptoms of infection (Pugh *et al.*, 2018). However, obtaining data from large breeding nursery requires substantial amount of time and have higher chances of producing biased results. The assessment of disease severity is

possible with the use of UAS that was used in this study as we were able to generate orthomosaics with ~0.7cm resolution. Consistent, repeatable measurements obtained in both years show the potential of using this tool for improving accuracy in disease severity quantification. This study contained several released varieties and advanced lines comprising a wide range of genetic variability. This might be one of the reasons that UAS-based vegetation indices were able to dissect variation in terms of disease severity. Future studies are needed to confirm its suitability for evaluating early generation breeding lines.

A linear relationship between vegetation indices and CI was found in this study. At leaf level, Ashourloo et al. (2014) also found a strong relationship between several vegetation indices derived from hyperspectral sensor and disease severity obtained from digital camera. In particular, the GI used in this study had a significant association with wheat leaf rust severity. Su *et al.* (2018) ranked GI and GLI within top seven vegetation indices to discriminate healthy and yellow rust infected plants. The vegetation indices obtained in the visible region rely on several factors such as concentrations of chlorophyll and non-chlorophyll pigments in the leaves, level of chlorophyll degradation, color of the leaves, and spectral characteristics of pustules that appear on the leaves. A significant correlation was obtained between vegetation indices and leaf rust severity in our study. NDI, GLI, and NDVI were negatively associated with CI whereas GI was positively related to CI. NDI, GLI, and NDVI provides an indirect measurement of green vegetation. GI, which is the ratio of reflectance in the R and G bands, estimates the non-green portion of the vegetation. In other words, increased

disease severity reduces the green vegetative parts of the wheat canopy and increases the dead biomass. Although, NDVI measurements were made using handheld green seeker, it had highest R^2 value compared to other three UAS-based indices. It was also selected as the best predictor of CI. Zang et al. (2018) also found NDVI as best performing index for detecting different levels of rice sheath blight severity. NDVI is sensitive to the changes in the color of the plant canopy which is caused by leaf rust infestation (Haboudane *et al.*, 2004). GLI, which measures the green leaf area derived from the reflectance obtained in the G and R band, was one of the best predictors among UAS-based vegetation indices. This index can be used to rank genotypes based on disease severity using a simple UAS platform equipped with digital camera. Reflectance observed in the R waveband which is one of the major components of GLI can play a vital role in separating healthy and rust infested wheat plants (Su *et al.*, 2018).

Small UAS equipped with consumer grade digital camera with easy operational procedure are readily available at low cost. The availability of software applications to plan and design the flight mission have made it easier to use UAS in breeding programs. Under naturally inoculated field conditions, there are several factors that influence UAS measurements. The appearance and spread of diseases such as leaf rust in the field is largely determined by variety, disease epidemiology, and virulence (Roelfs *et al.*, 1992) which is attributed to higher R^2 and repeatability values obtained in 2017 compared to 2018. Plant physiological factors such as senescence, leaf optical

properties, presence of multiple diseases, CC, and growth stage can have significant influence on data if we are using this tool for assessing severity of a specific disease.

REFERENCES

AgiSoft. 2016. Metashape Professional. Version 1.2.6. AgiSoft, St. Petersburg, Russia. http://www.agisoft.com/downloads/installer/

Ali, S., & Hodson, D. (2017). Wheat rust surveillance: Field disease scoring and sample collection for phenotyping and molecular genotyping. In *Methods in Molecular Biology* (Vol. 1659, pp. 3–11). https://doi.org/10.1007/978-1-4939-7249-4_1

Ashourloo, D., Mobasheri, M. R., & Huete, A. (2014). Evaluating the effect of different wheat rust disease symptoms on vegetation indices using hyperspectral measurements. *Remote Sensing*, *6*(6), 5107–5123. https://doi.org/10.3390/rs6065107

Carretero, R., Bancal, M. O., & Miralles, D. J. (2011). Effect of leaf rust (*Puccinia triticina*) on photosynthesis and related processes of leaves in wheat crops grown at two contrasting sites and with different nitrogen levels. *European Journal of Agronomy*, *35*(4), 237–246. https://doi.org/10.1016/j.eja.2011.06.007

Dash, J. P., Watt, M. S., Pearse, G. D., Heaphy, M., & Dungey, H. S. (2017). Assessing very high resolution UAV imagery for monitoring forest health during a simulated disease outbreak. *ISPRS Journal of Photogrammetry and Remote Sensing*, *131*, 1–14. https://doi.org/10.1016/j.isprsjprs.2017.07.007

Draz, I. S., Abou-Elseoud, M. S., Kamara, A. E. M., Alaa-Eldein, O. A. E., & El-Bebany, A. F. (2015). Screening of wheat genotypes for leaf rust resistance along with grain yield. *Annals of Agricultural Sciences*, *60*(1), 29–39. https://doi.org/10.1016/j.aoas.2015.01.001

Du, M., & Noguchi, N. (2017). Monitoring of wheat growth status and mapping of wheat yield's within-field spatial variations using color images acquired from UAV-camera System. *Remote Sensing*, *9*(3). https://doi.org/10.3390/rs9030289

Haboudane, D., Miller, J. R., Pattey, E., Zarco-Tejada, P. J., & Strachan, I. B. (2004). Hyperspectral vegetation indices and novel algorithms for predicting green LAI of crop canopies: Modeling and validation in the context of precision agriculture. *Remote Sensing of Environment*. https://doi.org/10.1016/j.rse.2003.12.013

Haghighattalab, A., González Pérez, L., Mondal, S., Singh, D., Schinstock, D., Rutkoski, J., Ortiz-Monasterio, I., Singh, R. P., Goodin, D., & Poland, J. (2016). Application of unmanned aerial systems for high throughput phenotyping of large wheat breeding nurseries. *Plant Methods*, *12*(1). https://doi.org/10.1186/s13007-016-0134-6

Iqbal, F., Lucieer, A., & Barry, K. (2018). Simplified radiometric calibration for UAS-mounted multispectral sensor. *European Journal of Remote Sensing*. https://doi.org/10.1080/22797254.2018.1432293

Kolmer, J. A., & Hughes, M. E. (2018). Physiologic specialization of *Puccinia triticina* on wheat in the United States in 2016. *Plant Disease*, *102*(6), 1066–1071. https://doi.org/10.1094/PDIS-11-17-1701-SR

Line, R. F., & Chen Xianming. (1995). Successes in breeding for and managing durable resistance to wheat rusts. *Plant Disease*, *79*(12), 1254–1255.

Louhaichi, M., Borman, M. M., & Johnson, D. E. (2001). Spatially located platform and aerial photography for documentation of grazing impacts on wheat. *Geocarto*

International, *16*(1), 65–70. https://doi.org/10.1080/10106040108542184

Mutka, A. M., & Bart, R. S. (2015). Image-based phenotyping of plant disease symptoms. In *Frontiers in Plant Science*. https://doi.org/10.3389/fpls.2014.00734

Nguyen, H. C., Jung, J., Lee, J., Choi, S. U., Hong, S. Y., & Heo, J. (2015). Optimal atmospheric correction for above-ground forest biomass estimation with the ETM+ remote sensor. *Sensors (Switzerland)*, *15*(8), 18865–18886. https://doi.org/10.3390/s150818865

Oelke, L. M., & Kolmer, J. A. (2004). Characterization of leaf rust resistance in hard red spring wheat cultivars. *Plant Disease*, *88*(10), 1127–1133. https://doi.org/10.1094/PDIS.2004.88.10.1127

Pathan, A. K., & Park, R. F. (2006). Evaluation of seedling and adult plant resistance to leaf rust in European wheat cultivars: Leaf rust resistance in European wheat cultivars. *Euphytica*, *149*(3), 327–342. https://doi.org/10.1007/s10681-005-9081-4

Pérez, A. J., López, F., Benlloch, J. V., & Christensen, S. (2000). Colour and shape analysis techniques for weed detection in cereal fields. *Computers and Electronics in Agriculture*, *25*(3), 197–212. https://doi.org/10.1016/S0168-1699(99)00068-X

Ponce-Molina, L. J., Huerta-Espino, J., Singh, R. P., Basnet, B. R., Lagudah, E., Aguilar-Rincón, V. H., Alvarado, G., Lobato-Ortiz, R., García-Zavala, J., & Lan, C. (2018). Characterization of adult plant resistance to leaf rust and stripe rust in Indian wheat cultivar ‘New pusa 876.’ *Crop Science*. https://doi.org/10.2135/cropsci2017.06.0396

Potgieter, A. B., George-Jaeggli, B., Chapman, S. C., Laws, K., Cadavid, L. A. S.,

Wixted, J., Watson, J., Eldridge, M., Jordan, D. R., & Hammer, G. L. (2017). Multi-spectral imaging from an unmanned aerial vehicle enables the assessment of seasonal leaf area dynamics of sorghum breeding lines. *Frontiers in Plant Science*, *8*:1532. https://doi.org/10.3389/fpls.2017.01532 https://doi.org/10.3389/fpls.2017.01532

Prescott, J. M., Burnett, P. A., Saari, E. E., Ransom, J. K., Bowman, J. D., De Milliano, W., ... & Geleta, A. B. (1986). Wheat diseases and pests: a guide for field identification. International Maize and Wheat Improvement Center (CIMMYT).

Pugh, N. A., Han, X., Collins, S. D., Thomasson, J. A., Cope, D., Chang, A., Jung, J., Isakeit, T. S., Prom, L. K., Carvalho, G., Gates, I. T., Vree, A., Bagnall, G. C., & Rooney, W. L. (2018). Estimation of plant health in a sorghum field infected with anthracnose using a fixed-wing unmanned aerial system. *Journal of Crop Improvement*, *32*(6), 861–877. https://doi.org/10.1080/15427528.2018.1535462

Qin, Z., & Zhang, M. (2005). Detection of rice sheath blight for in-season disease management using multispectral remote sensing. *International Journal of Applied Earth Observation and Geoinformation*, *7*(2), 115–128. https://doi.org/10.1016/j.jag.2005.03.004

Roelfs, P., Singh, R. P., & Saari, E. E. (1992). Rust Diseases of Wheat: Concepts and methods of disease management. *Rust Diseases of Wheat: Concepts and methods of disease management.* International Maize and Wheat Improvement Center (CIMMYT).

Rouse, J. W., Haas, R. H., Schell, J. A., & Deering, D. W. (1974). Monitoring vegetation

systems in the Great Plains with ERTS. *NASA special publication*, *351*, 309.

Rudd, J. C., Devkota, R. N., Ibrahim, A. M., Baker, J. A., Baker, S., Sutton, R., ... & Nelson, L. R. (2019). 'TAM 204'Wheat, Adapted to Grazing, Grain, and Graze-out Production Systems in the Southern High Plains. *Journal of Plant Registrations*, *13*(3), 377-382.

Rust Scoring Guide. 1986. International Maize and Wheat Improvement Center (CIMMYT). https://repository.cimmyt.org/bitstream/handle/10883/1109/13395.pdf?sequence=1&isAllowed=y

Shafian, S., Rajan, N., Schnell, R., Bagavathiannan, M., Valasek, J., Shi, Y., & Olsenholler, J. (2018). Unmanned aerial systems-based remote sensing for monitoring sorghum growth and development. *PLoS ONE*, *13*(5). https://doi.org/10.1371/journal.pone.0196605

Singh, R. P., & Huerta-Espino, J. (1997). Effect of leaf rust resistance gene Lr34 on grain yield and agronomic traits of spring wheat. *Crop Science*, *37*(2), 390–395. https://doi.org/10.2135/cropsci1997.0011183X003700020014x

Smith, G. M., & Milton, E. J. (1999). The use of the empirical line method to calibrate remotely sensed data to reflectance. *International Journal of Remote Sensing*. https://doi.org/10.1080/014311699211994

Stubbs, R. W., Prescott, J. M., Saari, E. E., & Dubin, H. J. (1986). Cereal disease methodology manual. International Maize and Wheat Improvement Center (CIMMYT).

Su, J., Liu, C., Coombes, M., Hu, X., Wang, C., Xu, X., Li, Q., Guo, L., & Chen, W. H. (2018). Wheat yellow rust monitoring by learning from multispectral UAV aerial imagery. *Computers and Electronics in Agriculture*, *155*, 157–166. https://doi.org/10.1016/j.compag.2018.10.017

Wang, C., & Myint, S. W. (2015). A Simplified Empirical Line Method of Radiometric Calibration for Small Unmanned Aircraft Systems-Based Remote Sensing. *IEEE Journal of Selected Topics in Applied Earth Observations and Remote Sensing*, *8*(5), 1876–1885. https://doi.org/10.1109/JSTARS.2015.2422716

Wang, H., Qin, F., Ruan, L., Wang, R., Liu, Q., Ma, Z., Li, X., Cheng, P., & Wang, H. (2016). Identification and severity determination of wheat stripe rust and wheat leaf rust based on hyperspectral data acquired using a black-paper-based measuring method. *PLoS ONE*, *11*(4). https://doi.org/10.1371/journal.pone.0154648

Wegulo, S., & Byamukama, E. (2012). Rust diseases of wheat. Univ. of Nebraska Ext., Lincoln. http://extensionpublications.unl.edu/assets/pdf/g2180.pdf

White, J. W., Andrade-Sanchez, P., Gore, M. A., Bronson, K. F., Coffelt, T. A., Conley, M. M., Feldmann, K. A., French, A. N., Heun, J. T., Hunsaker, D. J., Jenks, M. A., Kimball, B. A., Roth, R. L., Strand, R. J., Thorp, K. R., Wall, G. W., & Wang, G. (2012). Field-based phenomics for plant genetics research. In *Field Crops Research* (Vol. 133, pp. 101–112). https://doi.org/10.1016/j.fcr.2012.04.003

Yang, G., Liu, J., Zhao, C., Li, Z., Huang, Y., Yu, H., Xu, B., Yang, X., Zhu, D., Zhang, X., Zhang, R., Feng, H., Zhao, X., Li, Z., Li, H., & Yang, H. (2017). Unmanned aerial vehicle remote sensing for field-based crop phenotyping: Current status and

perspectives. In *Frontiers in Plant Science* (Vol. 8). https://doi.org/10.3389/fpls.2017.01111

Yu, K., Kirchgessner, N., Grieder, C., Walter, A., & Hund, A. (2017). An image analysis pipeline for automated classification of imaging light conditions and for quantification of wheat canopy cover time series in field phenotyping. *Plant Methods*, *13*(1). https://doi.org/10.1186/s13007-017-0168-4

Zhang, D., Zhou, X., Zhang, J., Lan, Y., Xu, C., & Liang, D. (2018). Detection of rice sheath blight using an unmanned aerial system with high-resolution color and multispectral imaging. *PLoS ONE*, *13*(5). https://doi.org/10.1371/journal.pone.0187470

CHAPTER III

UNMANED AERIAL SYSTEM (UAS)-BASED PLANT GROWTH ANALYSIS OF WINTER WHEAT

INTRODUCTION

Crop growth is a continuous process which is a result of genes, environment, and their interaction. Temperature is one of the most important environmental factors regulating winter wheat (*Triticum aestivum* L.) growth. Generally, winter wheat is planted in fall in the areas where the temperature does not go below freezing for longer periods. In the U.S, winter wheat is mostly grown in the Great Plains. However, phenological differences during wheat development are observed throughout the region because of microclimatic differences in the south, central, and northern regions. Seeds are sown in fall and seedlings are exposed to a lower temperature during early winter. This low temperature promotes vernalization and induce flowering (Dixon *et al.*, 2019). Winter wheat goes through a series of physiological changes from emergence to maturity. According to Feekes scale (Feekes, 1941), major stages of wheat growth are emergence, tillering, jointing, booting, heading, anthesis, and maturity (Large, 1954). These stages are critical in making management decisions such as fertilizer applications, irrigation requirements, and pest control. Numerous morphological and physiological parameters such as canopy architecture, dry matter accumulation, photosynthesis, and transpiration are vital plant properties that can be monitored during the growth cycle to understand crop physiological status and obtain optimum yield. In plant breeding, understanding the mechanisms of physiological growth can help in selecting parents,

evaluating genotypes, and making selection strategies. For example, early vigor, which is defined as rapid early growth and accumulation of above-ground biomass, has a positive relationship with final grain yield in wheat (Carmo-silva *et al.*, 2017). This is achieved by reducing evaporation and early competition of crops with weeds (Rebetzke and Richards, 1999; Lemerle *et al.*, 2001; Botwright *et al.*, 2002; Richards *et al.*, 2002; Ludwig and Asseng, 2010). However, this may not always be true under dryland conditions as higher growth and biomass accumulation early in the season may reduce available soil water later during anthesis and grain filling stage (Feekes, 194; Large, 1954) leading to the reduction in grain yield (Zhao *et al.*, 2019). Additionally, plant growth analysis can help to investigate the morphological, physiological, and environmental reasons behind yield variations between genotypes. Therefore, a high-throughput system capable of estimating biomass accumulation early in the season and enabling analysis of the rate of plant growth can provide additional information to determine factors responsible for grain yield.

Traditionally, above ground dry matter and green leaf area are determined by destructive sampling procedures. This method has limitations in scalability and repeatability because of labor, cost, and time consumption. Also, several samples are harvested during the growing season and their contribution to final grain yield will be neglected when using multi-temporal dry matter accumulation approach to predict final grain yield. Although green leaf area and biomass can be estimated by using different sensors that can capture the rate of photosynthesis, canopy light interception, and gas exchange at single plant and leaf level, it is limited to few measurements in a given time

and is highly affected by the weather variability between two measurements. The issue of labor, time and expenses of collecting many samples can be addressed by using Unmanned Aerial Systems (UAS). With the rapid advancement in UAS and sensor technology, we can obtain high spatial-temporal resolution data of plant morphological features such as plant height, green canopy cover, and canopy volume. These proxy measurements can be used to perform growth analysis and estimate biomass, and vegetation growth rate. UAS equipped with sensors can collect spectral data based on the reflectance properties of plants and other elements such as soil, plant internal structures, pigments, and plant water status (Yang *et al.*, 2017). This spectral data is further processed to generate multiple band images (for example, RGB band image) and can be used to obtain canopy features by following programmatic image processing approaches. Data obtained throughout the season using this technique can be used to perform growth analysis.

Plant growth is a dynamic process which is the result of genetics and environmental variations. Plant growth analysis is a holistic approach and integrates the shape, size, and efficiency function of a plant (Schurr *et al*. 2006; Szparaga and Kocira, 2018). It is either performed by simple calculations using growth equations to obtain growth parameters such as growth rate (GR), relative growth rate (RGR)) (Hunt and Parsons, 1974; Hunt, 1979; Glasbey and Hunt, 1983; Schurr *et al*., 2006; Szparaga and Kocira, 2018) or using the conceptual models obtained by fitting the nonlinear regression models (Sugar et al., 2017). Plant growth generally follows sigmoidal growth function characterized by an early lag phase when growth is slow, an exponential phase

when the growth is maximum, and a stationary phase when growth is saturated (Batchelor, 1997; Yin *et al.*, 2003). First order derivative of a fitted function forms a bell-shaped curve (Yin *et al.*, 2003) from which the growth parameters (GR and RGR) can be obtained. Some of the commonly used functions for analyzing plant growth are logistic function, Richard function, and Gompertz function (Yin *et al.*, 2003).

Logistic function was originally formulated by Verhulst (1838). The first derivative of this function is symmetrical around time and is described as

$$w = \frac{w_{max}}{1 + e^{-k(t-t_m)}}$$

where, w_{max} is maximum value, t_m is the time when growth rate reaches the maximum value, k is a constant that determines the growth pattern, the relative growth rate at t_m is $k/2$ and the value at tm is half of the maximum value (w_{max}).

Richard function was originally formulated by Richards (1959) to deal with the asymmetrical nature of growth and is described as

$$w = \frac{w_{max}}{[1 + ve^{-k(t-t_m}]^{1/v}}$$

where, w_{max} is maximum value, t_m is the time when growth rate reaches maximum value, k is a constant that determines growth pattern, v is an additional parameter which determines relative growth rate at t_m as $k/(1+v)$.

Gompertz (1815) developed another function that gives an asymmetrical sigmoid pattern with three parameters and is described

$$w = w_{max}e^{-e^{k(t-t_m)}}$$

where, w_{max} is maximum value, t_m is the time when growth rate reaches maximum value, w is equal to w_{max}/e, relative growth rate at t_m is k

There are several other equations used in the growth analysis of plants and other organisms. The selection of any of the available functions depends on the nature of plants and the trait being measured. One of the important selection criteria as described by Zeide (1993) is the flexibility of a function and it depends on number of parameters. The major objective of this study was to investigate if multi-temporal Canopy Cover (CC) parameter obtained throughout the growing season using UAS can be used to perform growth analysis using growth functions. Specific objectives were to: i) outline the procedure to obtain CC from small breeding plots using UAS system ii) fit growth functions and obtain daily CC estimates, and iii) obtain interpretable growth parameters, namely; average growth rate, maximum growth rate, and day at which maximum growth rate was achieved from the fitted growth curve.

MATERIALS AND METHODS

Study area

Forty-five winter wheat genotypes were planted in a field experiment at the Texas A&M University farm located at College Station, Texas. UAS data were collected in 2018-2019 winter wheat growing season. Experiment was a random block design with six replications. Three of those six replications were treated with fungicide (Trivapro at 0.95 kg/ha) during heading (10.5 in Feekes scale; Large (1954)). This resulted in fungicide-treated and control plots. Plots were 3.4 m × 1.52 m in size consisting of seven rows with 0.18 m spacing. Seeds were sown on October 29, 2018. Plots were irrigated

throughout the season and other agronomic practices were conducted as per the requirement (Kimura et al., 2018).

UAS platforms and sensors

DJI phantom 4 pro (SZ DJI Technology Co., Ltd, Shenzhen, China) was flown to collect high-resolution red green, and blue (RGB) images. Phantom 4 pro was equipped with 20 megapixels one-inch CMOS (Complementary metal-oxide-semiconductor) RGB sensor. UAS platform was flown at 20 m altitude with front and side overlap of 85 percent to obtain high resolution orthomosaic images. Data were collected multiple times during the growing season and are summarized in Table **6**.

Table 6. Unmanned Aerial System (UAS) data collection timeline
Red, green, and blue band images were collected using DJI phantom 4 pro at several Days after Planting (DAP) over winter wheat breeding trial at College Station, Texas. Raw images were processed to generate orthomosaic images with certain spatial resolution (ground resolution).

Time of year	Days after Planting (DAP)	Ground resolution
Oct 29, 2018	Planting date	-
Nov 20, 2018	21	0.75 cm/pixel
Dec 3, 2018	34	0.75 cm/pixel
Dec 21, 2018	52	0.75 cm/pixel
Jan 09, 2019	71	0.75 cm/pixel
Jan 16, 2019	78	0.75 cm/pixel
Jan 26, 2019	88	0.75 cm/pixel
Feb 13, 2019	105	0.75 cm/pixel
Mar 19, 2019	139	0.75 cm/pixel
Mar 26, 2019	146	0.75 cm/pixel
Apr 12, 2019	163	0.75 cm/pixel
Apr 16, 2019	167	0.75 cm/pixel
May 05, 2019	187	0.75 cm/pixel

Geo-referencing, image processing and data extraction

UAS platform was equipped with a Global Positioning System (GPS). However, the accuracy of collected geographic coordinate's data is low as the platform is distorted

by wind during data collection. Georeferencing of collected raw images is important to achieve a high level of accuracy in the orthomosaics. Using same plot boundary shapefile throughout the growing season can reduce time required to extract data from small breeding plots. Temporary Ground Control Points (GCPs) were placed in the field before the flight and surveyed to collect the coordinate data. The GCPs were 0.6 m × 0.6 m square plywood board, painted black and white to make them easily identifiable during image processing. V-Map Post Processing Kinematic (PPK) system (Micro Aerial Projects LLC., Gainsville, FL, US) was used to survey precise coordinates of GCPs. Thus, obtained V-map data was further processed to acquire and latitude, longitude, and elevation of the GCPs. This information was uploaded in the Agisoft Metashape software (Agisoft LLC, St. Petersburg, Russia, 191144) during image processing (Figure 7).

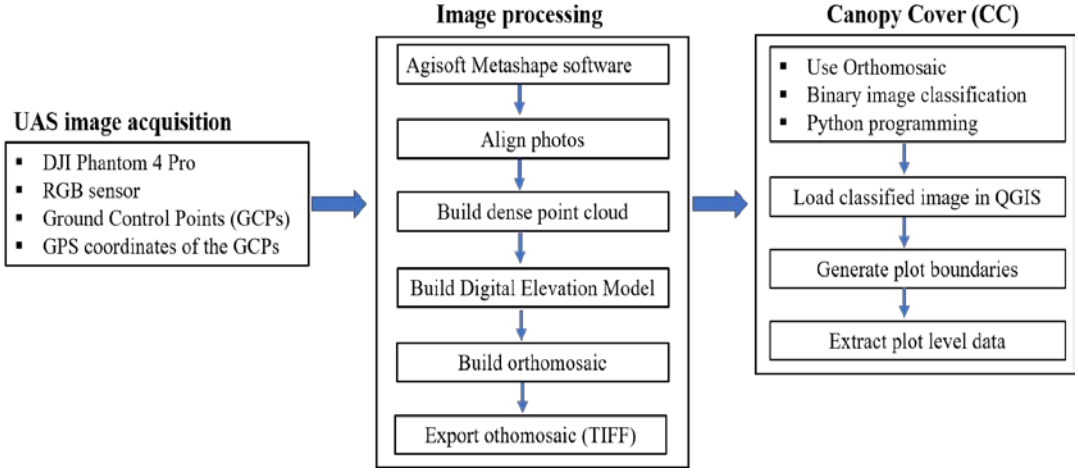

Figure 7. Unmanned Aerial System (UAS) workflow of data collection, processing, and analysis
RGB: Red, green and blue band, GPS: Global Positioning System.

Raw images obtained from the RGB sensor were processed using Agisoft Metashape software to generate a 3D point cloud, Digital Surface Model (DSM), and orthomosaic images (Jung, 2017; Jung *et al.*, 2018; Ashapure *et al.*, 2019). Figure **7** illustrates image processing workflow in AgiSoft Metashape software (Westoby *et al.*, 2012). After generating orthomosaic images, percentage of CC was calculated. CC is positively correlated with the dry matter accumulation and final grain yield in wheat. It considers the area covered by the canopy based on the intensity of greenness. Therefore, CC obtained from the UAS imagery was used to perform growth analysis and assess physiological changes in winter wheat genotypes. CC was obtained by following the Canopeo algorithm developed by Patrignani and Ochsner (2015). In this approach, a certain threshold was used to classify the image into canopy and non-canopy classes and a binary image was produced by applying following equations during image processing.

$$\frac{R}{G} < P1\ ,\ \frac{B}{G} < P2\ ,\ 2G - R - B > P3$$

where R, G, and B are Digital Number (DN) values for red, green and blue bands respectively. $P1$ and $P2$ are parameters to classify pixels in the green band and $P3$ sets the minimum value for excess green index to select green vegetation. In this study, parameter (*P1*, *P2*, and *P3*) values were set to default as explained in Canopeo (P1=0.95, P2=0.95, and P3=20). Figure **8** describes binary image classification and data extraction procedure, which classified, canopy pixels as white color and soil pixels as black color. A plot boundary shape file was created to extract data from the orthomosaic. The shapefile was overlaid on the classified image and total number of pixels and total

number of canopy pixels within the plot boundary were extracted using zonal statistics tool in QGIS software (www.qgis.org).

Average CC within the plot was calculated using the following formula.

$$\text{Canopy Cover (CC)} = \frac{\text{Number of canopy pixels}}{\text{Total number of pixels}} \times 100$$

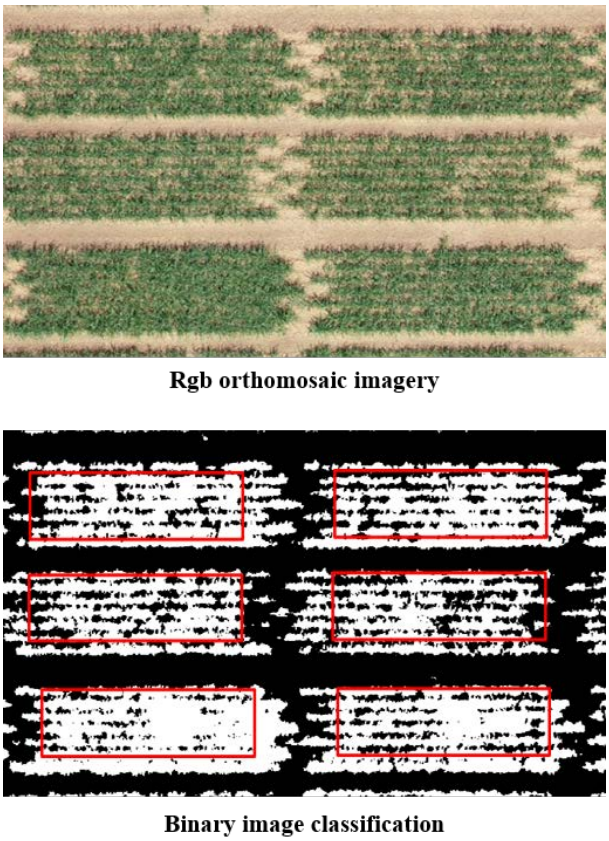

Figure 8. Binary image classification and data extraction to generate plot level canopy cover (CC)
Black color in the image is non-canopy pixels, white color is canopy pixels, red colored boundary is used to calculate CC and extract data from each plot.

Ground measurements

Biomass was harvested at 88 Days after Planting (DAP) from first two replications representing 20 genotypes to study the relationship between early growth

parameters and biomass. Samples were oven dried at 60°C for 48 hours to obtain dry matter content. Each plot was harvested using combine harvester (Classic Plus, Wintersteiger AG, Germany) to determine final grain yield.

Growth analysis

Logistic function, Richard, and Gompertz function were tested for their use in growth analysis using UAS obtained CC data. CC values obtained throughout the growing season from each plot were averaged to obtain mean value of CC for each of the measurement days. Growth analysis was performed using a dynamic fit wizard tool available in SigmaPlot (Systat Software, Inc). The decision to select the best function for further parameter extraction was based on adjusted R^2 and Root Mean Square Error (RMSE). RMSE measures the error obtained between the observed and predicted values. It is calculated using the following formula:

$$RMSE = \sqrt{\sum_{i}^{n} \frac{(\widehat{Y}i - Yi)^2}{n}}$$

where, $\widehat{Y}i$ are predicted values, Yi are observed values, and n is the number of observations

Statistical analysis

Growth parameters (maximum CC, maximum growth rate in CC, day of maximum CC) were obtained from the first derivative of the growth functions. Linear regression was performed between the growth parameters, biomass and yield to study the relationship between these variables. Coefficient of determination (R^2) was calculated to study the relationship.

RESULTS

Growth analysis

CC data obtained from emergence to 146 DAP followed a sigmoidal growth pattern (Figure **9**). Canopy growth was slow in the beginning until 20 DAP which is the early lag phase. An exponential growth occurred from 20 DAP to 66 DAP. There were no significant variations in CC from 66 DAP to 146 DAP which is often termed as a saturated phase in growth analysis. All the growth functions fitted well with CC data. Table **7** summarizes the statistical parameters used to assess the validity of growth functions. Growth functions applied in this study are nonlinear models consisting of different set of parameters. Four parameters logistic function had highest R^2 value and lowest RMSE. However, it predicted negative CC estimates in the early ten days. To remove negative estimates during growth analysis, a three-parameter sigmoid function was fitted in CC data obtained during 0 to 146 DAP. It had a higher RMSE and lower adjusted R^2. All four equations estimated similar growth parameters. In most cases, logistic function had a better fit than three other functions. Therefore, it was selected for further growth parameter calculations.

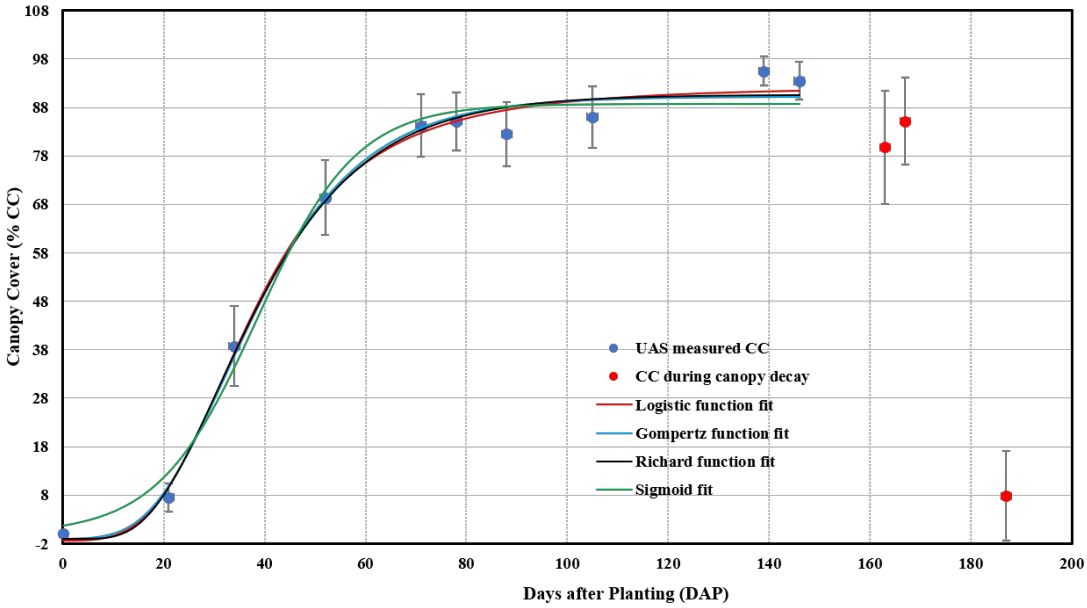

Figure 9. Fitting growth functions over a seasonal Canopy Cover (CC) distribution of winter wheat

Solid lines are fitted lines using growth functions. Vertical bars represent standard deviation. Each data point is the average of all CC values obtained on that day from three replications.

Following functions were used to perform growth analysis in this study:

Logistic function:

$$y = y_0 + \frac{a}{1 + \left(\frac{x}{x_0}\right)^b}$$

where, y_0 is estimated response at zero Days after Planting (DAP), a represents asymptote which is the maximum Canopy Cover (CC), b is slope factor, x_0 is mid-range DAP

Gompetz function:

$$y = y_0 + ae^{-e^{\frac{x-x_0}{b}}}$$

where, y_0 is estimated response at zero Days after Planting (DAP), a represents asymptote which is the maximum Canopy Cover (CC), b is slope factor, x_0 is mid-range DAP

Richard function:

$$y = y_0 + a\left(1 - e^{-bx_0}\right)c$$

where, y_0 is estimated response at zero DAP, a represents asymptote which is the maximum Canopy Cover (C), b is slope factor, x_0 is mid-range DAP

Sigmoid three parameter function:

$$y = \frac{q}{1 + e^{-\left(\frac{x - x_0}{b}\right)}}$$

where, q represents asymptote which is the maximum Canopy Cover (CC), b is slope factor, x_0 is mid-range DAP

Table 7. Statistical parameters of growth functions

Growth functions	Parameters	R^2	adj. R^2	RMSE
Richard	4	0.99	0.98	3.82
Gompretz	4	0.99	0.98	3.98
Logistic	4	0.99	0.99	3.43
Sigmoid	3	0.98	0.98	4.84

R^2: coefficient of determination; adj. R^2: adjusted coefficient of determination; RMSE: root-mean-square error.

Growth parameters

Three different parameters, namely maximum CC during 0-146 DAP (CC_{max}), maximum canopy growth rate per day (CC_{MGR}), and day at which CC had maximum growth rate ($CCGR_{DAP}$) were calculated based on a four parameter logistic growth function.

$CC_{max,}$ which is represented by "a" is shown in Figure **10**. CC_{GR} was calculated using the following formula:

$$\text{Canopy growth rate } (CC_{GR}) = \frac{CC_2 - CC_1}{T}$$

Where, CC_{GR} is the canopy growth rate, CC_2 and CC_1 are Canopy Cover measurements obtained in Day 2 and Day 1, respectively, and T is the number of days between each measurement.

Once CC_{GR} values were obtained, a graph was generated to plot the growth rate against DAP. As shown in Figure **11**, growth rate was asymmetrical and maximum growth of canopy in terms of CC took place during 35-40 DAP. Value falling at the top of the bell-shaped curve is CC_{MGR}.

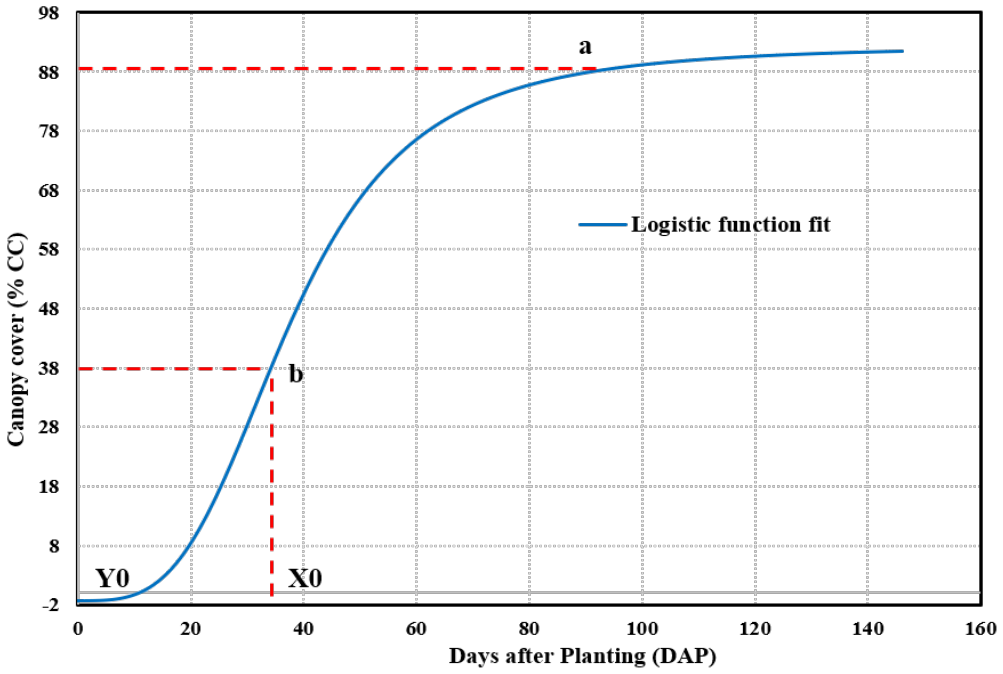

Figure 10. Description of logistic function and its related parameters
a represents asymptote which is the maximum Canopy Cover (CC), *b* is the mid-point slope, *X0* is the mid-point at which canopy growth rate reaches maximum, *Y0* is the amount of CC during lag phase.

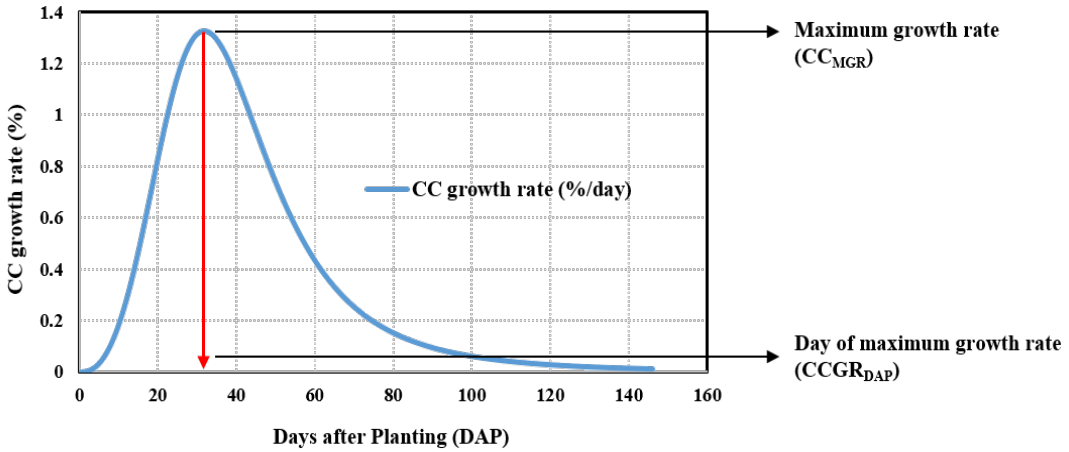

Figure 11. Growth parameters extracted from logistic growth function
Daily Canopy Cover (CC) measurements were estimated using logistic function and canopy growth rate was calculated by obtaining daily CC estimates.

Relationship between growth parameters, biomass, and grain yield

One of the major objectives of this study was to investigate if growth parameters extracted from growth functions can be used to assess genotypes for early vigor and grain yield. CC_{MGR} was positively associated to biomass (R^2=0.70, $p<0.05$) (Figure **12**A). However, it was not correlated to grain yield (Figure **12**B). Therefore, we wanted to study if canopy greenness after 146 DAP contributed to grain yield in this study. As shown in Figure 13 (A-B), CC measured at 163 DAP and 167 DAP had a strong relationship with grain yield (R^2=0.65, R^2=0.51, $p<0.01$). These two dates of UAS measurement coincided with grain filling stage (10.54 to 11.1 in Feekes scale; Large (1954)). Genotypes with lower CC values had lower yield compared to those with higher CC values. Images in Figure **14** clearly explain this variation in canopy greenness. At 146 DAP CC was 85-100 percent in the entire trial (Figure **9**). As the season progressed,

intensity of greenness decreased, and plots started to turn yellow (Figure **14**).

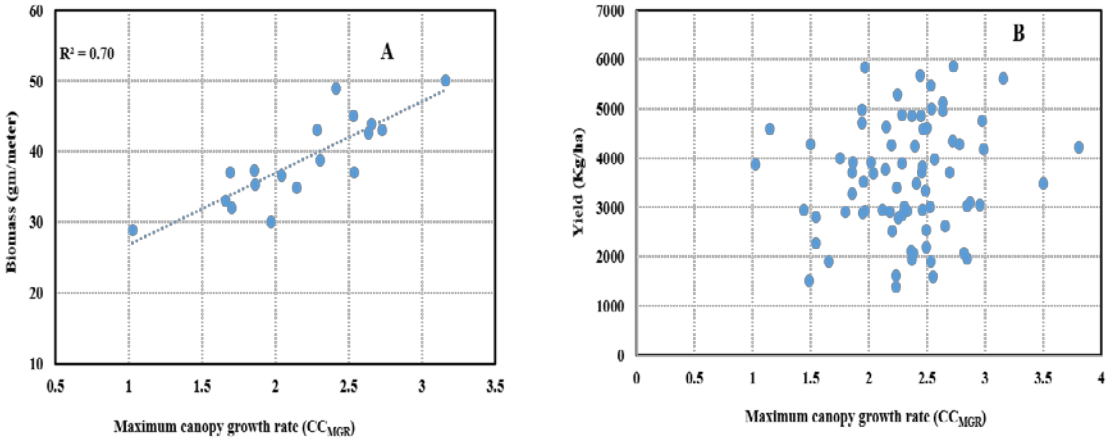

Figure 12. Scatter plot showing the relationship of canopy growth rate with biomass (A) and grain yield (B)
Each data point represents a genotype which is the average value of two replicates.

Leaf rust (*Puccinia triticina f. sp. tritici*) which is one of the major fungal diseases of wheat appears during last week of March in the southern region of Texas. Some of the susceptible genotypes such as 'TAM 204' (Rudd et al., 2019) had leaf rust infection at 140-145 DAP which is visible in some plots in the RGB image taken at 146 DAP (Figure **14**). The rate of canopy decay due to the disease infection was higher as the season progressed which is visible in Figure **14** on the images taken at 163 DAP and 167 DAP. CC measured at 163 DAP and 167 DAP had a positive relationship with grain yield (Figure 13). R^2 was higher (R^2=0.65, $p<0.05$) at 163 DAP (Figure **13**A) compared to 167 DAP (R^2=0.52, $p<0.05$; Figure **13**B). The results show that the slow rate of canopy decay during the reproductive stage leads to higher grain yield under the wheat growing conditions at College Station, TX. Strong relationship between the change in CC from 146 DAP to 163 DAP resulted into another approach of determining the rate of

canopy decay during this period. The rate of canopy decay based on CC values was calculated using the following formula:

$$\text{Rate of canopy decay} = \frac{\text{CC}_{163\text{DAP}} - \text{CC}_{146\text{DAP}}}{17}$$

where CC_{163DAP} and CC_{146DAP} is Canopy Cover (CC) obtained from UAS data at 163 and 146 DAP respectively, denominator value (17) is the number of days between those measurements

The relationship between the rate of canopy decay and grain yield is presented in Figure 15 (R^2=0.65, $p<0.05$). As shown in the figure, genotypes with slow canopy decay produced higher yield compared to those with faster decay. This study demonstrates the importance of maintaining canopy health to produce a better yield. Genotypes resistant to fungal diseases maintained green foliage for a longer period and had higher chances of producing better yield.

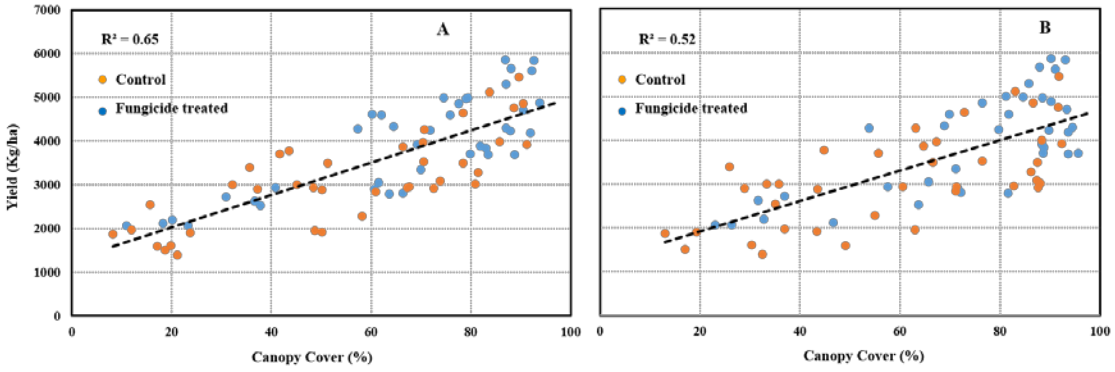

Figure 13. Scatter plot showing the relationship between grain yield and Canopy Cover (CC) measured at 163 (A) and 167 (B) Days after Planting (DAP)
Each data point represents a genotype which is the average value of three replicates.

Figure 14. Orthomosaic images taken at different times during the growing season of winter wheat
DAP is Days after Planting.

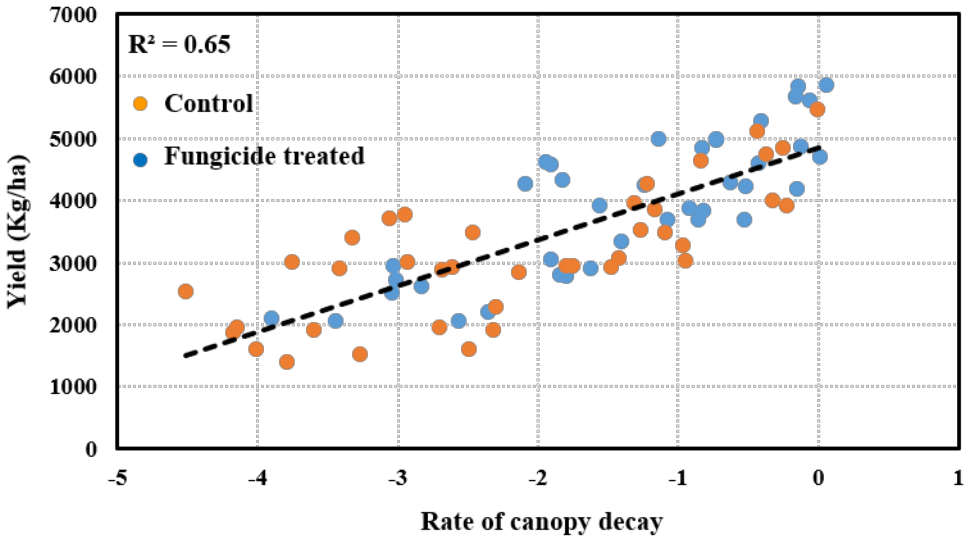

Figure 15. Scatter plot showing the relationship between grain yield and rate of canopy decay obtained from Unmanned Aerial System (UAS)
Each data point represents a genotype which is the average value of three replicates.

Effect of fungicide application on canopy cover (CC) and yield

Figure **16** shows the differences in CC values obtained between fungicide-treated and control plots. CC values were averaged across genotypes and standard error was calculated to show the statistical significance between the two treatments.

$$SE = \frac{SD}{\sqrt{n}}$$

Where *SE* is standard error, *SD* is standard deviation and *n* is the total number of observations.

Fungicide application reduced the rate of canopy decay and maintained greener canopy compared to untreated ones. CC values were significantly higher at 163 DAP and 167 DAP in the treated plots. The application of fungicide significantly improved grain yield (Figure **17**).

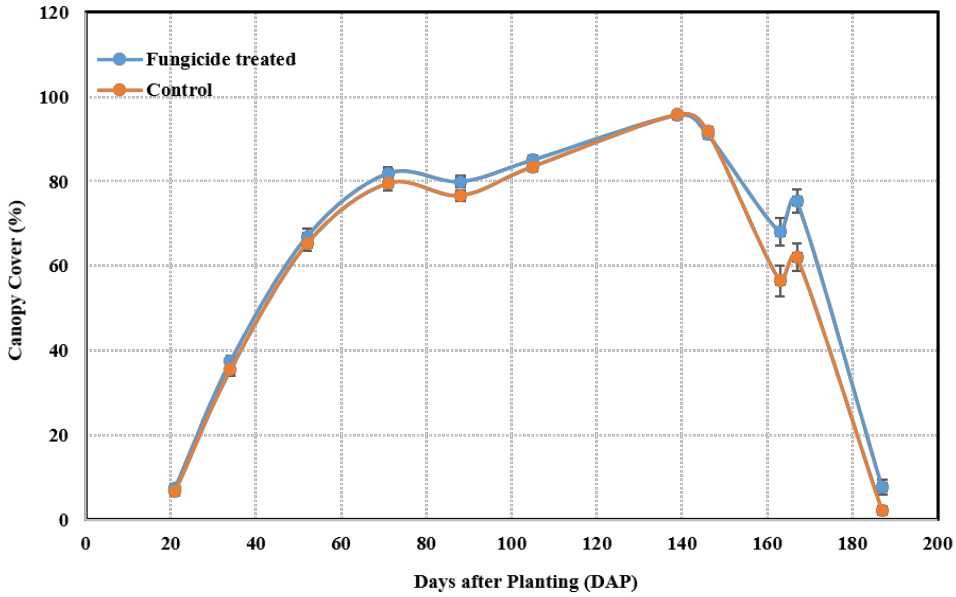

Figure 16. Unmanned Aerial System (UAS) obtained Canopy Cover distribution of fungicide-treated and control plots measured over a wheat growing season
Vertical bars represent standard error.

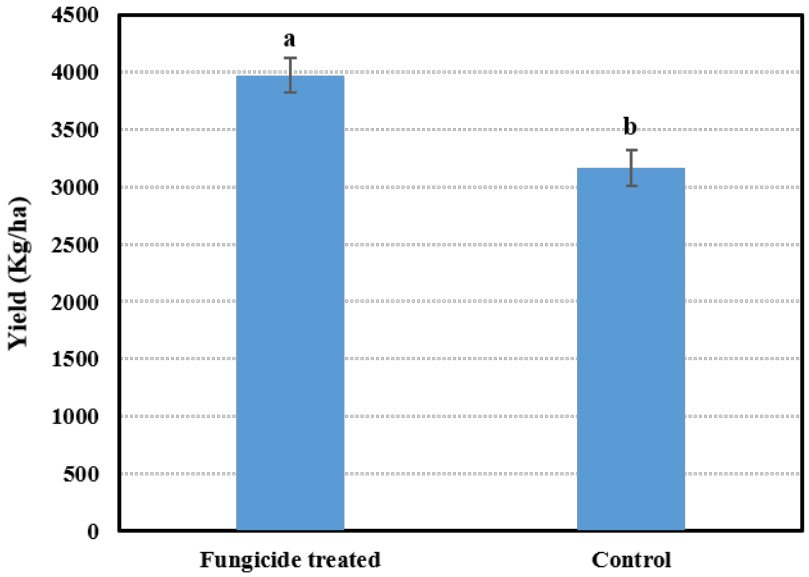

Figure 17. Bar graph showing grain yields of fungicide-treated and control plots
Yield was averaged across treatments. Vertical bar represents standard error. Letter a, b indicate significant difference between two treatments.

DISCUSSION

UAS equipped with RGB camera was useful in obtaining high-resolution orthomosaics. Easy operational procedures added benefits in collecting data multiple times during the growing season. In this study, the importance of GCPs during image processing and data extraction was realized. It is very important to install semi-permanent GCPs to speed up image processing and data extraction. Temporary GCPs were used which needed to be placed before flights and collected after flights. It took a sizable amount of time to place GCPs, obtain coordinates, and collect them. Technical malfunction of GPS at some dates of data collection resulted in additional work to generate plot boundaries. There was equal possibility of losing the pixels that lie in the exact same location because of GPS inaccuracies. Therefore, to improve the efficiency

of image processing and data extraction, it is important to install semi-permanent GCPs mobile during agronomic operations and place them back throughout the growing season. UAS resulted in a large amount of high-resolution multi-temporal data with the potential to be used at multiple dimensions to understand crop growth and development. Importance of GCPs was highlighted in several previous studies (Jung, 2017; Jung *et al.*, 2018; Ashapure *et al.*, 2019).

UAS data acquired multiple times over the growing season can be used for crop growth analysis. Application of non-linear growth functions to study plant growth dynamics has been considered since the early times. Fresco (1973) illustrated the use of a logistic function to model plant growth. Use of non-linear models came with an understanding that the relative and absolute growth of plants differ with environmental conditions and growth stages. Growth models need to account for this temporal dynamics of growth and varying relative growth rates that happen as plants increase in biomass and achieve its potential biomass accumulation (Paine *et al.*, 2012). Growth functions have been developed and used in modeling emergence of winter rapeseed (*Brassica napus L.*) (Szparaga and Kocira, 2018), modeling plant growth, and calculate growth rate (Paine *et al.*, 2012). Liu et al. (2018) derived an improved sigmoidal model to estimate maximum crop biomass to forecast yield. Derived functions were fitted in dry biomass content in eight crop species. They concluded that the use of growth functions can be helpful to understand the growth of different plant species. Traditional way of harvesting biomass to determine dry matter content and use it to develop growth functions is time-consuming and laborious process. This method is totally based on a

destructive sampling procedure where the same plants samples are not used to determine future growth and yield. Additionally, plant growth parameters such as relative and absolute growth were calculated by fitting a curve entirely in a small number of biomass samples. Therefore, this study is an improvement over the traditional approach of crop growth analysis. Indirect estimates of green biomass through CC measurements allowed the fitting of a non-linear growth curve and derivation of important growth parameters.

Wheat growth followed a sigmoidal pattern in this study, including the lag phase, linear phase, and stationary phase. It is important to determine a growth function that can fit across all these growth phases (Batchelor, 1997). In wheat, it is important to consider the longer lag phase in case of low temperatures during the first three week of planting. Low temperature early in the season slow down the rate of canopy growth. Therefore, a four-parameter logistic function was selected as a best fit model in this study to account for a longer lag phase. The results showed a negative estimation of CC for the first ten DAP which might be attributed to a longer interval between the first and second measurements after planting. It is suggested to improve the frequency of measurements (3-5 days interval) during the early stage of growth. However, growth parameters extracted in this study showed large variation and were significantly different among genotypes. Based on the statistics, four-parameter logistic function was selected as the best fit and its first derivative resulted in asymmetrical bell-shaped growth rate curve. The logistic function is commonly used to quantify growth and compute growth rate in several studies (Hunt and Parsons, 1974; HUNT, 1979, 1982; Hunt, 1990; Batchelor, 1997; Hunt *et al.*, 2002; Yin *et al.*, 2003). But its use for analyzing UAS data was not

found in literature. This study aimed to test a simple approach for understanding wheat growth using UAS data rather than developing and defining new growth functions. The quantification of growth by using this method can be adopted by crop physiologists and breeders as an additional trait to characterize genotypes in different environments and design varieties for target environments. For example, growth parameters can be used to assess genotypes for early CC which is an important trait to breed for developing forage wheat genotypes. This approach can also be used to assess early season freezing damage by quantifying the change in green CC.

The nature of canopy growth can improve canopy architecture and affect light interception, absorption, distribution within the plant canopy, and also affect crop yield (Gifford *et al.*, 1984; Dreccer *et al.*, 1997; Bruin and Pedersen, 2008; Eberhard *et al.*, 2008; Giunta *et al.*, 2008; Acreche *et al.*, 2009; Cossani *et al.*, 2009; Distelfeld et al., 2014; Feng *et al.*, 2016). One of the hypotheses tested in this study was the relationship between early growth of canopy and final grain yield based on the assumption that a genotype with a bigger canopy can produce higher yield (De Bruin and Pedersen, 2008). This is because of the availability of large photosynthetic area (Gifford *et al.*, 1984; Eberhard *et al.*, 2008; Fischer, 2011). However, there was no significant relationship between early canopy growth and final grain yield. Another important physiological factor contributing to grain yield is the efficiency of a canopy in converting the available sunlight into biomass and produce better yield (Loss and Siddique, 1994; Maddonni and Otegui, 1996; Reta-Sánchez and Fowler, 2002; Richards *et al.*, 2002; Stewart *et al.*, 2003; Nielsen *et al.*, 2012; Sandaña *et al.*, 2012). In wheat, flag leaf contributes about 60

percent of grain yield. Spectral indices measured during anthesis and grain filling stages are correlated with grain yield of wheat in several studies (Marti *et al.*, 2007; Jin *et al.*, 2017; Kyratzis *et al.*, 2017; Olanrewaju *et al.*, 2019; Thapa *et al.*, 2019; Zhang *et al.*, 2019). Positive relation of CC measured during the reproductive stage with grain yield suggested the importance of canopy greenness during reproductive stage to convert the captured energy into grain yield. Therefore, it is important to maintain canopy health after heading until the late grain filling stage.

Fungicide was applied after heading (10.51 in Feekes scale; Large (1954)) following the onset of leaf rust infection in susceptible varieties. The objective of using three replications for fungicide treatment was to quantify the effect of leaf rust on CC values and differentiate it from normal physiological changes. Although we were able to see the differences in greenness of the canopy, it was not enough to isolate the differences in the decrease in CC due to leaf rust infection or physiological changes.

REFERENCES

Acreche, M. M., Briceño-Félix, G., Martín Sánchez, J. A., & Slafer, G. A. (2009). Radiation interception and use efficiency as affected by breeding in Mediterranean wheat. *Field Crops Research, 110*(2), 91–97. https://doi.org/10.1016/j.fcr.2008.07.005

Ashapure, A., Jung, J., Yeom, J., Chang, A., Maeda, M., Maeda, A., & Landivar, J. (2019). A novel framework to detect conventional tillage and no-tillage cropping system effect on cotton growth and development using multi-temporal UAS data. *ISPRS Journal of Photogrammetry and Remote Sensing, 152,* 49–64. https://doi.org/10.1016/j.isprsjprs.2019.04.003

Batchelor, W. D. (1997). Modelling potential crop growth processes. In *Agricultural Systems* (Vol. 54, Issue 1). https://doi.org/10.1016/s0308-521x(97)86669-3

Botwright, T. L., Condon, A. G., Rebetzke, G. J., & Richards, R. A. (2002). Field evaluation of early vigour for genetic improvement of grain yield in wheat. *Australian Journal of Agricultural Research, 53*(10), 1137–1145. https://doi.org/10.1071/AR02007

Calderini, D. F., Dreccer, M. F., & Slafer, G. A. (1997). Consequences of breeding on biomass, radiation interception and radiation-use efficiency in wheat. *Field Crops Research, 52*(3), 271–281. https://doi.org/10.1016/S0378-4290(96)03465-X

Cossani, C. M., Slafer, G. A., & Savin, R. (2009). Yield and biomass in wheat and barley under a range of conditions in a Mediterranean site. *Field Crops Research, 112*(2–3), 205–213. https://doi.org/10.1016/j.fcr.2009.03.003

De Bruin, J. L., & Pedersen, P. (2008). Effect of row spacing and seeding rate on soybean yield. *Agronomy Journal*, *100*(3), 704–710. https://doi.org/10.2134/agronj2007.0106

Distelfeld, A., Avni, R., & Fischer, A. M. (2014). Senescence, nutrient remobilization, and yield in wheat and barley. In *Journal of Experimental Botany* (Vol. 65, Issue 14, pp. 3783–3798). https://doi.org/10.1093/jxb/ert477

Dixon, L. E., Karsai, I., Kiss, T., Adamski, N. M., Liu, Z., Ding, Y., Allard, V., Boden, S. A., & Griffiths, S. (2019). VERNALIZATION1 controls developmental responses of winter wheat under high ambient temperatures. *Development (Cambridge, England)*, *146*(3). https://doi.org/10.1242/dev.172684

Eberhard, S., Finazzi, G., & Wollman, F.-A. (2008). The Dynamics of Photosynthesis. *Annual Review of Genetics*, *42*(1), 463–515. https://doi.org/10.1146/annurev.genet.42.110807.091452

Feng, G., Luo, H., Zhang, Y., Gou, L., Yao, Y., Lin, Y., & Zhang, W. (2016). Relationship between plant canopy characteristics and photosynthetic productivity in diverse cultivars of cotton (Gossypium hirsutum L.). *Crop Journal*, *4*(6), 499–508. https://doi.org/10.1016/j.cj.2016.05.012

Fischer, R. A. (2011). Wheat physiology: A review of recent developments. In *Crop and Pasture Science* (Vol. 62, Issue 2, pp. 95–114). https://doi.org/10.1071/CP10344

Fresco, L. F. M. (1973). a Model for Plant Growth. Estimation of the Parameters of the Logistic Function. *Acta Botanica Neerlandica*, *22*(5), 486–489. https://doi.org/10.1111/j.1438-8677.1973.tb00868.x

Gifford, R. M., Thorne, J. H., Hitz, W. D., & Giaquinta, R. T. (1984). Crop productivity and photoassimilate partitioning. *Science*, *225*(4664), 801–808. https://doi.org/10.1126/science.225.4664.801

Giunta, F., Motzo, R., & Pruneddu, G. (2008). Has long-term selection for yield in durum wheat also induced changes in leaf and canopy traits? *Field Crops Research*, *106*(1), 68–76. https://doi.org/10.1016/j.fcr.2007.10.018

Glasbey, C. A., & Hunt, R. (1983). Plant Growth Curves-the Functional Approach to Plant Growth Analysis. *Biometrics*, *39*(2), 537. https://doi.org/10.2307/2531040

Gompertz, B. (1815). On the Nature of the Function Expressive of the Law of Human Mortality, and on a New Mode of Determining the Value of Life Contingencies. *Proceedings of the Royal Society of London*, *2*(0), 252–253. https://doi.org/10.1098/rspl.1815.0271

Hunt, R. (1979). Plant Growth Analysis: The Rationale Behind the Use of the Fitted Mathematical Function. *Annals of Botany*, *43*(2), 245–249. https://doi.org/10.1093/oxfordjournals.aob.a085632

Hunt, R. (1982). Plant Growth Analysis: Second Derivatives and Compounded Second Derivatives of Splined Plant Growth Curves. *Annals of Botany*, *50*(3), 317–328. https://doi.org/10.1093/oxfordjournals.aob.a086371

Hunt, R., Causton, D. R., Shipley, B., & Askew, A. P. (2002). A modern tool for classical plant growth analysis. *Annals of Botany*, *90*(4), 485–488. https://doi.org/10.1093/aob/mcf214

Hunt, R. (1990). Basic Growth Analysis*: Plant Growth Analysis for Beginners*. Springer

Science & Business Media. https://doi.org/10.1007/978-94-010-9117-6

Hunt, R., & Parsons, I. T. (1974). A Computer Program for Deriving Growth-Functions in Plant Growth-Analysis. *The Journal of Applied Ecology*, *11*(1), 297. https://doi.org/10.2307/2402022

Jin, X., Li, Z., Yang, G., Yang, H., Feng, H., Xu, X., Wang, J., Li, X., & Luo, J. (2017). Winter wheat yield estimation based on multi-source medium resolution optical and radar imaging data and the AquaCrop model using the particle swarm optimization algorithm. *ISPRS Journal of Photogrammetry and Remote Sensing*, *126*, 24–37. https://doi.org/10.1016/j.isprsjprs.2017.02.001

Jung, J. (2017). UAS data processing. *Auvsi Xponential 2017*.

Jung, J., Ashapure, A., Maeda, M., Landivar, J., Chang, A., Yeom, J., Hague, S., & Smith, W. (2018). *Unmanned aerial system based cotton genotype selection using machine learning (Conference Presentation)*. 36. https://doi.org/10.1117/12.2323858

Kyratzis, A. C., Skarlatos, D. P., Menexes, G. C., Vamvakousis, V. F., & Katsiotis, A. (2017). Assessment of vegetation indices derived by UAV imagery for durum wheat phenotyping under a water limited and heat stressed Mediterranean environment. *Frontiers in Plant Science, 8*. https://doi.org/10.3389/fpls.2017.01114

Lemerle, D., Gill, G. S., Murphy, C. E., Walker, S. R., Consens, R. D., Mokhtari, S., Peltzer, S. J., Coleman, R., & Luckett, D. J. (2001). Genetic improvement and agronomy for enhanced wheat competitiveness with weeds. In *Australian Journal of Agricultural Research* (Vol. 52, Issue 5, pp. 527–548).

https://doi.org/10.1071/AR00056

Large, E. C. (1954). Growth stages in cereals illustration of the Feekes scale. *Plant Pathology*, *3*(4), 128-129.

Loss, S. P., & Siddique, K. H. M. (1994). Morphological and Physiological Traits Associated with Wheat Yield Increases in Mediterranean Environments. *Advances in Agronomy*, *52*(C), 229–276. https://doi.org/10.1016/S0065-2113(08)60625-2

Ludwig, F., & Asseng, S. (2010). Potential benefits of early vigor and changes in phenology in wheat to adapt to warmer and drier climates. *Agricultural Systems*, *103*(3), 127–136. https://doi.org/10.1016/j.agsy.2009.11.001

Maddonni, G. A., & Otegui, M. E. (1996). Leaf area, light interception, and crop development in maize. *Field Crops Research*, *48*(1), 81–87. https://doi.org/10.1016/0378-4290(96)00035-4

Marti, J., Bort, J., Slafer, G. A., & Araus, J. L. (2007). Can wheat yield be assessed by early measurements of Normalized Difference Vegetation Index? *Annals of Applied Biology*, *150*(2), 253–257. https://doi.org/10.1111/j.1744-7348.2007.00126.x

Nielsen, D. C., Miceli-Garcia, J. J., & Lyon, D. J. (2012). Canopy cover and leaf area index relationships for wheat, triticale, and corn. *Agronomy Journal*, 104(6), 1569-1573. https://doi.org/10.2134/agronj2012.0107n

Olanrewaju, S., Rajan, N., Ibrahim, A. M. H., Rudd, J. C., Liu, S., Sui, R., Jessup, K. E., & Xue, Q. (2019). Using aerial imagery and digital photography to monitor growth and yield in winter wheat. *International Journal of Remote Sensing*, *40*(18), 6905–6929. https://doi.org/10.1080/01431161.2019.1597303

Paine, C. E. T., Marthews, T. R., Vogt, D. R., Purves, D., Rees, M., Hector, A., & Turnbull, L. A. (2012). How to fit nonlinear plant growth models and calculate growth rates: An update for ecologists. *Methods in Ecology and Evolution*, *3*(2), 245–256. https://doi.org/10.1111/j.2041-210X.2011.00155.x

Patrignani, A., & Ochsner, T. E. (2015). Canopeo: A powerful new tool for measuring fractional green canopy cover. *Agronomy Journal*, *107*(6), 2312–2320. https://doi.org/10.2134/agronj15.0150

Rebetzke, G. J., & Richards, R. A. (1999). Genetic improvement of early vigour in wheat. *Australian Journal of Agricultural Research*, *50*(3), 291–301. https://doi.org/10.1071/A98125

Reta-Sánchez, D. G., & Fowler, J. L. (2002). Canopy light environment and yield of narrow-row cotton as affected by canopy architecture. *Agronomy Journal*, *94*(6), 1317–1323. https://doi.org/10.2134/agronj2002.1317

Richards, F. J. (1959). A flexible growth function for empirical use. *Journal of Experimental Botany*, *10*(2), 290–301. https://doi.org/10.1093/jxb/10.2.290

Richards, R. A., Rebetzke, G. J., Condon, A. G., & Van Herwaarden, A. F. (2002). Breeding opportunities for increasing the efficiency of water use and crop yield in temperate cereals. *Crop Science*, *42*(1), 111–121. https://doi.org/10.2135/cropsci2002.1110

Sandaña, P., Ramírez, M., & Pinochet, D. (2012). Radiation interception and radiation use efficiency of wheat and pea under different P availabilities. *Field Crops Research*, *127*, 44–50. https://doi.org/10.1016/j.fcr.2011.11.005

Schurr, U., Walter, A., & Rascher, U. (2006). Functional dynamics of plant growth and photosynthesis - From steady-state to dynamics - From homogeneity to heterogeneity. In *Plant, Cell and Environment* (Vol. 29, Issue 3, pp. 340–352). https://doi.org/10.1111/j.1365-3040.2005.01490.x

Stewart, D. W., Costa, C., Dwyer, L. M., Smith, D. L., Hamilton, R. I., & Ma, B. L. (2003). Canopy Structure, Light Interception, and Photosynthesis in Maize. *Agronomy Journal*, *95*(6), 1465–1474. https://doi.org/10.2134/agronj2003.1465

Szparaga, A., & Kocira, S. (2018). Generalized logistic functions in modelling emergence of Brassica napus L. *PLoS ONE*, *13*(8). https://doi.org/10.1371/journal.pone.0201980

Thapa, S., Rudd, J. C., Xue, Q., Bhandari, M., Reddy, S. K., Jessup, K. E., Liu, S., Devkota, R. N., Baker, J., & Baker, S. (2019). Use of NDVI for characterizing winter wheat response to water stress in a semi-arid environment. *Journal of Crop Improvement*, *33*(5), 633–648. https://doi.org/10.1080/15427528.2019.1648348

Westoby, M. J., Brasington, J., Glasser, N. F., Hambrey, M. J., & Reynolds, J. M. (2012). "Structure-from-Motion" photogrammetry: A low-cost, effective tool for geoscience applications. *Geomorphology*, *179*, 300–314. https://doi.org/10.1016/j.geomorph.2012.08.021

Yin, X., Goudriaan, J., Lantinga, E. A., Vos, J., & Spiertz, H. J. (2003). A flexible sigmoid function of determinate growth. *Annals of Botany*, *91*(3), 361–371. https://doi.org/10.1093/aob/mcg029

Zeide, B. (1993). Analysis of Growth Equations. *Forest Science*, *39*(3), 594–616.

https://doi.org/10.1093/forestscience/39.3.594

Zhang, L. X., Chen, Y. Q., Li, Y. X., Ma, J. C., Du, K. M., Zheng, F. X., & Sun, Z. F. (2019). Estimating Above Ground Biomass of Winter Wheat at Early Growth Stages Based on Visual Spectral. *Guang Pu Xue Yu Guang Pu Fen Xi/Spectroscopy and Spectral Analysis*, *39*(8), 2501–2506. https://doi.org/10.3964/j.issn.1000-0593(2019)08-2501-06

Zhao, Z., Rebetzke, G. J., Zheng, B., Chapman, S. C., & Wang, E. (2019). Modelling impact of early vigour on wheat yield in dryland regions. *Journal of Experimental Botany*, *70*(9), 2535–2548. https://doi.org/10.1093/jxb/erz069

CHAPTER IV

WINTER WHEAT YIELD PREDICTION USING UNMANNED AERIAL SYSTEM (UAS)-BASED CANOPY FEATURES

INTRODUCTION

Estimating wheat (*Triticum aestivum* L.) yield before harvest can be of great importance to plant breeders, farmers, and policy makers. Precise estimates of yield early in the season can help breeders to evaluate genotypes efficiently and accurately. The prediction tools can be used by the farmers and production industries to make in-season management and financial decisions. Wheat grain yield is a function of total biomass and harvest index (Reynolds and Langridge, 2016). Harvest index, which is the ratio of harvested grain yield to above ground biomass measures the efficiency of plants in allocating biomass to the grain (Calderini *et al.*, 1997; Hütsch *et al.*, 2019). Biomass is the product of incident solar radiation during the growing season, the amount of light intercepted by the canopy, and the its conversion into plant dry matter (Stöckle and Kemanian, 2009; Bai *et al.*, 2016). Establishment of Canopy Cover (CC) earlier in the growing season to maximize light interception can increase dry matter production in wheat through increased photosynthetic duration. Assessing biomass and canopy features throughout the growing season is useful for crop growth monitoring and grain yield estimation (Shi *et al.*, 2019). The three yield components: 1) number of heads per unit area, 2) number of kernels per head, or 3) kernel weight, which determine yield per plant either alone or in combinations are affected by the physiological changes that occur

during the growing season (Pennacchi *et al.*, 2018). Therefore, continuous monitoring of canopy features such as plant height, CC, and Leaf Area Index (LAI) can provide crucial information about biomass, crop growth and yield (Richards, 2000; Yield, 2002). LAI is directly proportional to light interception by the canopy and gross primary production in wheat. Incorporating genes (Rht) targeted to dwarfing of plants reduced height in wheat and prevented lodging. This improved harvest index and increased wheat yield (Richards, 2000; Araus *et al.*, 2008). Reduced plant height increases leaf area and light interception as more dry matter can be allocated to the growth of leaves rather than stems. Breeders select for short high-yielding lines to maintain dwarfing genes in the population so that they will be able to select for high yielding semi-dwarf lines in the advanced generations (Law *et al.*, 1978). CC, a.k.a. ground cover, is the area covered by the canopy per unit area of the land surface. It is positively correlated with LAI and biomass (Gamon *et al.*, 1995). In wheat breeding, one of the reasons for determining CC is to assess genotypes in terms of early vigor. It can also be used as an indirect measure of photosynthetic duration of individual genotypes. Additionally, assessing growth of winter wheat genotypes can be helpful for plant breeders to determine tolerance to abiotic and biotic stresses such as freezing, water stress, diseases, and pests. Optimization of canopy features is important for determining photosynthetic efficiency, biomass, and yield of selected genotypes. For this, it is important to have precise, reliable and efficient methods to measure all traits associated with yield. Measuring LAI and biomass throughout the growing season using destructive sampling method takes significant amount of time and the measurements are often inaccurate. Therefore, there

is a need to develop and evaluate a high-throughput field phenotypic system for making precise phenotypic measurements and assessing wheat growth and yield (Crain *et al.*, 2016, 2018).

Remote sensing based on Unmanned Aerial System (UAS), is gaining interest for high-throughput field phenotyping (Yang *et al.*, 2017). Development of lightweight, low-cost portable sensors had added benefits of using UAS for obtaining high spatial and temporal resolution data (Xu, Li and Paterson, 2019). UAS equipped with digital, thermal and multispectral sensors have been used to estimate several crop biophysical parameters such as LAI (Yang *et al.*, 2017), the fraction of intercepted photosynthetically active radiation (Bendig *et al.*, 2014, 2015; Bendig, 2015), plant height (Anderson *et al.*, 2019), canopy temperature (Berni *et al.*, 2009), disease assessment (Pugh *et al.*, 2018), growth status (Du and Noguchi, 2017), and yield prediction (Potgieter *et al.*, 2017). Red, green, and blue band (RGB) images obtained by flying small UAS at low altitude can be used to develop Digital Surface Model (DSM) of the bare ground and the surface of the canopy which can be used to determine canopy height. Biomass can be estimated using plant height derived from DSM in wheat (Anderson *et al.*, 2019). RGB and multispectral imagery can be used to obtain reflectance measurements in the R, G, B, red edge and near infrared (NIR) wavebands and calculate spectral vegetation indices. Numerous indices have been developed so far and are used to study vegetation growth and development. For example, reflectance observed in the green, NIR and red channels can be used to obtain indices such as Normalized Difference Vegetation Index (NDVI), Normalized Difference Red Edge

Index (NDRE), Simplified Canopy Chlorophyll Content Index (SCCCI), and Green Normalized Difference Vegetation Index (GNDVI). These indices can be used to estimate LAI, CC, and canopy chlorophyll content and provide an indirect assessment of canopy growth and health (Xue and Su, 2017). A strong correlation was found between vegetation indices, LAI and biomass in several studies (Calderini *et al.*, 1997; Bala and Islam, 2009; Bendig *et al.*, 2015; Xu, Li and Paterson, 2019). NDVI, which is one of the widely used indices was correlated with CC in cotton (Xue and Su, 2017), yield (Hassan *et al.*, 2019) and above ground biomass in wheat (Gamon *et al.*, 1995). NDRE, which uses the reflectance obtained in the red edge region of the spectrum can be used in vegetation stress detection and crop canopy senescence (Potgieter *et al.*, 2017).

Determining the right time to obtain imagery data during the crop growing season is another challenge faced by the breeders to evaluate genotypes for biomass, LAI, and yield as flying UAS platforms several times during the growing season can be costly. While there are several studies on the use of UAS as a high-throughput phenotyping (HTP) tool in wheat breeding, very few of them are focused on developing UAS parameters-based yield prediction models to predict grain yield in wheat. In the recent years, machine learning (ML) methods have been developed and used in prediction modeling. Some of the common ML methods are random forest (RF), support vector machine (SVM), and neural network models, such as the artificial neural network (ANN), and deep neural network (DNN). ML techniques have several advantages over traditional linear regression to predict crop yield. The ML methods can handle huge data with the problems of complexity and non-linearity (Jiang *et al.*, 2004).

Chlingaryan *et al.* (2018) reviewed ML research and development works and concluded that the advancement in remote sensing techniques coupled with ML techniques can provide better crop yield estimations. Khaki and Wang (2019) used DNN to predict grain yield in corn by using genotype, weather and soil information. They found a strong correlation between the predicted and actual corn yield and DNN outperformed Lasso, shallow neural networks (SNN), and regression tree. Kim *et al.* (2019) tested several ML methods with crop land information, vegetation indices derived from satellite images, meteorological and hydrological data and found that ANN and DNN can predict corn and soybean yield with high accuracy. ANN is one of the mostly used ML approaches in recent years to predict crop yield. ANN consists computational models and functions as an analogy with human neural system consisting of computational units called neurons (Zhelavskaya et al., 2017). In this model, a network structure that has at least one hidden layer and multiple neurons is created, and nonlinear response function is employed to reiterate many times to understand the complex relationships between input and output in training data. Jiang *et al.* (2004) used ANN for estimating wheat yield using back propagation algorithms based on satellite imagery data. They found that the performance of ANN was better than traditional linear regression methods. Use of ANN to predict yield is found in several crops such as wheat (Pantazi *et al.*, 2016), maize (*Zea mays* L.) (Kaul, Hill and Walthall, 2005), soybean (*Glycine max* L.) (Kaul, Hill and Walthall, 2005), potato (*Solanum tuberosum* L.) (Gómez *et al.*, 2019). Much of the work on using ANN to predict crop yield has been done by using either satellite imagery or weather and soil data. There are limited studies

that used season-long multi-temporal UAS data for developing ML models. In this study, the potential use of UAS equipped with RGB and multispectral sensor to predict grain yield was evaluated. This was tested by obtaining measurements on multiple traits including plant height, CC, and vegetation indices by flying UAS multiple times during the winter wheat growing season. These traits were used to study wheat growth and yield prediction. Thus, the objectives of this study were to i) obtain canopy features from UAS imagery and test the accuracy of the methods ii) assess the relationship between UAS parameters and grain yield in wheat iii) test ANN based-ML model for its potential to predict grain yield

MATERIALS AND METHODS

Study area

A field experiment was conducted at the Texas A&M AgriLife Research Experiment Station at Bushland, Texas (35º11'N, 102º06'W, and elevation 1170 m) in 2017-2018 winter wheat growing season. Sixty-two wheat cultivars and advanced lines were grown following a randomized complete block design with three replications under full irrigation. Plots were 3.4 m × 1.52 m in size consisting of seven rows with 0.18 m spacing. Seeds were sown on October 17, 2017. Agronomic practices such as nutrient management and weed management were carried out as per the requirement (Kimura et al., 2018).

UAS platforms and sensors

UAS platforms and sensors used in this study are shown in Figure **18**. To obtain multispectral images, a 4-band multispectral camera; SlantRange 3P (SlantRange, Inc., California, USA) was flown using DJI Matrice 100 quadcopter (SZ DJI Technology Co., Ltd, Shenzhen, China). SlantRange 3p is a multispectral sensor with 410-950 nm spectral range availability and have 1.2-megapixel resolution. It has a global shutter module which helps to capture data on G, R, red edge, and NIR wavebands. The center wavelengths of each bands are 550 nm, 650 nm, 720 nm, and 850 nm. Low accuracy Global Positioning System (GPS) was mounted on Matrice 100 and connected to the sensor to capture the geographic coordinates of the image. Another platform, DJI phantom 4 pro (SZ DJI Technology Co., Ltd, Shenzhen, China) was flown to collect high resolution RGB images. Phantom 4 pro is equipped with 20 megapixels one-inch CMOS (Complementary metal-oxide-semiconductor) RGB sensor. Both platforms have the advantage of flying at low altitude, which is helpful for obtaining high resolution orthomosaic images. UAS mission planning software: Pix4Dcapture (Pix4D S. A, Switzerland) and DroneDeploy (DroneDeploy, San Francisco, US), were used to plan UAS flights for phantom 4 pro and Matrice 100, respectively.

Figure 18. Unmanned Aerial System (UAS) platforms and sensors used in this study
Matrice 100 was used to carry SlantRange 3p (multispectral sensor).

UAS mission details and image acquisition timeline are summarized in Table **8**. UAS data were collected right after planting to generate Digital Elevation Model (DEM) to determine the elevation of the field. Data were collected by Ms. Shannon Baker, Research Associate at Texas A&M AgriLife at Amarillo, Texas over winter wheat breeding nursery maintained by Dr. Jackie Rudd.

Table 8. Unmanned Aerial System (UAS) flight details and data collection timeline
Red, green, and blue band (RGB) images were collected using DJI phantom 4 pro, multispectral sensor was used to collect data on R, G, red edge, near infrared (NIR) band using Matrice 100 platform at several Days after Planting (DAP) over winter wheat breeding trial at Bushland, Texas. Raw images were processed to generate orthomosaic images with certain spatial resolution (ground resolution).

		Multispectral sensor		RGB sensor	
Date	DAP	Flight altitude (m)	Ground resolution (cm/pixel)	Flight altitude (m)	Ground resolution (cm/pixel)
03-Jan-18	78	-	-	12.4	0.52
16-Jan-18	91	36.7	1.44	-	-
23-Jan-18	98	33.0	1.31	9.7	0.482
31-Jan-18	106	32.9	1.30	19.0	0.493
07-Feb-18	113	32.2	1.28	17.6	0.463
01-Mar-18	135	31.6	1.24	17.5	0.494
06-Mar-18	140	33.3	1.32	19.3	0.474
12-Mar-18	146	32.9	1.30	17.6	0.462
20-Mar-18	154	38.6	1.52	18.3	0.487
28-Mar-18	162	39.1	1.55	19.3	0.484

Table 8 continued

		Multispectral sensor		RGB sensor	
Date	DAP	Flight altitude (m)	Ground resolution (cm/pixel)	Flight altitude (m)	Ground resolution (cm/pixel)
05-Apr-18	170	38.7	1.53	19.7	0.503
09-Apr-18	174	42.0	1.66	21.9	0.543
15-Apr-18	180	34.1	1.35	19.9	0.489
23-Apr-18	188	28.3	1.12	16.5	0.446
04-May-18	199	29.2	1.13	50.8	0.510
08-May-18	203	30.9	1.19	22.0	0.543
14-May-18	209	30.3	1.18	30.7	0.528
21-May-18	216	29.8	1.17	19.0	0.460
30-May-18	225	30.9	1.19	21.3	0.536
05-Jun-18	231	30.6	1.20	17.3	0.515
12-Jun-18	238	30.3	1.20	15.2	0.375

Geo-referencing and radiometric calibration

It is important to overlay all the multi-temporal orthomosaics on a same geographic location of the plots so that same plot boundary shape file can be used to extract data from the orthomosaic to reduce error on the obtained data. Semi-permanent ground control points (GCPs) were placed across the field after planting and precise coordinates of the GCPs were surveyed using Real-time kinematics (RTK) GPS. The GCPs were surveyed after every flight throughout the growing season.

Vegetation indices are based on the reflectance measurements. The data collected by the UAS sensors was in the form of image digital numbers (DN). The DN values are affected by solar illumination patterns, angle of the sun, and cloud coverage when data was collected multiple times during the season. The conversion from DN into reflectance values, also known as radiometric calibration, should be done to calculate vegetation

indices. In this study, vegetation indices were developed using the reflectance obtained in the R, G, red edge, and NIR wavebands of the multispectral sensor. Thus, the radiometric calibration was performed on the data obtained using multispectral sensor. SlantRange 3p camera used in this study had an on-board Ambient Illumination Sensor (AIS) which is capable of correcting sunlight variations when flying. The AIS sensor measures incident light and adjusts the exposure time for each frame during data collection. Therefore, data captured throughout a single flight and from flight-to-flight during the growing season was comparable and consistent with respect to changing weather conditions. In this study, SlantView software (SlantRange, Inc., California, USA) was used to perform radiometric calibration of multispectral raw dataset.

Image processing and data extraction

Raw images obtained from the RGB sensor were processed using Agisoft metashape software (Agisoft LLC, St. Petersburg, Russia, 191144) to generate 3D point cloud, DSM, and orthomosaic images (Chang *et al.*, 2017; Du and Noguchi, 2017; Jung, 2017; Ashapure, Jung, Yeom, *et al.*, 2019). Several canopy features (CC, canopy height) and vegetation indices (Table 9) data were extracted from DSM and orthomosaic images. Canopy height was calculated by subtracting DEM obtained after planting from DSM generated after every flight during the crop growth. Figure **19** shows the procedure for developing Canopy Height Model (CHM).

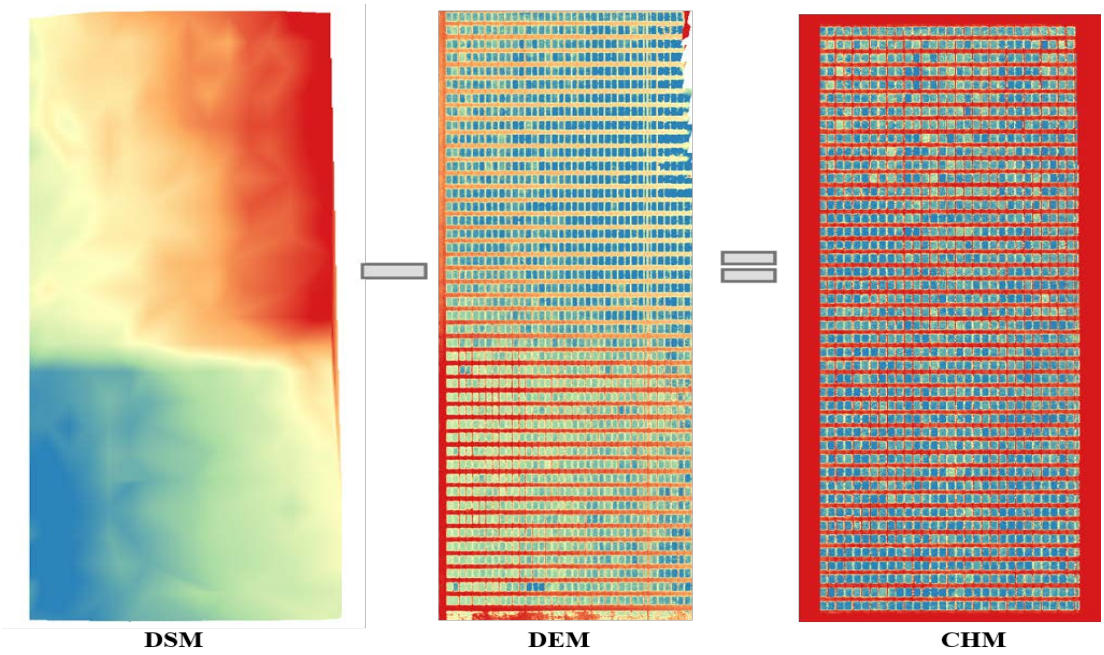

Figure 19. Determination of Canopy Height Model (CHM) from Unmanned Aerial System (UAS)
CHM was generated by subtracting Digital Elevation Model (DEM) from Digital Surface Model (DSM). DEM and DSM are surface models generated from UAS data using Agisoft Metashape software.

Percentage of CC was calculated by two different approaches following Jung et al. (2018) and Ashapure et al. (2019). In the first approach, CC was obtained by applying a threshold value in the NDVI map to separate vegetation and non-vegetation pixels and generate a binary image. NDVI map was generated from the calibrated multispectral imagery. In this study, an NDVI value of 0.6 was used as a threshold for separating vegetation from the soil. In the second approach, Canopeo algorithm (Patrignani and Ochsner, 2015) was used to classify the image into canopy and non-canopy classes.

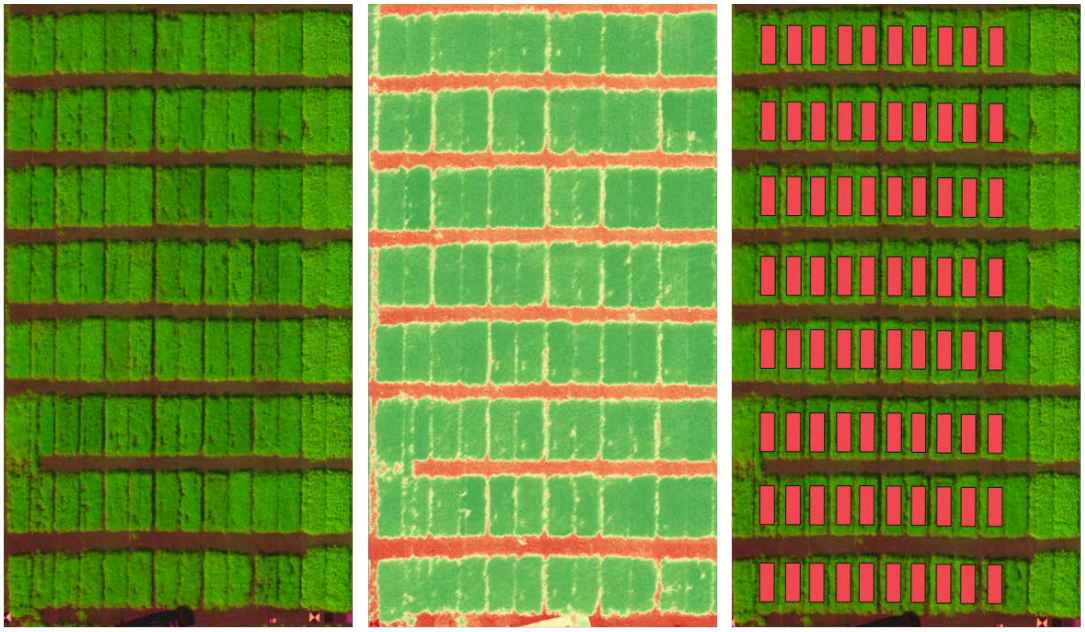

A. Orthomosaic B. Vegetation index map C. Plot boundary shapefile

Figure 20. Image processing and data extraction workflow after developing orthomosaic from Unmanned Aerial System (UAS) raw imagery
Vegetation index map is generated from spectral band combinations and is overlaid by plot boundary shape file to extract plot measurements.

Plot boundary shape file with individual plots was created to extract the data from individual plots (Figure 20C). This shapefile was overlaid on the canopy feature and vegetation indices maps. Data were extracted using zonal statistics tool in QGIS software (www.qgis.org). After the images were classified, CC in each plot was calculated using the following equation.

$$CC = \frac{Number\ of\ canopy\ pixels}{Total\ number\ of\ pixels}$$

Where CC is Canopy Cover

Spectral vegetation indices

Reflectance measurements obtained in four different spectral bands can be used to calculate several vegetation indices. In this study, eight vegetation indices commonly used to assess vegetation biomass, disease and senescence were calculated (Table 9).

Table 9. List of spectral vegetation indices used in this study
Reflectance obtained in the red band is denoted by R, green band by G, red edge by RE, and near infrared by NIR.

Vegetation indices	Formula	References
Normalized Difference Vegetation Index (NDVI)	$\frac{NIR - R}{NIR + R}$	Rouse *et al.*, 1974
Excess Green Index (ExG)	$ExG = 2G - R - B$	Patrignani and Ochsner, 2015
Normalized Difference Red Edge Index (NDRE)	$\frac{NIR - RE}{NIR + RE}$	Barnes *et al.*, 2000
Simplified Canopy Chlorophyll Content Index (SCCCI)	$\frac{NDRE}{NDVI}$	Raper and Varco, 2015
Green Normalized Difference Vegetation Index (GNDVI)	$\frac{NIR - G}{NIR + G}$	Giletson *et al.*, 2003
Soil Adjusted Vegetation Index (SAVI)	$\frac{1.5(NIR - R)}{NIR + R + 0.5}$	Huete, 1988
Modified Soil Adjusted Vegetation Index (MSAVI)	$\frac{2\mathrm{NIR} + 1 - \sqrt{(2NIR + 1)^2 - 8(\mathrm{NIR} - \mathrm{R})}}{2}$	Qi *et al.*, 1994
Modified Triangular Vegetation Index (MTVI2)	$\frac{1.5[1.2(NIR - G) - 2.5(R - G)}{\sqrt{[(2NIR + 1)^2 - (6NIR - 5\sqrt{R}) - 0.5}}$	Haboudane *et al.*, 2004

Ground measurements

Each plot was harvested by plot combine (Classic Plus, Wintersteiger AG, Germany) to determine final grain yield. Manual plant height measurements were

collected before harvest. A single measurement was taken per plot from the soil to the top of the plant.

Statistical analysis

Plant height obtained from the imagery data was used to study wheat growth and development. However, CC and vegetation indices were used to indirectly estimate grain yield. Data from UAS imagery can provide measurements on several traits that can be used to evaluate genotypes for higher grain yields. Data were analyzed using SAS version 9.4 (Statistical Analysis System Institute, Cary, NC, USA) and R programming language (R Development Core Team, 2014).

The relationship of wheat grain yield with multi-temporal CC and spectral vegetation indices measurements was assessed using coefficient of determination (R^2) and a significance level of 0.05 was used throughout. Significant temporal autocorrelation and multi-collinearity among the variables were found. Thus, appropriate variables contributing to grain yield were selected based on the variation observed in the temporal measurements of UAS features and R^2. After selecting appropriate variables, multi-temporal parameters were concatenated as a single feature vector to develop and train a neural network model.

RESULTS

Canopy height

Canopy height obtained from UAS imagery during the growing season is presented in Figure **21**. As shown in this figure, plants started to gain height at 100 Days after Planting (DAP). Tillers were formed early in the growing season until late tillering (Feekes scale: 2 to 4; Large (1954)) which was followed by stem elongation and increase in height. This behavior was clearly demonstrated when plotting multi-temporal UAS data against DAP. A sigmoidal growth pattern was found in canopy height. A four-parameter sigmoid function was fitted across the multi-temporal dataset and a highly accurate sigmoid fitting line with R^2=0.98 and RMSE=0.03 m was found. Growth in canopy height accelerated after 150 DAP and reached a maximum at 220 DAP. At this point, canopy height ranged from 0.7 to 0.9 m. Plot variability was larger in canopy height once the growth accelerated and when the plants reached maximum height. UAS-obtained canopy height was validated using the actual measurements obtained in the field (Figure **22**). UAS-based canopy height measurements correlated well with the ground measurements. Since ground measurements were obtained before harvest when the crop was at final growth stage, canopy height obtained at 225 (Figure **22**a), 231 (Figure **22**b), 238 DAP (Figure **22**c) from UAS imagery were used to validate the accuracy with ground data. Canopy height obtained at 225 (R^2=0.67) and 238 DAP (R^2=0.61) had better accuracy with ground measurements.

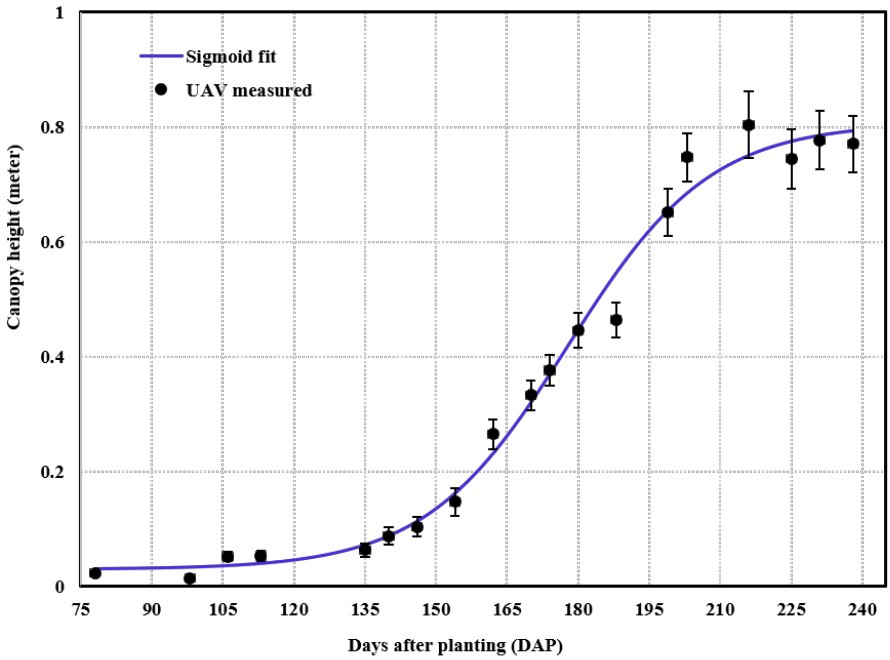

Figure 21. Canopy height obtained over an entire winter wheat growing season from Unmanned Aerial System (UAS)-based Digital Surface Models (DSM)
Vertical bars represent standard deviation.

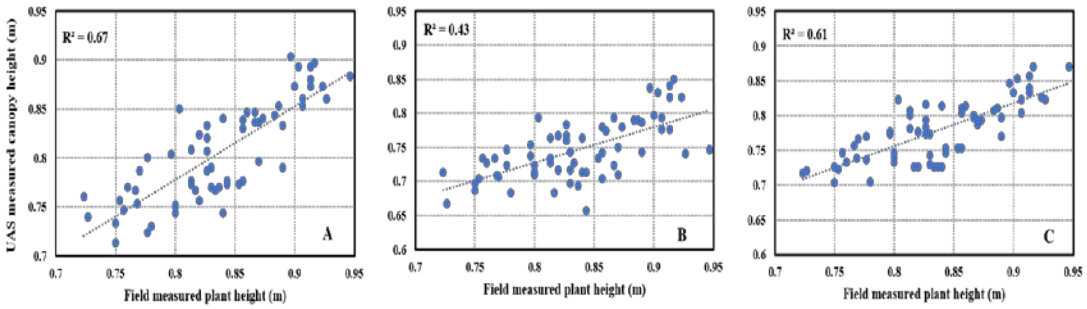

Figure 22. Relationship between field measured plant height and Unmanned Aerial System (UAS) obtained canopy height.
Each data point represents a genotype which is the average of three replicates.

Vegetation indices

Vegetation indices obtained from the multispectral sensor are shown in Figure **23** and Figure **24**. GNDV, Modified Soil Vegetation Index (MSAVI), NDVI, SCCI, and Soil Adjusted Vegetation Index (SAVI) had lower variation among eight indices derived from multispectral imagery. NDRE, and Modified Triangular Vegetation Index (MTVI2) had higher variability. These indices were compared to assess their once the ground is fully covered by canopy. Almost all these vegetation indices had higher variability early and at the end of the season. However, MTVI2 and NDRE showed higher variability among genotypes during later growth stages (10.1 to 11.1 in Feekes scale; Large (1954)). NDRE had highest variability among all other indices after heading. Genotypes usually start senescing after anthesis. When the NDRE values of highest and lowest yielding genotypes were compared across the growing season, differences in NDRE values were found after heading. This shows the importance of NDRE which might not get saturated once a plot is fully covered by the canopy. However, if we assess Excess Green Index (ExG) obtained using RGB sensor, a higher variability was observed among genotypes throughout the growing season (Figure **25**). ExG values were low early and started to increase after 140 DAP and reached maximum at 174 DAP. ExG being highly sensitive to change in color of the canopy might have attributed this variation in ExG. Another interesting difference noted in this study was that ExG was never saturated. It reached the peak and again started to decrease rapidly. Two major dips were found at 180 and 188 DAP which was not seen in any of the vegetation indices obtained from multispectral sensor. reached 0.35 at 199 DAP. Visual inspection of orthomosaic images

was done to find the reason behind this decrease in ExG values at those two specific days. The difference in the brightness of the sun can be seen in the pictures. ExG is highly sensitive to weather conditions as this index was not radiometrically calibrated. Heading date was noted at 199 to 230 DAP. Once plots reached heading, ExG values decreased and was minimum during the late grain filling stage. This shows its sensitivity to change in color of the canopy and growth stage. Compared to ExG, vegetation indices obtained from multispectral imagery showed higher stability across the season.

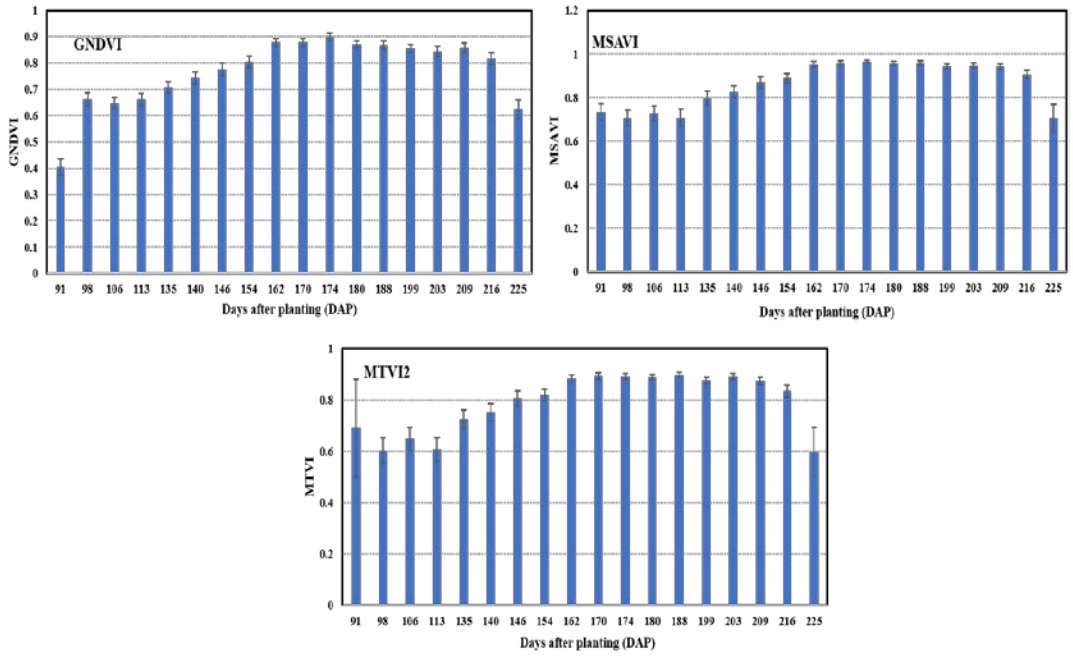

Figure 23. Vegetation indices obtained over the winter wheat growing season from Unmanned Aerial System (UAS)-based multispectral imagery (Group A)
GNDVI: Green Normalized Difference Vegetation Index, MSAVI: Modified Soil Adjusted Vegetation Index, MTVI2: Modified Triangular Vegetation Index. Vertical bars represent standard deviations.

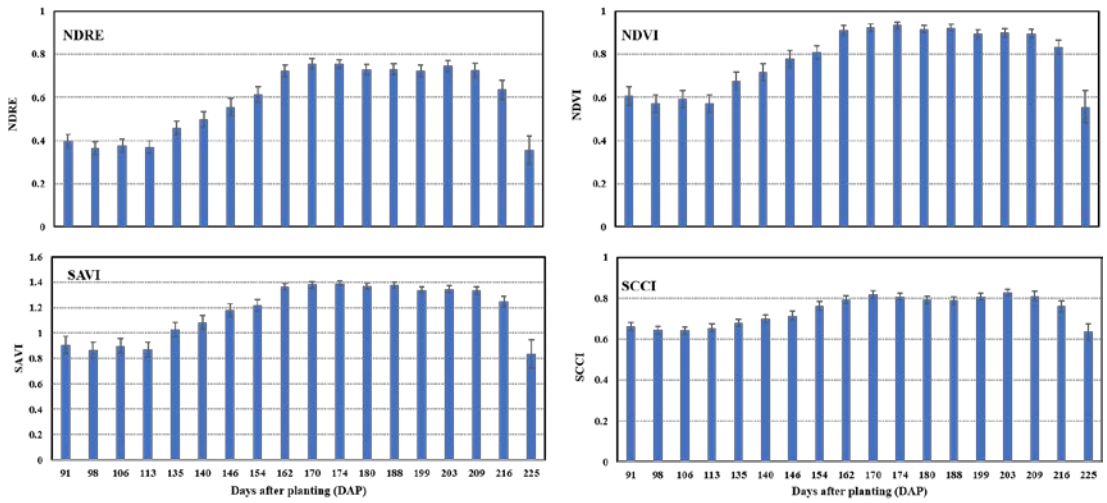

Figure 24. Vegetation indices obtained over the winter wheat growing season from Unmanned Aerial System (UAS)-based multispectral indices (Group B)
NDRE: Normalized Difference Red Edge Index, NDVI: Normalized Difference Vegetation Index, SAVI: Soil Adjusted Vegetation Index, SCCI: Simplified Canopy Chlorophyll Content Index. Vertical bars represent standard deviations.

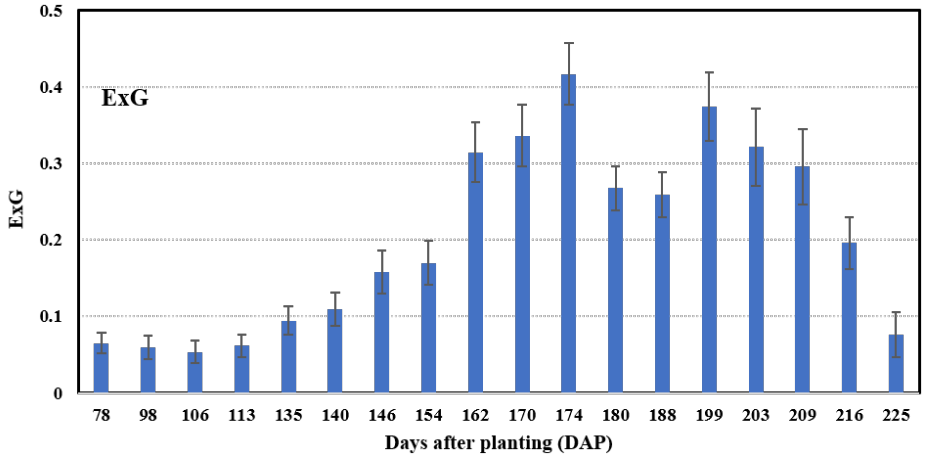

Figure 25. Excess Green Index (ExG) obtained over the winter wheat growing season from Unmanned Aerial System (UAS)-based digital imagery
Vertical bars represent standard deviations.

Canopy cover (CC) obtained from RGB and multispectral sensors

CC obtained by processing RGB and multispectral images is presented in Figure **26**. Applying threshold in NDVI values is a common approach to obtain precise

vegetation estimates. Potgieter et al. (2017) applied 0.5 as a threshold in NDVI to capture reflectance from green leaves in sorghum. In this study, pixels with NDVI values greater than 0.6 were considered as green vegetation. For obtaining CC measurements from RGB orthomosaic, canopeo algorithm developed by Patrignani and Ochsner (2015) was used. CC was generated using the digital number values and threshold was used as follows to classify green vegetation with respect to background soil.

$$\frac{R}{G} < 0.95\,, \qquad \frac{B}{G} < 0.95\,, \qquad 2G - R - B > 20$$

where, R, G, and B are the digital numbers in RGB imagery.

As shown in Figure **26**, CC obtained from RGB imagery (CC_RGB) was significantly lower than CC obtained from NDVI map (CC_NDVI) until 170 DAP. At 170 DAP, CC reached maximum and plots were fully covered by green foliage. Lower CC_RGB values were caused by burned foliage tips due to low temperature. Minimum temperature reached below freezing during this time (Figure **27**). On an average, CC_RGB values decreased from 40 % to 20 % from 106 DAP to 135 DAP. However, on those same dates, CC_NDVI remained constant. It was not affected by the change in vegetation color caused by lower temperature during those measurement dates. CC obtained from both methods increased as the temperature increased. CC_RGB was not significantly different than CC_NDVI from 170 DAP to 203 DAP. Wheat plots headed at 199 to 203 DAP, and as shown in Figure 26, CC_RGB started decreasing and it was significantly lower than CC_NDVI until 231 DAP. Abrupt decrease in CC_NDVI

occurred at 231 DAP.

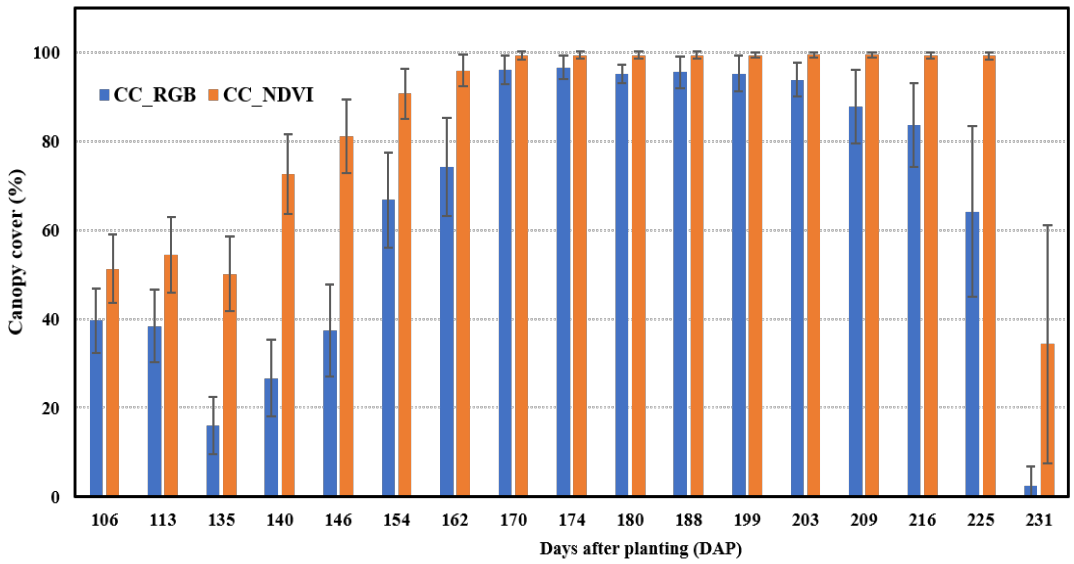

Figure 26. Comparison of Canopy cover obtained by using different Unmanned Aerial System (UAS) sensors over the entire season

CC_RGB: Canopy Cover obtained from red, green, and blue band (RGB) orthomosaics, CC_NDVI: Canopy Cover obtained from Normalized Difference Vegetation Index (NDVI) map. Vertical bars represent standard deviations.

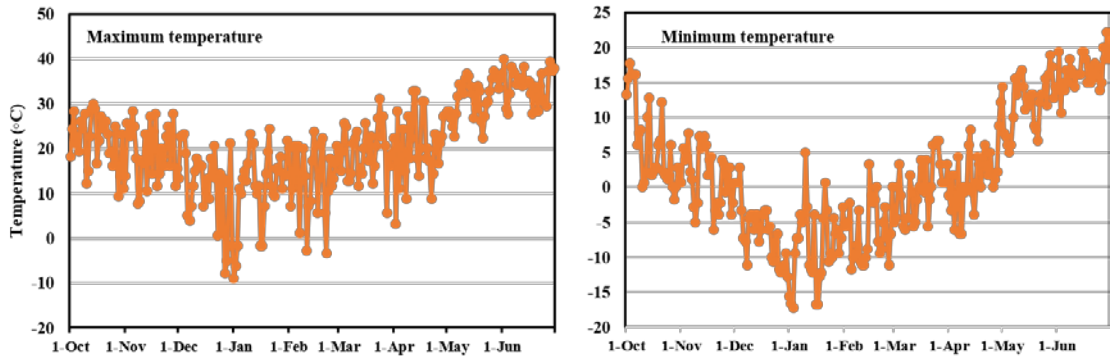

Figure 27. Maximum and minimum temperature during winter wheat growing season at Bushland, TX during 2017-2018 growing season

Relationship between UAS features and grain yield

Linear regression was performed between vegetation indices, canopy features and grain yield of wheat. All variables had positive relationship with grain yield. Most of the variables indicate leaf chlorophyll content which might be one of the reasons for positive relationship with grain yield. Relationship was strong at later growth stages specifically after flowering (10.51 to 11.1 in Feekes scale; Large (1954)). Table **10** shows the R^2 values obtained during the growing season. Among 11 different UAS features obtained in this study, NDRE, NDVI, SAVI, MSAVI, and CC_RGB were top five variables explaining maximum variation in grain yield (R^2~0.3-0.35, $p<0.05$). NDVI and MSAVI had similar R^2 values throughout the growing season. Highly significant multi-collinearity and autocorrelation was found between the UAS features. Features obtained from multispectral sensors were highly correlated with one another. Canopy features measured early in the growing season (during early vegetative stage) did not explain variability in yield. However, CC_RGB measured after 146 DAP started to show some impact on yield variation ($R^2 > 0.15$).

Variables were selected based on the physiological property of UAS features, variability, available literature and hit-trial method to develop a prediction model. NDRE, ExG, CC_RGB, CH, and NDVI were selected to develop machine learning model based on neural network architecture. Features that were able to measure the rate of senescence were highly associated with grain yield. NDRE can measure the rate of senescence (Potgieter et al., 2017). CC_RGB had strong association with grain yield compared to CC_NDVI. Another aspect of using this approach is to find the determinants of photosynthetic efficiency and assimilatory area of a plant. For example, CC determines the size of photosynthetic area and the ExG which measures the intensity of greenness in a canopy and determines assimilation efficiency.

Table 10. Coefficient of determination (R^2) values obtained between the linear relationships of Unmanned Aerial System (UAS)-based vegetation indices and canopy features with wheat grain yield

DAP: Days after planting, GNDVI: Green Normalized Difference Vegetation Index, MSAVI: Modified Soil Adjusted Vegetation Index, MTVI2: Modified Triangular Vegetation Index, NDRE: Normalized Difference Red Edge Index, NDVI: Normalized Difference Vegetation Index, SAVI: Soil Adjusted Vegetation Index, SCCI: Simplified Canopy Chlorophyll Content Index, ExG: Excess Green Index, CH: Canopy height, CC_RGB: Canopy Cover obtained from RGB orthomosaic, CC NDVI: Canopy Cover obtained from NDVI.

	Vegetation indices							Canopy features			
DAP	GNDVI	MSAVI	MTVI2	NDRE	NDVI	SAVI	SCCI	ExG	CH	CC_RGB	CC_NDVI
78								0.01	0.03	0.00	
91	0.00	0.00	0.00	0.00	0.00	0.00	0.01				0.00
98	0.00	0.00	0.00	0.00	0.00	0.00	0.02	0.00	0.02	0.00	0.00
106	0.01	0.01	0.00	0.01	0.01	0.00	0.01	0.00	0.02	0.00	0.01
113	0.00	0.01	0.00	0.02	0.01	0.00	0.01	0.01	0.02	0.04	0.01
135	0.00	0.01	0.01	0.02	0.01	0.01	0.02	0.01	0.00	0.06	0.02
140	0.01	0.05	0.06	0.03	0.05	0.04	0.00	0.02	0.00	0.09	0.06
146	0.05	0.11	0.10	0.10	0.11	0.09	0.05	0.03	0.01	0.10	0.12
154	0.06	0.10	0.10	0.12	0.10	0.09	0.05	0.04	0.02	0.13	0.08
162	0.12	0.19	0.14	0.16	0.19	0.18	0.04	0.04	0.03	0.14	0.01
170	0.12	0.14	0.08	0.09	0.14	0.14	0.01	0.06	0.03	0.14	0.00
174	0.03	0.15	0.10	0.12	0.14	0.14	0.02	0.01	0.02	0.10	0.01
180	0.13	0.24	0.17	0.18	**0.24**	0.23	0.04	0.11	0.02	0.24	0.02
188	0.13	0.20	0.10	0.18	0.20	0.19	0.06	0.11	0.02	**0.31**	0.05
199	0.19	**0.30**	0.23	0.22	**0.29**	**0.28**	0.06	0.14	0.02	0.23	0.00
203	**0.25**	**0.27**	0.14	**0.28**	**0.26**	**0.25**	0.11	0.16	0.07	0.22	0.00
209	**0.28**	**0.32**	0.19	**0.32**	**0.32**	**0.31**	0.17	0.18	0.14	**0.23**	0.00
216	**0.27**	**0.33**	**0.27**	**0.35**	**0.33**	**0.31**	**0.26**	0.22	0.07	**0.33**	0.02
225	**0.21**	**0.33**	**0.32**	**0.33**	**0.33**	**0.32**	**0.25**	**0.28**	0.15	**0.20**	**0.30**

Values in bold letters are statistically significant at $p<0.05$.

Prediction model

A three layered Artificial Neural Network (ANN), which consists of one input layer, one hidden layer, and one output layer was designed for predictive analysis (Mishra and Datta-Gupta, 2017). There were only 210 plots in the UVT and TXE trial. This data set was not enough to train the model. Therefore, data collected from other varietal trials was included in this study to train and test the neural network model. The data set comprised of 731 total samples, out of which 70% was divided into training set and 30% was used as a testing set resulting into 511 samples for training and 220 for testing following the stratified sampling procedure. An input feature vector was formed by concatenating UAS obtained temporal parameters. NDRE, ExG, CC_RGB, canopy height, NDVI, standard deviation of NDRE and ExG were selected as best performers of the model. In the process of developing predictive model, temporal parameters (independent variables) were scaled and divided into training and testing sets. The training vector with independent variables comprised the input layer and related to a hidden layer and yield was output layer of the network. Figure **28** shows the overall design of the network. A three-layered sequential model was created in Keras Python library. A sigmoid function was used as an activation function in the hidden layer, and the performance of the model was evaluated using mean absolute error. When a minimum error was achieved, the training of the model was stopped, and current parameter weights were used to predict the yield over the test samples. Model was trained using all UAS parameters measured across the season and using only the data collected after heading.

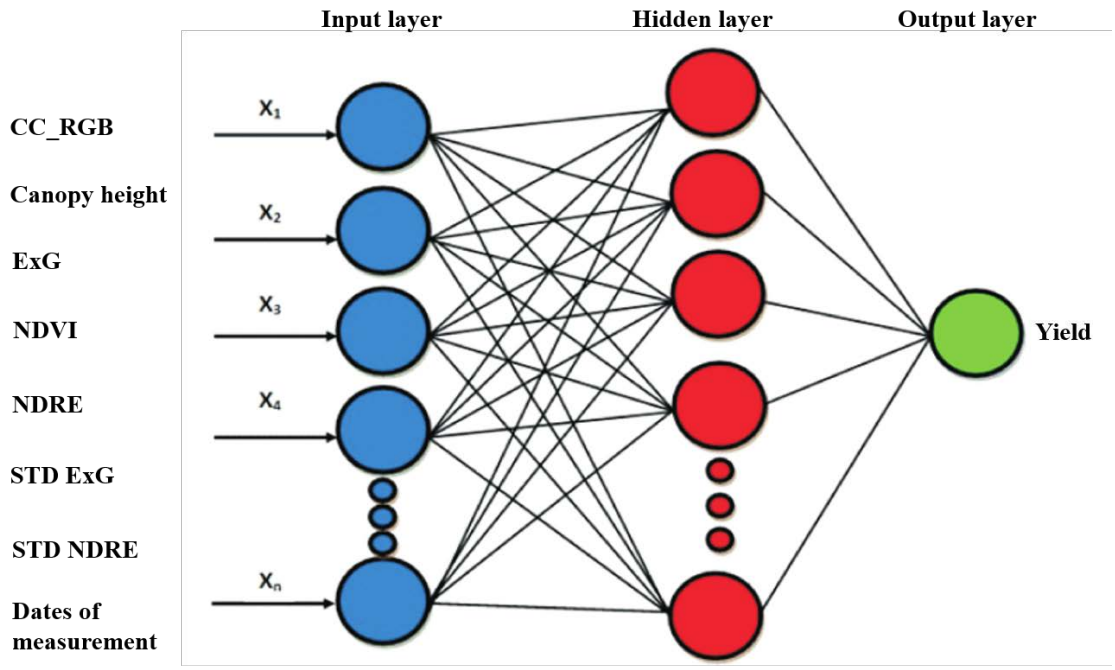

Figure 28. Artificial Neural Network (ANN) architecture based on Unmanned Aerial System (UAS) parameters

CC_RGB: Canopy Cover obtained from RGB orthomosaic, ExG: Excess Green Index, NDVI: Normalized Difference Vegetation Index, NDRE: Normalized Difference Red Edge Index, STD: Standard deviation of a plot. Adapted from Mishra and Gupta (2018).

Figure **29** shows the results of the model trained using data collected over entire season. R^2 values between the predicted and observed yield were 0.78 and 0.56 ($p<0.05$) for training and testing sets respectively. Figure **30** shows the results of the model trained using only the data collected after heading. R^2 values between the predicted yield and observed yield were 0.78 and 0.60 ($p<0.05$) for training and testing sets respectively.

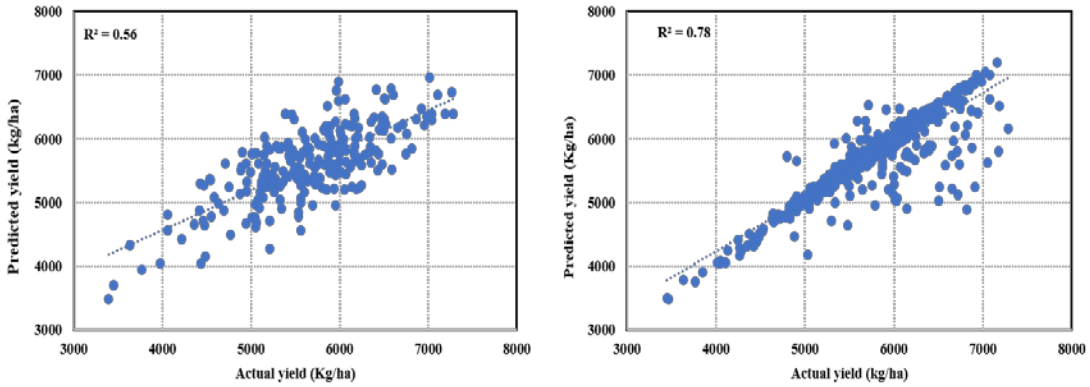

Figure 29. Artificial Neural Network (ANN) performance results for training and testing data from all measurement dates

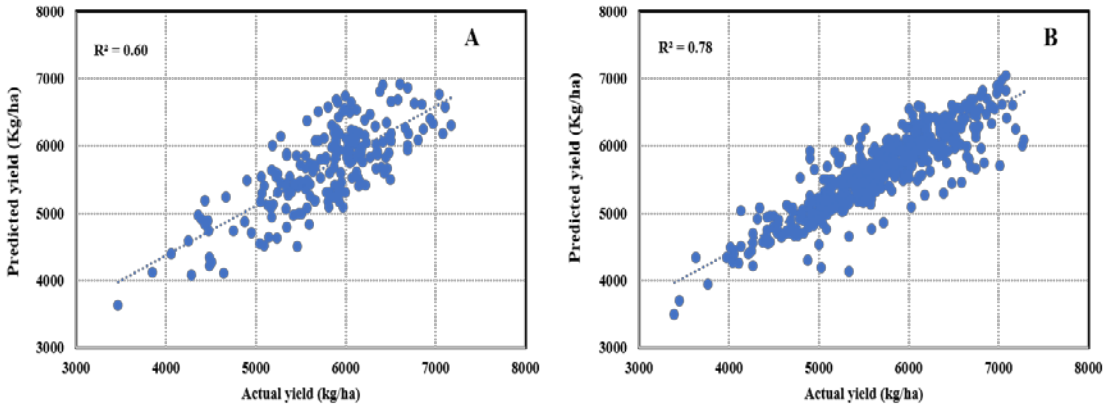

Figure 30. Artificial Neural Network (ANN) performance results for training and testing data from measurements taken after heading

DISCUSSION

UAS equipped with multispectral and RGB sensors were used to collect data efficiently over an entire growing season. Huge data set was collected over the entire season resulting in high spatial and temporal resolution data. It is important to understand the information provided by the UAS data. Analyzing UAS data from multiple dimensions is important to make their meaningful interpretation and use in

wheat breeding. Acquisition of several canopy features has enabled an approach to look at a canopy from different perspectives. Several vegetation indices were extracted from multispectral sensor and compared with RGB sensor. Although, spectral indices provide indirect estimates of several canopy features, they are subjected to errors caused by the soil, non-photosynthetic surfaces, canopy saturation, and angle of sun, etc. For example, NDVI is saturated when the vegetation is dense, and the canopy is fully closed. NDRE is less prone to saturation (Delegido *et al.*, 2013). The Soil Adjusted Vegetation Index (SAVI) minimizes the influence of background soil (Huete, 1988). Therefore, it is necessary to test the utility of UAS parameters specific to crops and their growing conditions. CC obtained from multispectral and RGB sensors was compared to test the stability and sensitivity of sensors. In terms of determining the canopy area coverage, multispectral sensor-based CC estimates were more stable compared to RGB-based CC estimates. RGB was more responsive to changes in canopy color, while multispectral measurements, which include reflectance in the NIR region, were more sensitive to change in canopy water content. This might be one of the reasons that CC obtained from multispectral sensor dropped during the end of the growing season whereas RGB-based CC was changing with the change in color of the canopy during freeze and senescence. (Ashapure *et al.*, 2019) found similar pattern in cotton. In addition to CC, vegetation indices based on NIR reflectance were highly stable but at the same time saturated. They were not responsive to change in growth stage of wheat. However, RGB-based indices were highly sensitive and resulted in larger variability among plots. Radiometric calibration of multispectral sensor and lower spatial resolution of orthomosaic images

obtained from this sensor can attributed to its stable measurements. Although, multispectral sensor provides a better stability of multi-temporal UAS measurements, they are expensive, and image processing procedure is comparatively more tedious than RGB sensors. It also limits the variability among plots. In case of canopy height, ground measurements were taken from single plant per plot during maturity which is associated to lower R^2 values between the UAS measured and actual plant height. In an experiment conducted by Anderson et al. (2019), canopy height measurements were reduced once the canopy started to dry. However, severe drop in canopy height was not observed in this study. A slight decrease in canopy height was observed once canopy reached maximum height. After that a reduction in 5-7 cm was found.

All the vegetation indices and canopy features were highly correlated with grain yield. Some indices had better correlation. One of the interesting findings in this study was the amount of variability explained by UAS features measured after heading on grain yield. The finding of chapter III is supported by the results obtained in this chapter. Genotypes senesced too rapidly during grain filling stage were prone to low yielding potential. Genotypes which senesce slowly can maintain biomass conversion efficiency and produce higher yield. This information can be helpful to design canopy properties of a genotype in a breeding program. Therefore, continuous monitoring of canopy features such as plant height, CC, and vegetation indices can provide crucial information about biomass, crop growth and yield. Use of UAS can make it possible to obtain information about all these features that may be used to determine plant health, canopy architecture, nature of growth, and grain yield in wheat.

In this study, ANN-based model to predict wheat grain yield was developed using multi-temporal UAS parameters. Encouraging results were obtained and a potential of using machine learning models to predict grain yield was explored. Results obtained from the developed model demonstrated the potential of predicting grain yield using data acquired after heading. Data obtained before heading were used to develop models to predict grain yield, but accurate results were not obtained. Training data was over-fitted and did not predict yield with low mean square errors. Machine learning tool to predict yield before heading would be an important asset to plant breeders to analyze the performance of a genotype and make early decisions. If highly accurate, it will reduce the amount of time and labor required to harvest genotypes. UAS measurements collected from multiple environments and multiple year if combined with weather information can result in a better prediction of grain yield. A lower testing accuracy indicates the need for additional tuning of the model. This can be achieved by training the model with large datasets collected from multiple environments. Larger sample size can have better generalization capability of the model and can improve predictability. Acquiring enough variation in the training data is important to improve model accuracy. Once the desired accuracy of the model is acquired, it is important to design a model that can be replicated across environments and years. The input parameters for the models are the multi-temporal data obtained from UAS imagery. It is challenging to maintain similar data collection schedule across environment because of the weather conditions and the availability of resources. Therefore, UAS measurements obtained across the growing season can be interpolated to create a data framework. Ashapure et al. (2019)

used radial basis function neural network (RBFNN)-based regression model to interpolate UAS measurement to predict tomato yield. Daily UAS measurements obtained from the first day after transplanting to final harvest accounts for all the physiological changes of canopy growth and fosters the application of the model in multiple years and multiple environments. There are other several other methods such as spline interpolation, cubic interpolation, or linear interpolation to determine time-series measurements (Lepot *et al.*, 2017). These approaches can be considered in future studies.

REFERENCES

Anderson, S. L., Murray, S. C., Malambo, L., Ratcliff, C., Popescu, S., Cope, D., ... & Thomasson, J. A. (2019). Prediction of maize grain yield before maturity using improved temporal height estimates of unmanned aerial systems. *The Plant Phenome Journal*, *2*(1). https://doi.org/10.2135/tppj2019.02.0004

Araus, J. L., Slafer, G. A., Royo, C., & Serret, M. D. (2008). Breeding for yield potential and stress adaptation in cereals. In *Critical Reviews in Plant Sciences*. https://doi.org/10.1080/07352680802467736

Ashapure, A., Jung, J., Chang, A., Oh, S., Maeda, M., & Landivar, J. (2019). A comparative study of RGB and multispectral sensor-based cotton canopy cover modelling using multi-temporal UAS data. *Remote Sensing*. https://doi.org/10.3390/rs11232757

Ashapure, A., Jung, J., Yeom, J., Chang, A., Maeda, M., Maeda, A., & Landivar, J. (2019). A novel framework to detect conventional tillage and no-tillage cropping system effect on cotton growth and development using multi-temporal UAS data. *ISPRS Journal of Photogrammetry and Remote Sensing*. https://doi.org/10.1016/j.isprsjprs.2019.04.003

Bai, Z., Mao, S., Han, Y., Feng, L., Wang, G., Yang, B., Zhi, X., Fan, Z., Lei, Y., Du, W., & Li, Y. (2016). Study on light interception and biomass production of different cotton cultivars. *PLoS ONE*. https://doi.org/10.1371/journal.pone.0156335

Bala, S. K., & Islam, A. S. (2009). Correlation between potato yield and MODIS-derived vegetation indices. *International Journal of Remote Sensing*.

https://doi.org/10.1080/01431160802552744

Bendig, J., Bolten, A., Bennertz, S., Broscheit, J., Eichfuss, S., & Bareth, G. (2014). Estimating biomass of barley using crop surface models (CSMs) derived from UAV-based RGB imaging. *Remote Sensing*. https://doi.org/10.3390/rs61110395

Bendig, J. (2015). Unmanned aerial vehicles (UAVs) for multi-temporal crop surface modelling. A new method for plant height and biomass estimation based on RGB-imaging. Doctoral dissertation, Universität zu Köln.

Bendig, J., Yu, K., Aasen, H., Bolten, A., Bennertz, S., Broscheit, J., Gnyp, M. L., & Bareth, G. (2015). Combining UAV-based plant height from crop surface models, visible, and near infrared vegetation indices for biomass monitoring in barley. *International Journal of Applied Earth Observation and Geoinformation*. https://doi.org/10.1016/j.jag.2015.02.012

Berni, J. A. J., Zarco-Tejada, P. J., Suárez, L., González-Dugo, V., & Fereres, E. (2009). Remote sensing of vegetation from UAV platforms using lightweight multispectral and thermal imaging sensors. *Int. Arch. Photogramm. Remote Sens. Spatial Inform. Sci*. https://doi.org/10.1007/s11032-006-9022-5

Calderini, D. F., Dreccer, M. F., & Slafer, G. A. (1997). Consequences of breeding on biomass, radiation interception and radiation-use efficiency in wheat. *Field Crops Research*. https://doi.org/10.1016/S0378-4290(96)03465-X

Chang, A., Jung, J., Maeda, M. M., & Landivar, J. (2017). Crop height monitoring with digital imagery from Unmanned Aerial System (UAS). *Computers and Electronics in Agriculture*. https://doi.org/10.1016/j.compag.2017.07.008

Crain, J. L., Wei, Y., Barker, J., Thompson, S. M., Alderman, P. D., Reynolds, M., Zhang, N., & Poland, J. (2016). Development and deployment of a portable field phenotyping platform. *Crop Science*, *56*(3), 965–975. https://doi.org/10.2135/cropsci2015.05.0290

Crain, J., Mondal, S., Rutkoski, J., Singh, R. P., & Poland, J. (2018). Combining High-Throughput Phenotyping and Genomic Information to Increase Prediction and Selection Accuracy in Wheat Breeding. *The Plant Genome*. https://doi.org/10.3835/plantgenome2017.05.0043

Delegido, J., Verrelst, J., Meza, C. M., Rivera, J. P., Alonso, L., & Moreno, J. (2013). A red-edge spectral index for remote sensing estimation of green LAI over agroecosystems. *European Journal of Agronomy*. https://doi.org/10.1016/j.eja.2012.12.001

Du, M., & Noguchi, N. (2017). Monitoring of wheat growth status and mapping of wheat yield's within-field spatial variations using color images acquired from UAV-camera System. *Remote Sensing*, *9*(3). https://doi.org/10.3390/rs9030289

Gamon, J. A., Field, C. B., Goulden, M. L., Griffin, K. L., Hartley, A. E., Joel, G., Penuelas, J., & Valentini, R. (1995). Relationships between NDVI, canopy structure, and photosynthesis in three Californian vegetation types. *Ecological Applications*, *5*(1), 28–41. https://doi.org/10.2307/1942049

Gómez, D., Salvador, P., Sanz, J., & Casanova, J. L. (2019). Potato yield prediction using machine learning techniques and Sentinel 2 data. *Remote Sensing*. https://doi.org/10.3390/rs11151745

Hassan, M. A., Yang, M., Rasheed, A., Yang, G., Reynolds, M., Xia, X., Xiao, Y., & He, Z. (2019). A rapid monitoring of NDVI across the wheat growth cycle for grain yield prediction using a multi-spectral UAV platform. *Plant Science*. https://doi.org/10.1016/j.plantsci.2018.10.022

Hütsch, B. W., Jahn, D., & Schubert, S. (2019). Grain yield of wheat (Triticum aestivum L.) under long-term heat stress is sink-limited with stronger inhibition of kernel setting than grain filling. *Journal of Agronomy and Crop Science*. https://doi.org/10.1111/jac.12298

Jiang, D., Yang, X., Clinton, N., & Wang, N. (2004). An artificial neural network model for estimating crop yields using remotely sensed information. *International Journal of Remote Sensing*, *25*(9), 1723–1732. https://doi.org/10.1080/0143116031000150068

Jung, J. (2017). UAS data processing. *AUVSI XPONENTIAL 2017*.

Kaul, M., Hill, R. L., & Walthall, C. (2005). Artificial neural networks for corn and soybean yield prediction. *Agricultural Systems*. https://doi.org/10.1016/j.agsy.2004.07.009

Kimura, E., Bell, J., Trostle, C., & Neely, C. (2018). Winter wheat management calander for rolling plains and high plains of Texas. Texas A&M Extension.

Law, C. N., Snape, J. W., & Worland, A. J. (1978). The genetical relationship between height and yield in wheat. *Heredity*. https://doi.org/10.1038/hdy.1978.13

Large, E. C. (1954). Growth stages in cereals illustration of the Feekes scale. *Plant Pathology*, *3*(4), 128-129.

Lepot, M., Aubin, J. B., & Clemens, F. H. L. R. (2017). Interpolation in time series: An introductive overview of existing methods, their performance criteria and uncertainty assessment. In *Water (Switzerland)*. https://doi.org/10.3390/w9100796

Mishra, S., & Datta-Gupta, A. (2017). Applied statistical modeling and data analytics: A practical guide for the petroleum geosciences. Elsevier.

Pantazi, X. E., Moshou, D., Alexandridis, T., Whetton, R. L., & Mouazen, A. M. (2016). Wheat yield prediction using machine learning and advanced sensing techniques. *Computers and Electronics in Agriculture*. https://doi.org/10.1016/j.compag.2015.11.018

Patrignani, A., & Ochsner, T. E. (2015). Canopeo: A powerful new tool for measuring fractional green canopy cover. *Agronomy Journal, 107*(6), 2312–2320. https://doi.org/10.2134/agronj15.0150

Pennacchi, J. P., Carmo-Silva, E., Andralojc, P. J., Feuerhelm, D., Powers, S. J., & Parry, M. A. J. (2018). Dissecting wheat grain yield drivers in a mapping population in the UK. *Agronomy*. https://doi.org/10.3390/agronomy8060094

Potgieter, A. B., George-Jaeggli, B., Chapman, S. C., Laws, K., Cadavid, L. A. S., Wixted, J., Watson, J., Eldridge, M., Jordan, D. R., & Hammer, G. L. (2017). Multi-spectral imaging from an unmanned aerial vehicle enables the assessment of seasonal leaf area dynamics of sorghum breeding lines. *Frontiers in Plant Science, 8:1532*. https://doi.org/10.3389/fpls.2017.01532

Pugh, N. A., Han, X., Collins, S. D., Thomasson, J. A., Cope, D., Chang, A., Jung, J., Isakeit, T. S., Prom, L. K., Carvalho, G., Gates, I. T., Vree, A., Bagnall, G. C., &

Rooney, W. L. (2018). Estimation of plant health in a sorghum field infected with anthracnose using a fixed-wing unmanned aerial system. *Journal of Crop Improvement*, *32*(6), 861–877. https://doi.org/10.1080/15427528.2018.1535462

Reynolds, M., & Langridge, P. (2016). Physiological breeding. In *Current Opinion in Plant Biology*. https://doi.org/10.1016/j.pbi.2016.04.005

Richards, R. A. (2000). Selectable traits to increase crop photosynthesis and yield of grain crops. *Journal of Experimental Botany*. https://doi.org/10.1093/jexbot/51.suppl_1.447

Sankaran, S., Khot, L. R., Espinoza, C. Z., Jarolmasjed, S., Sathuvalli, V. R., Vandemark, G. J., Miklas, P. N., Carter, A. H., Pumphrey, M. O., Knowles, R. R. N., & Pavek, M. J. (2015). Low-altitude, high-resolution aerial imaging systems for row and field crop phenotyping: A review. In *European Journal of Agronomy*. https://doi.org/10.1016/j.eja.2015.07.004

Shi, Z., Chang, T. G., Chen, G., Song, Q., Wang, Y., Zhou, Z., Wang, M., Qu, M., Wang, B., & Zhu, X. G. (2019). Dissection of mechanisms for high yield in two elite rice cultivars. *Field Crops Research*. https://doi.org/10.1016/j.fcr.2019.107563

Stöckle, C. O., & Kemanian, A. R. (2009). Crop radiation capture and use efficiency: a framework for crop growth analysis. In *Crop Physiology*. https://doi.org/http://dx.doi.org/10.1016/B978-0-12-374431-9.00007-4

Xu, R., Li, C., & Paterson, A. H. (2019). Multispectral imaging and unmanned aerial systems for cotton plant phenotyping. *PLoS ONE*. https://doi.org/10.1371/journal.pone.0205083

Xue, J., & Su, B. (2017). Significant remote sensing vegetation indices: A review of developments and applications. In *Journal of Sensors*. https://doi.org/10.1155/2017/1353691

Yang, G., Liu, J., Zhao, C., Li, Z., Huang, Y., Yu, H., Xu, B., Yang, X., Zhu, D., Zhang, X., Zhang, R., Feng, H., Zhao, X., Li, Z., Li, H., & Yang, H. (2017). Unmanned aerial vehicle remote sensing for field-based crop phenotyping: Current status and perspectives. In *Frontiers in Plant Science*. https://doi.org/10.3389/fpls.2017.01111

Yield, C. (2002). Crop physiology & metabolism: Breeding Opportunities for Increasing the Efficiency of Water Use and Crop Yield. *Crop Science, 42*(1), 111–121. http://cat.inist.fr/?aModele=afficheN&cpsidt=13440698

Zhelavskaya, I. S., Shprits, Y. Y., & Spasojević, M. (2017). Empirical Modeling of the Plasmasphere Dynamics Using Neural Networks. *Journal of Geophysical Research: Space Physics*. https://doi.org/10.1002/2017JA024406

CHAPTER V

CONCLUSIONS

This study demonstrates the potential use of Unmanned Aerial System (UAS) in high-throughput phenotyping (HTP). UAS comes with efficient data collection advantages which has opened several avenues to study agronomic and physiological properties of crops. Major focus was placed on UAS collection, processing, and utilization of collected data to assess foliage disease severity, growth, and yield of winter wheat genotypes.

Identification of sensors, data collection and processing procedure applicable to wheat breeding trials are outlined in each research chapter. Multiple UAS platforms equipped with Red Greed, and Blue (RGB) and multispectral sensors were flown over wheat breeding nurseries at Castroville, College Station, and Bushland, Texas. Image processing was mainly conducted using Agisoft Metashape, QGIS, and Python.

As shown in Chapter II, a low cost, consumer grade UAS equipped with a high-resolution RGB camera was used to capture imagery data of winter wheat breeding trials in 2017 and 2018. Raw images were processed to obtain orthomosaics which were radiometrically calibrated to generate vegetation index maps. Three different vegetation indices were developed and data from individual plots was extracted from the orthomosaics. All the image-based vegetation indices were highly associated with Coefficient of Infection (CI) that measured the leaf rust severity in both years. In addition, ground measured Normalized Difference Vegetation Index (NDVI) had a significant negative association with CI. These measurements can help to evaluate

genotypes for disease resistance on a large scale. Prediction models were developed, and their ability was tested to estimate disease severity based on vegetation index values. A very high association between the predicted and observed CI shows the ability of remotely measured data to estimate CI. Ability to significantly discriminate genotypes for disease severity, high repeatability, strong relationship between CI and vegetation indices, consistent results in both years, and reduced time to collect and process data show the significance of this approach as a HTP tool for foliage disease severity in wheat.

Chapter III demonstrated the potential of utilizing UAS obtained temporal data to understand plant growth. A phenotyping tool for growth analysis can be developed based on high-throughput data collection combined with the simple approach of fitting non-linear growth functions to derive multiple growth parameters. The rate of maximum canopy growth obtained using a logistic function can be useful to understand and predict plant biomass growth. In addition, it has the potential of serving as an additional trait to assess genotypes for early vigor and as a selection tool in forage breeding. A significant relationship between Canopy Cover (CC) during the reproductive phase shows the importance of slow canopy decay either due to disease infection or physiological changes (senescence). Genotypes capable of producing larger canopy and maintaining green canopy relatively longer can produce higher yield under biotic and abiotic stress conditions.

In Chapter IV, several spectral vegetation indices and canopy features obtained from multispectral and RGB sensors were evaluated for their relationship with grain

yield. In addition, the behavior of these UAS parameters was analyzed to diagnose the sensitivity, stability, and saturation of vegetation indices across growing season. Results indicated that vegetation indices obtained using near infrared reflectance measurements are comparatively stable compared to RGB-based features in response to canopy color, growth stage and atmospheric conditions. Measurements taken after heading were highly correlated to grain yield. However, reflectance from wheat head may be different than that of canopy which needs further investigation. Additionally, difference in canopy color among genotypes needs to be addressed. This study also reveals that UAS measurements should be taken frequently early in the season until plots are fully covered by the canopy. If disease is not present, then longer intervals can reduce the cost of data collection and processing. After heading and during late grain filling period more frequent UAS measurements are recommended to isolate the rate of maturity. This study further reveals that use of machine learning models can be helpful to predict yield early in the season, but the models should be trained with large dataset obtained from multiple environments and multiple years. These models can be combined with weather data and initial soil parameter dataset to predict genotype performance early in the season which can save the cost of harvesting. Assessing spatial variability based on soil water content and nutrient content across the field can provide additional accuracy. Additionally, highly trained models can act as a tool to assess genotypes by growing them in small plots which can reduce space and increase the throughput of evaluating more genotypes. Predicting yield early in the season can help farmers to make informed decisions about crop management and marketing.

Development of autonomous and semi-autonomous UAS system that can automate data acquisition, processing and analysis can play a vital role in phenotyping multiple traits in wheat breeding. These measurements will help to select parents and evaluate progenies on a large scale. Additionally, this tool can complement traditional methods of disease phenotyping and improve the precision of collected data and produce reliable disease estimates. Ultimately, HTP technologies combined with machine-learning algorithms can improve genetic gain by increasing the size and efficiency of breeding programs.